Photoluminescence Studies of Certain RE ions Doped Phosphate Glasses for Photonic Applications

Thesis

Submitted to

Delhi Technological University

In Partial Fulfillment of the Requirements for the Degree of

DOCTOR OF PHILOSOPHY

in

APPLIED PHYSICS

Submitted By

Ms. KARTIKA MAHESHWARI

Reg. Number: 2K17/Ph.D./AP/12

Under the Supervision of

Prof. A. S. RAO

Department of Applied Physics

Delhi Technological University

Delhi-110 042, INDIA

August, 2023

DEDICATED TO….

MY PARENTS

Delhi Technological University

(Govt. of National Capital Territory of Delhi)
Bawana Road, Delhi-110042

CERTIFICATE

This is to certify that the thesis titled "***Photoluminescence Studies of Certain RE ions Doped Phosphate Glasses for Photonic Applications***" is being submitted by ***Ms. KARTIKA MAHESHWARI*** with registration number ***2K17/Ph.D./AP/12*** to the Delhi Technological University for the award of the degree of Doctor of Philosophy in Applied Physics. The work embodied in this thesis is a record of bonafide research work carried out by me in the Materials and Atmospheric Sciences Research (MASR) Lab, Applied Physics Department, Delhi Technological University, New Delhi under the guidance of ***Prof. A. S. Rao***. It is further certified that this work is original and has not been submitted in part or fully to any other University or Institute for the award of any degree or diploma.

Ms. Kartika Maheshwari
Roll No. 2K17/PHDAP/12

This is to certify that the above statement made by the candidate is correct to the best of our knowledge.

Prof. A. S. Rao
Supervisor
Department of Applied Physics
Delhi Technological University
Delhi, India

Prof. A. S. Rao
Head
Department of Applied Physics
Delhi Technological University
Delhi, India

ACKNOWLEDGEMENTS

The journey of my research is accomplished with the valuable support of many people. I feel truly grateful to acknowledge all those people who have assisted me directly or indirectly for the finalization of my research work. It is a pleasant aspect that I have now the opportunity to express my gratitude for all of them. Firstly, I am grateful to goddess Saraswati, enduring me with strength and provide directions, motivating me throughout this journey towards the research.

At the outset, I would like to share my profound sense of gratitude, indebtedness and reverence to my supervisor, ***Professor A. S. Rao****, Head & Chairman, Department Research Committee (DRC), Department of Applied Physics, Delhi Technological University, Delhi, who nurtured my research capabilities for a successful scientific career. It has been an honor to work under excellent, enthusiastic and distinguished supervisors. His unremitting encouragement, constant help and meticulous supervision throughout the course of my study for carving another milestone in my academic journey. His immense knowledge of the subject, analytic gaze, farsightedness and perseverance were a constant source of inspiration during the course of this thesis work. I feel privileged to have worked under such a great supervision.*

My heartfelt recognitions for ***Dr. Amrish Panwar****, Department of Applied Physics, DTU for his timely support. I am also thankful to* ***Dr. M. Jayasimhadri****, Department of Applied Physics, DTU for granting their lab facilities to furnish the research work. I am thankful to the DRC chairman, DRC members, SRC members and other teaching and non-teaching staff of the department of Applied Physics, DTU for their help and advice.*

I am also thankful to ***Dr. K. Swapna, Dr. M. Venkateswarlu, Dr. Rekha Rani*** *from K.L. University, Vijayawada, A.P. for providing the characterization facilities for my research work and necessary advices. Above board I would like to express my sincere gratitude towards*

Dr. Sk. Mahamuda, K.L. University, Vijayawada, A.P. *for her precious time, support, motivation and advices throughout the tenure of my research work.*

It is my pleasure to thank my seniors ***Dr. Nisha Deopa, Dr. Sumandeep Kaur****,* ***Dr. Aman Prasad****, for their precious suggestions and assistance. I sincerely thank to my dear friends, former and present lab-mates and my colleagues whose support helped in accomplishing my work. I thank my fellow researchers* ***Dr. Ravita****,* ***Mr. Mukesh K. Sahu****,* ***Mr. Rajat Bajaj, Ms. Pooja Rohilla, Mr. Mohit Tyagi, Ms. Shristy, Ms. Anu, Ms. Sheetal, Mr. Videsh, Ms. Deepali, Mr. Vikas, Mr. Indrajeet*** *for the help whenever needed in completing my research work.*

I also desire to thank the Head of the department of ***AS&H ABES Engineering College****, Ghaziabad and all my fellow colleagues in AS&H department for all the guidance and motivation for pursuing my research work. Sincere gratitude to* ***Dr. Yasha Tayal*** *for extended support during research work and* ***Dr. Satyendra Kumar*** *for their timely support and encouragement in pursuing research work.*

Finally, I would like to thanks my family for their support and motivation during every moment of my research period. With heartful gratitude and love, I express my gratefulness to my father ***Mr. B M Maheshwari,*** *my mother* ***Mrs. Usha Maheshwari*** *for their continual love and encouragement over the entire course of my life. I am thankful to my father-in-law* ***Mr. Pawan Kumar Maheshwari*** *and my mother-in-law* ***Mrs. Veena Maheshwari*** *for their encouragement, support, care, love and having faith in me throughout my existence. I desire to reveal my admiration towards my husband* ***Mr. Bharat Maheshwari****, my son* ***Ravit Maheshwari****, they have been source of motivation, encouragement and source of energy throughout this research work and stood by me as strong pillars always. I am always thankful to all my family members and friends.*

I thank one and all for helping me accomplish the successful realization of the thesis.

Thank you all!!!

Kartika Maheshwari

LIST OF PUBLICATIONS

1. **Kartika Maheshwari,** A.S. Rao "Photoluminescence downshifting studies of thermally stable Dy^{3+} ions doped phosphate glasses for photonic device applications"

   Optical Materials 129 (2022) 112518. **(IF: 3.9)**

2. **Kartika Maheshwari**, A.S. Rao "Down-shifting Photoluminescent properties of Tb^{3+} doped Phosphate Glasses for intense Green-emitting device applications"

   Optical Materials 137 (2023) 113533 **(IF: 3.9)**

3. **Kartika Maheshwari**, Ravita, Aman Prasad, Yasha Tayal, AS Rao "Spectroscopic studies of Pr^{3+} doped red-emitting $BaO–ZnO–Li_2O–P_2O_5$ glasses for luminescent devices applications"

   Optical Materials 140 (2023) 113910] (**IF: 3.9**)

ABSTRACT

Photoluminescence Studies of Certain RE ions Doped Phosphate Glasses for Photonic Applications

Recent innovations based on solid-state lighting (SSL) have contributed significantly and practically to the lighting sectors. Small size, durable, and environmentally friendly, SSL devices consumed very little energy. When compared to other convectional light sources such as incandescent lamps, electric bulbs, and fluorescent tubes, The SSL based w-LEDs are more superior because they have a longer lifespan, use less energy, have great color rendering, small size, and environmental friendly nature. The advancement of superior white light-emitting diodes (w-LEDs) as lighting sources has become crucial for lowering global energy consumption in artificial lighting. Currently, the blue LED and YAG: Ce^{3+} phosphor serve as the foundation of the produced commercial w-LED. The w-LEDs that are now in use have various drawbacks, including a low color rendering index, an incorrect color temperature, and a halo effect. Phosphors can be replaced with RE activated glass to overcome the limitations. Glass also possesses a number of unique qualities, including a simple, efficient production method, strong chemical and thermal stability, as well as a high level of RE solubility. In light of this, various photonic devices, including w-LEDs, may benefit from effective RE activated glass.

The RE-activated glasses are directly useful for a variety of applications, including solid-state lasers, optical fibre, sensors, light converters, and other innovative optoelectronic devices. The efficacy of the glass matrix host for all of these photonic device applications is investigated through spectroscopic analyses of characteristics including absorption, excitation, emission, and temperature-dependent photoluminescence (PL) characteristics recorded for the RE ions

doped glasses. By selecting the right host glass composition or altering the RE ion concentration in a glass, one may change certain spectral properties. Based on special applications like solid-state lasers, RE doped glasses exhibit distinctive optical characteristics in a variety of host glasses like phosphate, borate, silicate, telluride, and chalcogenides. A good former along with intermediates and network modifier can help in improving the lasing characteristics of glass hosts. Choosing a host glass with different RE ions for the optimal optical and lasing capabilities is still a challenging task. A dependable material for the construction of lighting devices is host glass with relatively low phonon energy, which increases the stimulated emission cross-section and quantum efficiency.

There are several glass formers, including fluorides, phosphates, borates, tellurites, silicates, and borosilicate, that have been created and used to study different spectroscopic characteristics. Due to its unique characteristics, including clear visibility in a broad spectrum, softening, a lower melting point, good thermal stability, high RE solubility, and low dispersion, phosphate is one of the most ideal glass formers. Although phosphate glasses have several uses in photonic devices, their hygroscopic nature and weak chemical stability pose certain restrictions. The main focus of the current work is to investigate the benefits of heavy metal oxide glasses that are well suited for photonic devices such as lasers, fiber amplifiers, and light-emitting diodes. We looked into these RE-ionized glasses because of the importance of heavy metal oxides in research and technology. In accordance to the aforementioned discussion, the combination of BaO, ZnO, Li_2O, and P_2O_5 glasses can fulfil the requirement. constituent parts after assessing all the scientific patronages supplied by for the present inquiry. To improve the composition and concentration of RE ions for greater luminescence efficiency, we considered creating a suitable optical system, namely Barium Zinc Lithium Phosphate (BZLP) glasses.

Several chapters make up this thesis' structure in order to meet all of the objectives of the research. Each chapter is structured such that it may be read alone.

Chapter 1 begins with a clarified introduction, the cause of the issue, the inspiration behind the study, and a summary of recent literature. This chapter describes why 15 BaO-15ZnO-10Li_2O-60P_2O_5 glasses are preferred for photonic devices like lasers and w-LEDs over a variety of other glasses. The characteristics of the various chemical components found in the host glass have been explored in length in this approach. Further research was done on the utility of RE ions when they are doped with glasses for usage in photonic devices. Several radiative metrics, including transition probabilities, branching ratios, radiative durations, stimulated emission cross-sections, and quantum efficiencies of the major excited levels, have been compiled using Judd-Ofelt (J-O) theory. The Inokuti-Hirayama (I-H) model, which is used to investigate the mechanisms of luminescence decay and energy transfer, has been explained. It has also been detailed how to use the luminescence spectra to calculate the CIE chromaticity color coordinates (x, y) to assess the white light tunability. Temperature dependent PL emission investigation signifies the utility of thermal stability of the prepared glasses in W-LEDs applications.

Chapter 2 focuses on the experimental procedure utilized to prepare RE doped glasses as well as the procedures for analyzing the luminescence characteristics of the as prepared glasses. The melt quench method, which is used to synthesize the as-prepared glasses, is also thoroughly discussed. In order to study different properties, including thermal, structural, PL, and colorimetric properties, this chapter describes the use of numerous advanced experimental techniques, including differential scanning calorimetry (DSC), thermo gravimetric analysis (TGA), X-ray diffraction (XRD), Fourier-transform infrared spectroscopy (FT-IR), UV-VIS spectrophotometer, and spectrofluorophotometer.

Chapter 3 develops trivalent dysprosium (Dy^{3+}) activated BZLP glasses for the possible applicability of prepared glasses in photonic device applications, numerous structural, optical, and radiative characteristics have been explored in detail. The non-crystalline character of BZLP glass has been confirmed with the help of an XRD pattern. The titled glasses doped with Dy^{3+} ions show several absorption peaks in 330-2000 nm range with an indirect optical band gap of 3.41-3.76 eV. The J-O theory was employed on the absorption profiles and estimated various radiative parameters for the Dy^{3+} ions activated BZLP glasses. The Dy^{3+} ions activated glasses exhibit intense excitation at 350 nm and three sharp visible emissions at blue ($^4F_{9/2}\rightarrow{}^6H_{15/2}$), yellow ($^4F_{9/2}\rightarrow{}^6H_{13/2}$), and red ($^4F_{9/2}\rightarrow{}^6H_{11/2}$). To ascertain the lasing potentialities of BZLP glasses, the stimulated emission cross-section and branching ratios have been assessed by correlating the emission spectral information with the radiative parameters calculated from the absorption spectral features. The colorimetric properties show the coordinates situated in a bright white region. Temperature-dependent photoluminescence (TD-PL) spectral features recorded revealed the thermal stability of as-prepared glasses. The explored distinctive features for Dy^{3+} ions activated BZLP glasses suggested the superiority and direct utility of the as-prepared glasses in advanced photonic device applications such as lasers and w-LEDs. The content of this chapter has been published in an international journal **Optical Materials** 129 (2022) 112518] **(IF: 3.754)**

Chapter 4 deals with Tb^{3+} doped BZLP glasses and investigated thoroughly using spectroscopic techniques such as XRD, UV-VIS absorption and PL to explore their utility in visible photonic device applications. The information pertaining glass transition temperature, melting temperature and thermal stability were understood by using recording the DSC spectrum for an un-doped BZLP glass. The total weight loss during the glass composition melting process was analyzed using thermo gravimetric curves. The UV spectral information recorded for the titled

glasses reveal the optical band gap falling in the range from 4.57 to 4.19 eV. The prepared Tb^{3+} doped BZLP glasses exhibit intense green emission along with relatively less intense blue, yellow and red peaks under 373 nm excitation. In the resultant PL spectra, the emission intensity increases with the activator concentration of Tb^{3+} ions from 0.5 to 5.0 mol%. The estimated CIE chromaticity coordinates falling in the green region reveals the aptness of the titled glasses as a green constituent in visible photonic devices. The PL decay curves show the bi-exponential behaviour with an average decay time of 2-3 ms. The temperature-dependent PL profile shows fewer changes in spectra and has a relatively high activation energy value, confirming the high thermal stability. Various results obtained for Tb^{3+} doped BZLP glasses finally reveal their usage as a green emitter needed to fabricate w-LEDs and other green emitting photonic device applications.

The results of this chapter has already appeared in an International Journal ***Optical Materials*** *137 (2023) 113533*] **(IF: 3.754)**

Chapter 5 describes the structural, physical and spectral analysis Pr^{3+} doped BZLP glass samples synthesized through melt quenching route were studied. The x-ray diffraction (XRD) confirms the amorphous non-crystalline nature of an un-doped and doped BZLP glass. Absorption spectra show several bands in ultraviolet, visible and infrared regions. The absorption data was used in J-O theory to evaluate various radiative parameters. Three peaks are visible in the PL emission spectra with the strongest peak positioned at 604 nm for which stimulated emission cross section and quantum efficiency has been assessed. The CIE color coordinates of the samples lie in the red region. The decay time values for 604 nm emission decreased with increased Pr^{3+} concentration. The luminescence intensity decreased to 88.12% and 82.61% of maximum value at 423 K and 473 K respectively showing high thermal stability.

These BZLP glasses can work as an effective deep red-emitting component for w-LEDs and other photonic applications. The content of this chapter *has been published in* ***Optical Materials*** *140 (2023) 113910* **(IF: 3.754)**

Chapter 6 provides a summary of the general research effort given in this dissertation as well as the specific conclusions reached from the findings. This chapter also explores how the current work might be expanded and utilized upon going forward to guide new lines of investigation.

LIST OF FIGURES

Figure No.	Caption	Page No.
1.1	Schematic representation of glass formers and glass network modifiers.	6
1.2	V-T diagram showing glass formation.	8
1.3	Mechanism of Luminescence involving activator and sensitizer	14
1.4	Schematic representation of (a) excitation and emission, (b) excitation, energy transfer and emission in the host lattice.	21
1.5	An illustration of the ET processes using a schematic diagram	22
1.6	Excitation and de-excitation Process of RE ions.	27
1.7	Many tetrahedral structures of phosphate glass.	29
2.1	Preparation of glass samples by using melt quenching process	34
2.2	DSC/TGA simultaneous instrument (SETARAM, Labsys Evo)	40
2.3	(a) Brags law for diffraction (b) X-ray diffractometer instrument (Bruker D8 Advance).	42
2.4	Perkin Elmer's Frontier FT-IR spectrometer	43
2.5	Jasco V-770 UV/VIS/NIR spectrophotometer	44
2.6	(a) Jasco 8300FP spectrofluorophotometer (b) Edinburg, FLS 980 spectrofluorophotometer.	46
2.7	Schematic representation of Temperature-dependent spectrofluorophotometer.	48
3.1	XRD pattern of an un-doped BZLP glass.	53
3.2	(a) Density and molar volume variation with Dy^{3+} ions concentration in BZLP glasses.	54

3.2	(b) Variation of inter atomic distance and Field strength with Dy3+ ions concentration in BZLP glasses.	55
3.3	FT-IR spectrum of an un-doped BZLP glass.	58
3.4	Absorption spectra of Dy^{3+} ions doped BZLP glasses in UV-vis-NIR region.	59
3.5	(a) Indirect bandgap plot for Dy^{3+} ions doped BZLP glasses.	60
3.5	(b) Direct bandgap plot for Dy^{3+} ions doped BZLP glasses.	61
3.5	(c) Urbach energy plot for Dy^{3+} ions doped BZLP glasses.	62
3.6	Excitation spectrum of 1.0 mol% of Dy3+ ions in BZLP glasses under 575 nm emission wavelength	67
3.7	Emission spectra of Dy^{3+} ions in BZLP glasses monitored at 350 nm excitation wavelength. The inset plot shows the relative intensity variation of a most intense peak with different Dy-doped BZLP glasses.	68
3.8	Partial energy level diagram showing absorption, excitation, emission and cross-relaxation mechanism for Dy^{3+} ions in BZLP glasses.	70
3.9	CIE chromaticity coordinates of 1.5 mol% Dy^{3+}ions in BZLP glass.	73
3.10	Decay profile of Dy^{3+} ions in BZLP glasses for $^4F_{9/2} \rightarrow {}^6H_{13/2}$ (575 nm) transition under 350 nm excitation wavelength.	75
3.11	Temperature-dependent PL spectra for 1.5 mol% Dy^{3+} ions in BZLP glass.	77
3.12	Graph between $\ln[(I_o/I_T)-1]$ and $(1/K_BT)$ for 1.5 mol% Dy^{3+} ions in BZLP glass	78
4.1	Schematic diagram of a melt-quenching technique	84
4.2	DSC curve for un-doped BZLP glass.	86

4.3	TGA curve for un-doped BZLP glass.	86
4.4	XRD pattern of 5.0 mol% Tb^{3+} doped BZLP glass (PZBaLTb5.0).	89
4.5	Absorption spectra of Tb^{3+} doped BZLP glass with variable concentration of Tb^{3+} ions.	90
4.6	Indirect optical bandgap Tauc plot of Tb^{3+} doped BZLP glasses.	91
4.7	The excitation spectrum of the $PZBaLTb_{1.0}$ glass with monitoring the emission wavelength at 545 nm.	93
4.8	PL spectra of Tb^{3+} doped BZLP glasses with the doping concertation varying from 0.5 to 5.0 mol% at 373 nm excitation wavelength. The inset plot shows the variation of the emission intensity with Tb^{3+} ions concentration.	94
4.9	Partial energy level diagram of Tb^{3+} doped BZLP glass.	95
4.10	CIE chromaticity coordinates of $PZBaLTb_{5.0}$ glass.	96
4.11	Decay curves of Tb^{3+} doped BZLP glasses at 373 nm excitation and emission at 545 nm.	98
4.12	TDPL spectra of $PZBaLTb_{5.0}$ glass with the upsurge in temperature from 300 to 473 K at the excitation wavelength of 373 nm. The inset plot shows the decrease in relative emission intensity with the surge in temperature from 300 to 473 K.	99
4.13	Variation of $\ln[(I_o/I_T)-1]$ with $(1/K_BT)$ for $PZBaLTb_{5.0}$ glass.	100
5.1	XRD patterns recorded for BZLP and BZLP:0.1Pr glasses.	108
5.2	Absorption spectra of doped BZLP glasses with varying concentrations of Pr^{3+} from 0.01 to 2.5 mol%.	109
5.3	Indirect bandgap plot of Pr^{3+} doped BZLP glasses with varying concentration from 0.01 to 2.50 mol%.	114
5.4	The excitation spectrum recorded for BZLP:0.01Pr glass under 604 emission wavelength.	115

5.5	Emission spectra of Pr^{3+} doped BZLP glasses with varying the doping concentration from 0.01 to 2.50 mol%. Inset plot shows the variation of the emission intensity related to $^1D_2 \rightarrow {}^3H_4$ transition with Pr^{3+} ions concentration.	116
5.6	Energy level diagram of Pr^{3+} doped BZLP glasses.	118
5.7	Relation between log (I/c) and log (c) for different concentrations of Pr^{3+}.	119
5.8	Spectral overlap of absorbance & emission spectrum of BZLP:0.1 glass for transition $^1D_2 \rightarrow {}^3H_4$	123
5.9	CIE chromaticity coordinates of BZLP:0.10Pr glass.	125
5.10	PL decay curves of Pr^{3+} doped BZLP glasses with varying the doping concentration from 0.01 to 2.50 mol% under 445 nm excitation and emission at 604 nm.	126
5.11	TDPL spectra of optimized BZLP:0.10Pr glass with temperature varying from 27 ˚C to 200 ˚C under 445 nm excitation wavelength.	129
5.12	Graph between $\ln[(I_o/I_T)-1]$ and $(1/K_BT)$ for BZLP:0.10Pr glass. The inset plot shows the decrease in relative emission intensity with rise in temperature from 27 ˚C to 200 ˚C.	131

LIST OF TABLES

Table No.	Caption	Page No.
1.1	Electronic configurations of trivalent RE ions in ground state.	17
2.1	The list of chemicals and purity.	36
3.1	Various physical properties of Dy^{3+} ions in BZLP glasses.	56
3.2	Experimental (f_{exp}) ($x10^{-6}$), calculated (f_{cal}) ($x10^{-6}$) oscillator strengths, r.m.s deviation (δ_{rms}), nephelauxetic ratio ($\bar{\beta}$), bonding parameters (δ), and refractive index (n_d) for Dy^{3+} ions in BZLP glasses.	63
3.3	Judd-Ofelt parameters ($\Omega_\lambda \times 10^{-20} cm^2$) of Dy^{3+} ions in BZLP glasses along with various reported host glasses.	64
3.4	Transition probability (A_R) (s^{-1}), luminescence branching ratio (β_R), total transition probability (A_T) (s^{-1}) and radiative lifetime ($\boldsymbol{\tau_R}$) (μs) for the observed emission transitions of Dy^{3+} ions in BZLP glass.	65
3.5	Emission peak wavelength (λ_P)(nm), effective bandwidths ($\Delta\lambda_P$)(nm), measured and experimental branching ratios (β_R & β_{exp}), stimulated emission cross-sections (σ_{se}) (cm^2), gain bandwidth ($\sigma_{se} \times \Delta\lambda_P$) ($cm^3$) and optical gain parameter ($\sigma_{se} \times \tau_R$) ($cm^2$ s) parameters for the emission transitions for Dy^{3+} ions in BZLP glasses.	72
3.6	CIE coordinates of Dy^{3+} ions in BZLP glasses	74
3.7	Experimental lifetime (τ_{exp}) (μs), radiative lifetime (τ_R) (μs), quantum efficiency (η), Y/B ratio and non-radiative decay rates (W_{NR}) (s^{-1}), for Dy^{3+} ions in BZLP glasses.	76
4.1	Physical parameters of Tb^{3+} doped BZLP glasses.	87

4.2	CIE coordinates (*x*, *y*), CCT (K), color purity (%) and lifetime (ms) of Tb^{3+} doped BZLP glasses.	96
5.1	Physical Properties of Pr^{3+} doped BZLP glasses.	106
5.2	Experimental (f_{exp}) ($x10^{-6}$), calculated (f_{cal}) ($x10^{-6}$) oscillator strengths, r.m.s deviation (δ_{rms}), nephelauxetic ratio ($\bar{\beta}$), and bonding parameters (δ) for Pr^{3+} ions in BZLP glasses.	110
5.3	Judd-Ofelt Parameters ($\Omega_\lambda \times 10^{-20} cm^2$) of Pr^{3+} ions in BZLP glasses along with various reported hosts	112
5.4	Transition probability (A_R) (s^{-1}), luminescence branching ratio (β_R), total transition probability (A_T) (s^{-1}) and radiative lifetime ($\boldsymbol{\tau_R}$) (μs) for the observed emission transitions of Pr^{3+} ions in BZLP glass.	121
5.5	Emission peak wavelength (λ_P)(nm), effective band widths ($\Delta\lambda_P$)(nm), measured and experimental branching ratios (β_R & β_{exp}), stimulated emission cross-sections (σ_{se}) (cm^2), gain band width ($\sigma_{se} \times \Delta\lambda_P$) ($cm^3$) and optical gain parameter ($\sigma_{se} \times \tau_R$) ($cm^2$ s) parameters for the emission transitions for Pr^{3+} ions in BZLP glasses.	123
5.6	CIE co-ordinates of Pr^{3+} ions in BZLP glasses.	124
5.7	Experimental lifetime (τ_{exp}) (μs), radiative lifetime (τ_R) (μs), quantum efficiency (η), and non-radiative decay rates (W_{NR}) (s^{-1}) for Pr^{3+} ions in BZLP glasses.	127
5.8	Comparison of emission characteristics parameters like effective band widths ($\Delta\lambda_P$)(nm), measured branching ratio (β_R) and stimulated emission cross-sections (σ_{se} x 10^{-22}) (cm^2) of transition $\boldsymbol{^1D_2 \rightarrow {}^3H_4}$ in different Pr^{3+} doped glasses.	128

TABLE OF CONTENTS

Certificate……...……**i**

Acknowledgements…..……..……....**ii-iv**

List of Publications…….....**v**

Abstract…….…...…..**vi- xi**

List of Figures……...……**xii-xv**

List of Tables……....**xvi-xvii**

Chapter 1: Introduction, Motivation, Goals and Basics of The Research Work..…….....…….....**1**

1.1. Introduction and Motivation of the Work……2

1.2. Glass…..……...5

1.2.1. Glass Compositions…….....5

1.2.2. Formation of Glass ….…….....8

1.2.3. Glass Classifications …….....9

1.2.4. Glass Characteristics…….....11

1.3. Luminescence …….....13

1.3.1. Photoluminescence (PL)…….....15

1.4. RE Elements …….....16

1.4.1. Discrete $4f^n$– $4f^n$ transitions…….....18

1.4.2. $4f^{n-1} - 5d$ Transitions…….....20

1.4.3. Energy Transfer in RE ions…….....20

1.5. Judd-Ofelt (J-O) Theory ……23

1.6. Nephelauxetic Effect & Oscillator Strengths ……24

1.7. Radiative Characteristics of RE ions……25

1.8. Excited De-excitation Process of RE ions……..26

1.9. Inokuti-Hirayama (I-H) model……..28

1.10. Current Glass Composition Importance……29

1.11. Objectives of Thesis Work……30

Chapter 2: Experimental and Instrumentation Part of The Research Work……..……**32**

2.1. Glass Synthesis Procedure ……..33

2.1.1. Melt Quenching Procedure ……..……33

2.2. Calculation and Glass Preparation ……35

2.2.1. Precursor Materials ……..……35

2.2.2. Glass Preparation Procedure ……..……36

2.2.2. Physical Properties ……..……36

2.3. Characterization Techniques……..…38

2.3.1 Thermal Analysis……39

2.3.2. X-ray Diffraction ……..……38

2.3.3. Fourier Transform Infrared Spectroscopy (FT-IR) ……..42

2.3.4. UV/VIS/NIR Spectrophotometer……..……43

2.3.5. Spectrofluorophotometer Photoluminescent Studies……...…47

2.3.6. Temperature Dependent Emission Studies ……47

Chapter 3: Photoluminescence downshifting studies of thermally stable Dy^{3+} ions doped phosphate glasses for photonic device application.....49

3.1. Introduction……..50

3.2. Experimental Procedure and Characterizations……...……...52

3.3. Results & Discussion……..……..53

3.3.1. Structural Analysis…….…….....53

3.3.2. Physical properties ……..……..…...54

3.3.3. Vibrational Spectroscopy..…….…….....57

3.3.4. Absorption Spectral Analysis…..……...…..58

3.3.5. PL Excitation, PL Emission and Radiative Properties Analysis……...66

3.3.6. Colorimetric Properties…….…….....72

3.3.7. PL Decay Spectral Analysis……74

3.3.8. Temperature Dependent PL (TD-PL) Studies……76

3.4. Conclusions……...……78

Chapter 4: Down-shifting photoluminescent properties of Tb^{3+} doped phosphate glasses for intense green-emitting devices applications……81

4.1. Introduction……..81

4.2. Experimental Section……...…83

4.2.1. Synthesis……...83

4.2.2. Characterization……...84

4.3. Results and Discussion……...……..80

4.3.1. XRD and Structural Analysis…….…..……85

4.3.2. Physical Properties……..……87

4.3.3. Structural Analysis……..……88

4.3.4. Absorption Properties of Glass…….…..……89

4.3.5. PL Analysis……92

4.3.6. Colorimetric Study……95

4.3.7. Decay Profile Analysis……..…97

4.3.8. Temperature-Dependent PL Characteristics…….98

4.4. Conclusions…….100

Chapter 5: Spectroscopic Studies of Pr^{3+} Doped Red Emitting BaO-ZnO-Li_2O-P_2O_5 Glasses for Luminescent Devices Applications ……102

5.1. Introduction……....103

5.2. Experimental work and characterizations …….105

5.2.1. Preparation of glass……105

5.2.2. Preparation of glass……105

5.3. Results and Discussion……..103

5.3.1. Physical properties of Pr3+ doped BZLP glass samples…….....106

5.3.2. Glass Structural Analysis ……107

5.3.3. Absorption Properties of Glass..……..108

5.3.4. PL Characteristics of Glass……..114

5.3.5. Colorimetric Study…..…….123

5.3.6. PL Decay Analysis…….....125

5.3.7. Temperature-dependent PL (TD-PL) characteristics……127

5.4. Conclusions……..129

Chapter 6: Summary and Future Work……...131

6.1. Summary ……..……..132

6.2. Future Scope of the Work……...134

Refferences……..135

CHAPTER 1

Introduction, Motivation, Goals and Basics of the Research Work

The chapter begins with a clarified introduction, the cause of the issue, the inspiration behind the study, and a summary of recent literature. This chapter describes why BaO-15ZnO-10Li_2O-60P_2O_5 glasses are preferred for photonic devices applications like lasers and w-LEDs over a variety of other glasses. The characteristics of the various chemical components found in the host glass have been explored in length in this approach. Further research was done on the utility of RE ions when doped in to glasses for usage in photonic devices. The basics of the various models included, which is used to investigate the mechanisms of luminescence decay and energy transfer, has been explained. Temperature dependent emission investigation signifies the thermal stability of the prepared glasses for w-LEDs applications.

1.1. Introduction and motivation of the work

Spectroscopy is the study and measurement of the interaction of matter and electromagnetic radiation. It includes examining how light interacts with matter to reveal details on the structure, arrangement, and characteristics of substances. Numerous disciplines such as physics, applied sciences, chemistry, biology, astronomy and materials science will employ spectroscopy extensively to characterize the materials having applications in diversified fields. The fundamental idea behind spectroscopy is that various materials interact with light in distinctive ways, resulting in the absorption, emission, or scattering of particular light wavelengths. Scientists can identify and analyze a sample's constituent parts, ascertain its molecular structure, and learn more about its physical and chemical characteristics by investigating these interactions [1–3]. Optical spectroscopy, nuclear magnetic resonance (NMR), mass spectrometry, electron paramagnetic resonance (EPR) spectroscopy are numerous additional specialized types of spectroscopic techniques that are utilized for numerous scientific investigations. Science relies heavily on spectroscopy to examine a wide range of topics and events as well as comprehend the basic characteristics of matter [4–6].

Researchers in the fields of science and technology have become more interested in optical spectroscopy examinations of crystalline and non-crystalline materials during the past several decades. This could be because there are so many uses for luminous materials, which go well beyond just physics, biology, and chemistry. Examples include astrology, agriculture, defense, optical communication, geology, forensics, medicine, and a host of other professions [7,8]. The latest research and prospective scenarios demonstrate the continued scientific and technical interest in optical materials. A substance that transforms specific types of energy into visible light as well as the ultraviolet (UV) or infrared (IR) spectral spectrum is known as a luminescent material. Numerous optoelectronic applications, including contemporary displays, cutting-edge indoor-outdoor lighting, optical fiber amplifiers, scintillators, lasers, and sensors, have made extensive use of these luminous materials [9,10].

Crystalline and amorphous solid inorganic luminous materials fall into several types. Glass and other amorphous materials have a number of relevant and beneficial advantages over certain crystalline luminous materials [11,12]. Due to their photo-conducting qualities and excellent emission efficiencies, photonic glasses doped with different RE (RE) or transition metal ions have received a lot of interest in recent years. Major uses include emissive displays, fluorescent lighting, LEDs, and devices that detect X-rays or -rays, which are used in diversified field such physical, chemical, Technological, medical imaging, and other areas. For use in diode-based solid-state lighting devices, and visible colour display applications, luminescent materials are continuously aspired. In the past, this has taken a lot of experimental work. The use of data-driven methods in materials science has lately offered a different way to speed up the research and creation of luminous materials [13].

Phosphor converted white light emitting diodes (pc-wLEDs), which are transforming into a dynamic solid state light source, will be used in the next generation of lighting and display systems. The advantages of pc-wLEDs over incandescent and fluorescent lighting, include greater efficiency, lower energy consumption, a long operational lifetime (up to 100,000 h), ruggedness, and environmentally friendly features [14,15]. The white light can be attained in a variety of ways. The current commercial solution uses an InGaN chip that emits blue light along with a yellow-emitting (YAG: Ce^{3+}) phosphor. Due to the absence of red colors, this technique has drawbacks like halo effect, poor color rendering index (CRI) index, and high correlated color temperature (CCT). Another strategy, depends on an ultraviolet/near-ultraviolet (UV/n-UV) chip with a combination of RGB phosphors (red, green, and blue), has been extensively researched. Better CRI and CCT are provided by this method, but the device's cost and synthesis processing time are increased [16,17]. The different emitting centers or phosphors used in this technology also cause phase separation, re-absorption of blue light by green and red phosphors, poor RGB color mixing, and limited color stability. The fabrication of a single-phase white light illuminating phosphor is essential and has sparked a lot of interest in the field of solid-state lighting industry in order to solve the aforementioned issues. Additionally, in each of these methods, phosphors are enclosed in an epoxy resin that binds the powder in the w-LED package together. This

epoxy resin adds a number of drawbacks, such as the issues with epoxy encapsulations breaking or delaminating and the epoxy yellowing, which significantly affects the color output of the w-LEDs. Epoxy has recently been produced using silicone-based ingredients with exceptional temperature resistance. They also introduce new issues including w-LED performance degradation and shape distortion as a result of heat shrinkage. This results in the production process becomes challenging, time-consuming, and expensive, which lowers the manufacturing productivity of w-LED encapsulants [18–20].

RE ion-doped glasses are an excellent alternative to pc w-LEDs because of their benefits, including simplicity of manufacturing, ease of shaping any shape, reduced production costs, greater thermal stability, and notably epoxy resin-free manufacturing method. Also, the RE-doped glasses serve as an active medium for several technologically significant sectors, including fibers, optical amplifiers, and optical detectors [21,22]. There are several uses for luminescent materials. Glasses are thought to be the best hosts because they may display intriguing characteristics including wide inhomogeneous bandwidths, adjusting the wavelength, and significant doping capabilities. RE-doped glasses are preferable to phosphors due to their unique properties as well as their straightforward manufacturing procedure, low production costs, and strong thermal stability. We require a complete understanding of the optical absorption and photoluminescence characteristics of RE-doped glasses in order to forecast novel luminescent materials for their use in the diversified sectors of science and technology. Due to their ease of molding and shaping into larger sizes, glasses are potential hosts for various activator ions. The optical performance of glasses can be affected by the glass's structure, composition, optical quality, thermo-optical and thermo-mechanical capabilities, and chemical resistance. Among glasses' outstanding benefits include the flexibility of selecting glass composition over an extensive series [23–28]. Additionally, glasses are better than crystalline materials because they are less expensive and have a higher doping capacity for RE ions [29–32]. Additionally, glasses are readily made and molded. They are useful for the creation of luminous glass materials due to the above-mentioned fascinating characteristics. It is well knowledge that when compared to other glassy systems, oxide glasses are the

most stable. It is wanted to examine the relationship between local structure and fluorescence characteristics of oxide glasses in which RE ions are introduced in order to create novel laser glasses and glassy phosphors [33,34].

1.2. Glass

Glass is regarded as an amorphous solid in the realm of solids. When there is no regularity in the organization of a material's molecular elements on a scale more than a few times the size of these groups, a material is said to be amorphous. "An amorphous solid completely lacking in long-range, periodic atomic structure and exhibiting a region of glass transformation behavior" is the most accurate definition of glass . Glass is a typical transparent, brittle solid that is created by heating a chemical combination to a high temperature until it melts, followed by a quick cooling process. With evidence of its manufacturing stretching back thousands of years, it is one of the oldest and most adaptable materials utilized by mankind. Glass possesses several desirable properties, including transparency, durability, chemical inertness, and thermal resistance. These properties make it useful in a wide range of applications, including construction, packaging, electronics, and art. It is now possible to construct active devices like sensors, switches, solar cells, etc. out of glass, which was formerly thought of primarily as an optical and passivating medium[33,35].

1.2.1. Glass compositions:

Depending on the desired qualities and applications of the glass, glass compositions might vary greatly. The glass components are the primary determinants of the properties and uses of glass. Glass or network formers, network modifiers, and intermediates are three groups of glass components with varying binding strengths. It's vital to keep in mind that composition percentages might change based on the product, manufacturer, and application. Glass compositions can be adjusted to obtain desired features like transparency, strength, heat resistance, or optical characteristics by varying the quantities of certain constituents, adding extra components, or altering the production method [28,34].

- ***Glass Formers:***

  Glass formers are substances or elements that, when cooled from a molten state without crystallizing, can produce glass. They are crucial parts of the glass composition because they give it its distinctive amorphous or non-crystalline structure as shown in Fig. 1.1. The ability of glass formers to rapidly cool and solidify without passing through a crystalline phase transition is one of their main characteristics. As a result, they can "freeze" into a disorganized atomic configuration, which leads to the creation of glass. Oxides that have a bond strength greater than 80 kcal/mol often function as glass or network formers. The glass formers SiO_2, P_2O_5, PO_4, B_2O_3, V_2O_5, GeO_2, As_2O_5, and Sb_2O_5 were some of the more significant and widely utilized ones [9,36,37].

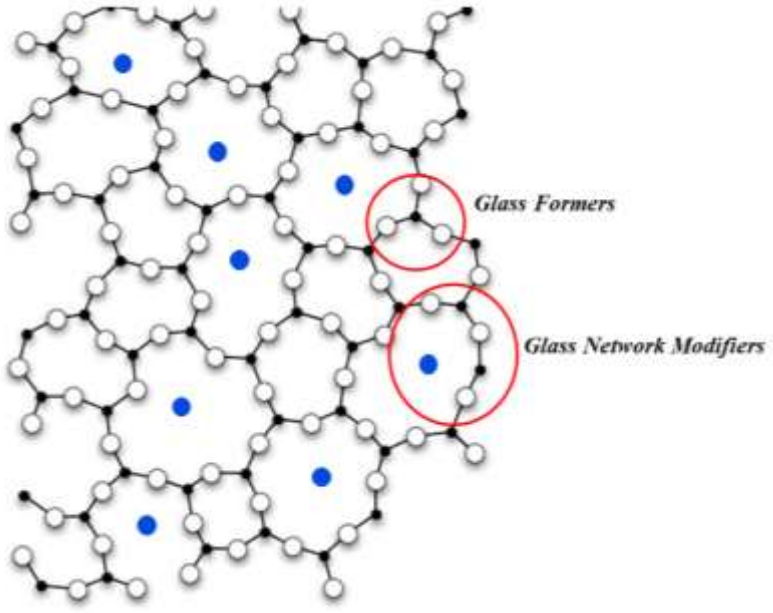

Fig. 1.1: *Schematic representation of glass formers and glass network modifiers.*

- ***Glass Network Modifiers:***

  Glass modifiers slackly connect with oxygen atoms to disrupt the regular bonding between glass-forming components and oxygen as shown in Fig. 1.1. Modifiers are oxides

with bond strengths in the 10 to 40 kcal/mol range that do not join the glass network former. The network modifiers' primary task is to change the glass's characteristics. Alkali oxides make up the majority of glass modifiers. Other oxide materials, however, can also be utilized as network modifiers. K_2O, CaO, NaO, MgO, LiO_2, BaO, SrO, and ZnO are a few significant network modifiers [38,39]. Choosing a modifier wisely, cation-oxide is a substance that has a wide range of modern uses, including sensors, bioactive materials, conducting glasses, and optoelectronic devices. The selection of a modifier is therefore of highest importance when preparing a particular type of glass for certain uses. The modifiers can therefore be added to glass formers as they still allow for the formation of glass, although in a changed structure [40,41].

- ***Glass Intermediates:***

  Glass intermediates, which are primarily metal oxides, are introduced to connect up with the core glass network and maintain structural continuity. The location of the intermediates is halfway among the glass modifiers and formers. The intermediates Al_2O_3, Be, TiO_2, ZnO, CdO, and PbO are a few of the most significant ones [42,43]. The phrases glass formers, modifiers, and intermediates are widely used to refer to the individual oxides' functions in multi-component glasses. Depending on the glass's composition, intermediate oxides may occasionally participate in the glass's network as well as serve as network modifiers.

1.2.2. Formation of Glass:

Materials with covalent, ionic, molecular, metallic, and hydrogen bonds all exhibit glass formation. Elements, simple chemical compounds, complex organic molecules, salt solutions, and alloys have all been used to make glasses. There is no particular arrangement of glass forming materials that is favourable. Practically all materials may be manufactured as amorphous solids by rapid cooling, which

avoids the crystallisation process and allows for the creation of glass [44]. Each substance cools at a different rate, which results in a different glass. When a substance is quickly chilled from a super cooled liquid, glass is created. The material is cooled to below what is known as the glass-transition temperature in order to create an amorphous solid. After then, the material starts to turn into glass as the atoms start to move more slowly in a molecular fashion. It is more organised than a liquid, but the freshly generated non-crystalline structure is not as organised as a crystal.

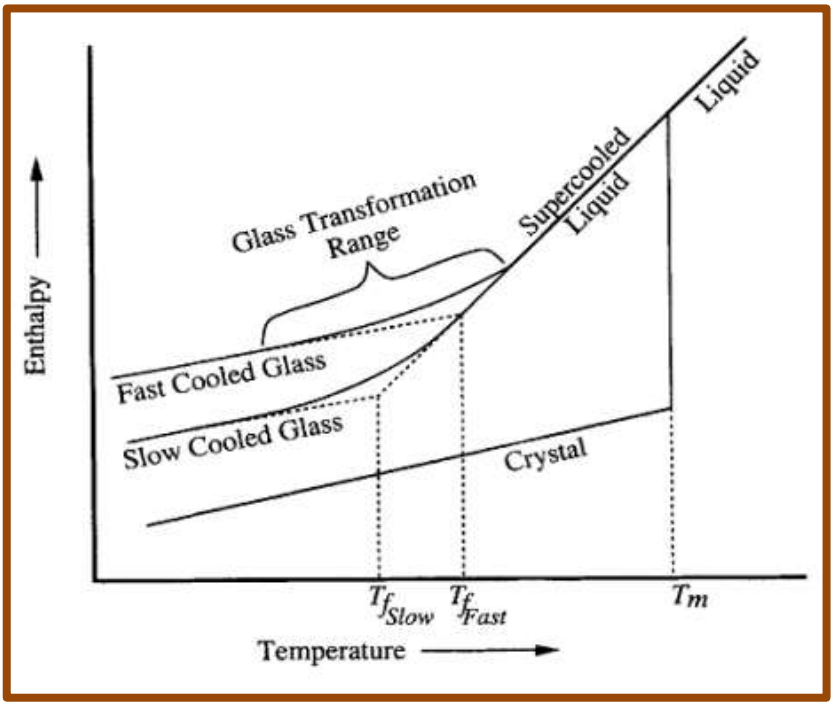

Fig.1.2. *V-T diagram showing glass formation*

The behavior of amorphous materials when they have transition from the super cooled state to glass must be plotted on a V-T diagram as depicted in Fig.1.2 to understand the glass transition process. The temperature is represented by the x-axis in the V-T diagram, while the volume and enthalpy of the material are represented by the y-axis. Melting point and glass transition temperatures are denoted by the letters Tm and Tg, respectively. When a super-cooled liquid freezes into an amorphous solid at or near the glass transition temperature, there is no abrupt discontinuity in volume. This is when the glass

transition occurs. The crystalline material state's Tg is shown to have a smaller value than its Tm. One of two things may happen as a liquid cool [44].

- Converted to super cooled below T_m
- Crystallization at T_m

As the temperature falls even further, the liquid becomes more viscous and crystallizes into glass. The main principles of glass transition are as follows:

- To prevent crystal development and nucleation, the cooling rate is increased for the creation of glass.
- Viscosity rises as temperature falls
- The V-T graphic shows that glasses have more free energy.
- The condition of the glass is metastable.

1.2.3. Glass Classifications:

Glass may be broadly divided into two categories: natural glass and manufactured glass. Natural glass is created by natural processes, as opposed to manufactured glass, which is created by melting a variety of basic ingredients. Obsidian and pumice creation has to be the most well-known of these processes. Lava from volcanic eruptions is the source of these organic varieties of glasses. Such natural glass was utilized by humans for a variety of reasons even a few millennia ago [45].

(i) Natural glasses:

Natural shockwaves like tektites that produce a rapid rise in temperature result in the formation of natural glasses. The alternative method for the creation of natural glasses involves biological activity and molten lava that has crossed the earth's crust and quickly cooled [46]. For instance, pechsteins, obsidian, and pumice.

(ii) Artificial glasses:

Artificial glasses, also known as engineered or synthetic glasses, are a category of glasses that are deliberately designed and manufactured with specific properties for various applications. Unlike naturally occurring glasses, such as obsidian or tektites, which form through natural processes like volcanic activity or meteorite impacts, artificial glasses are created in controlled laboratory or industrial settings. Many materials may be utilized to create artificial glasses, but only a select handful of them are useful in practice and can be employed as network formers.

- *Chalcogenide glasses:*

  Semiconductor glasses are another name for chalcogenide glasses. These glasses are made from a mixture of elements from the VI group (S, Te, Se), the V group (As, Sb, Bi), and the IV group (Ge, Si, Pb). They can be used as infrared deflectors, modulators, electrical switches, and infrared optical transmission [47,48].

- *Halide glasses:*

  The most suitable materials for thermonuclear fusions and high power lasers are the halide glasses. PbF_2, BeF_4, AlF_3, and GaF_3 are network formers and serve as a weak model of SiO_2 among the halide compounds. $ZnCl_2$ falls within the halide group as well. It does not, however, create glasses as quickly as BeF_2 [48].

- *Metallic glasses:*

  Metallic glasses have become quite important in recent years. Metal-metal alloy and metal-metalloid glasses have been divided into two categories for classification. Metallic glasses are distinguished by features including low magnetic loss, no magnetization, excellent hardness and strength, and strong resistance to chemical corrosion. Recording cartridges and high-frequency power transformers have both utilized the metallic glasses [49].

- *Oxide glasses:*

  These glasses are designed to have high transparency and excellent optical properties, making them suitable for lenses, prisms, optical fibers, and other components used in optics and photonics. Due to their greater bandgap, or more than 5eV, these glasses are extremely significant since they are color less and exceedingly transparent. Tellurite (TeO_2), germinate (GeO_2), phosphate (P_2O_5), silicate (SiO_2) and borate (B_2O_3) glasses are common examples of this glass, which functions as a glass former [49].

1.2.4. Glass characteristics:

Glass exhibits several characteristic properties that make it a unique and versatile material. Here are some key characteristics of glass [50]:

- *Transparency:* Owing to its extreme transparency, glass permits light to flow through it with little diffraction or absorption. Glass is useful for applications where visibility or light transmission are sought, such as windows, lenses, and optical equipment, because to its feature.
- *Hardness:* Glass is a material that is moderately durable and offers resistance to abrasion and scratching. It is not, however, as durable as substances like diamond or certain ceramics.
- *Brittle:* Due to its lack of ductility, glass is brittle and will shatter or fracture under stress as opposed to deforming. If treated to a severe impact or abrupt temperature fluctuations, it may be prone to breaking.
- *Amorphous structure:* Glass has a non-crystalline, amorphous structure as opposed to crystalline materials. This shape develops when molten glass cools quickly, delaying the creation of a normal crystal lattice. Glass has distinctive qualities due to its

amorphous structure, including transparency, isotropy (lack of preferred direction), and lack of grain boundaries.

- *Thermal stability:* Glass is capable of withstanding high temperatures without significantly deforming or melting because it has exceptional thermal stability. Thermal stress, on the other hand, can be brought on by abrupt temperature changes and may result in cracking or breaking.
- *Electrical insulation & conductivity:* Glass is a superb electrical insulator, making it appropriate for situations where electrical conductivity must be restricted or electrical insulation is necessary. The electrical conductivity of a material might change depending on its composition since electrical conductivity and resistance of materials are related to one another. In addition, the size of the ions in the network and the strength of their connections can have an impact on the electrical properties.
- *Chemical inertness:* Glass is appropriate for handling and storing corrosive substances since it is chemically inert and resistant to the majority of chemicals. However, some substances, especially powerful acids and alkalis, can interact with various forms of glass and etch or destroy them.
- *Recyclability:* Glass can be broken down and remade several times without significantly losing its qualities since it is extremely recyclable. Recycling glass contributes to resource conservation and trash reduction.
- *Optical properties:* Glass may be produced with a variety of optical qualities, including transmission, dispersion, and refractive index. Glass may be used in optical applications such lenses, prisms, and fibre optics. The highly transparent qualities of glasses have improved living conditions and has been employed as optical fibers for quick and improved communication as well as vision lenses, glass windows, and light bulbs. The

refractive index, transmission, and dispersion characteristics of glasses are primarily what determines their suitability for optical fiber communication. The composition of the glass can alter the refractive index and other optical characteristics. The pace of cooling has an impact on the refractive index of the glass as produced. Glasses with a high refractive index should be chilled more quickly. In the current work, the main focus is oriented towards the luminescence characteristics of the glasses doped with RE ions and their photonic applications [50].

1.3. Luminescence:

Luminescence is the emission of light from a material or substance as a result of various processes such as chemical reactions, electrical energy, or exposure to radiation. It is the phenomenon where energy is absorbed by a material and subsequently released as light. Luminescence is a general word used to describe cold body radiation scenarios that include energy absorption and subsequent light emission. Luminescent materials are those that have the ability to transform absorbed (invisible) energy like ultraviolet, x-rays, β, α and so forth into visible light [51]. Phosphor is a crystalline substance that falls under the category of luminous materials, while luminescent glass is often made of amorphous materials.

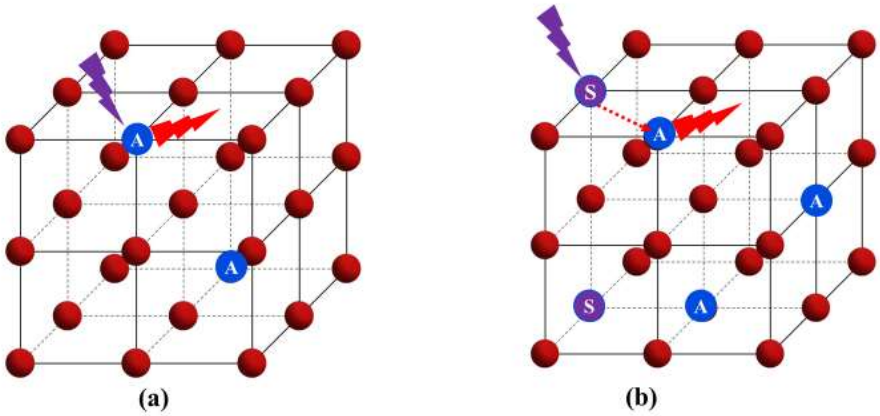

Fig.1.3. *Mechanism of luminescence involving activator and sensitizer*

Activators are certain substances that can emit immediately after being excited by suitable sources. When activator ions exhibit insufficient energy absorption, a different class of impurities called sensitizers may be added. The energy is transmitted to the activators by sensitizers after they have absorbed it. Energy is transported by the luminous materials during this process. The activator and sensitizer roles in the luminescence process are shown in Fig. 1.3. The basic building block of luminescent materials is an inert imperfect host lattice to which dopant ions and/or other deliberate imperfections have been introduced. Depending on their electrical configuration, solubility, and host lattice structure, the dopants perform diverse functions in various host lattices [35].

Activator: An activator (A) or luminous center is a dopant ion electron that jumps to the excited state after absorbing excitation energy and emits the energy as radiation when it returns to the ground state.

Sensitizer: When there are two dopants in a crystal lattice, one of them is referred to as an activator (A) and the other as a sensitizer (S) as displayed in Fig. 1.3 (b). The majority of the energy is absorbed by the "S" before being transferred to the "A" for emission [52].

There are several types of luminescence on the basis of source of excitation as discussed below, including photoluminescence:

Electroluminescence: When an electric current flows through a substance, it emits light, a process known as electroluminescence. Organic light-emitting diodes (OLEDs), light-emitting diodes (LEDs), and electroluminescent displays are just a few examples of the devices that make advantage of this phenomena.

Bioluminescence: A type of luminescence that occurs naturally in living things is called bioluminescence. It happens when certain species, such bacteria, deep-sea critters, and fireflies, emit light as a result of chemical processes taking place inside their bodies [51].

Chemiluminescence: Without the need for an external light source, chemiluminescence is the process by which light is emitted as a result of a chemical reaction, often an oxidation. Glow sticks and the light

produced by some chemical processes, such as the interaction between luminol and hydrogen peroxide, are typical examples[52].

Numerous industries use luminescence, including lighting, displays, forensics, environmental monitoring, medical diagnostics, and materials research. Scientific research imaging methods, fluorescence microscopy, and LED lighting have all benefited from the capacity to manipulate and utilize luminescence.

1.3.1. Photoluminescence (PL):

Photoluminescence is the term used to describe the phenomenon when light is released from molecules or atoms once they absorb photons. Electrons in the material migrate into allowable excited states as a result of photo-excitation. A phonon (a non-radiative process) or visible light (a radiative process) is produced when these electrons reach their lower energy or ground states, releasing the surplus energy. The energy of the light that is emitted (photoluminescence) is determined by the energy levels at which the two-electron states that are engaged in the process of transition across the higher energy excited state and the equilibrium (lower energy) state are at different energy levels . PL can be categorized into two ways based on emission or decay time [35].

Fluorescence: In fluorescence, a substance swiftly reemits energy as visible light after rapidly absorbing energy from an external source, such as ultraviolet (UV) radiation. Once the excitation source has been removed, the emission stops quickly. When emission happens within 10^{-8} seconds of the excitation source being removed, fluorescence occurs in PL. As electrons transition from an excited state to a different ground state energy level, a rapid emission of visible photons occurs [53].

Phosphorescence: The main distinction between phosphorescence and fluorescence is the time lag between the emission of light from the phosphor even after the source of excitation is stopped. When the excitation source is taken away, the material continues to emit energy after it has been absorbed as light over a longer time. Glow-in-the-dark stickers and other phosphorescent materials continue to

generate light after being exposed to a light source for a while. While the excited electron gradually returns to the ground state, the materials that exhibit phosphorescence light for several minutes to hours [53] Thus delayed fluorescence process is otherwise called as phosphorescence.

1.4. RE elements:

Rare-earth ions are chemical elements that belong to the rare-earth elements family and have distinct optical and electrical characteristics. They are situated in the f-block, a group of elements in the periodic table. The 15 elements ranging from lutetium (Lu) to lanthanum (La) make up the lanthanides. When these elements gain or lose electrons, rare-earth ions are produced, creating a charged species. Despite being referred to as "REs," lanthanides are not as scarce as their name would imply. However, they are normally present in low quantities in the crust of the earth and frequently co-occur with other rare-earth elements. They can be difficult and expensive to extract and refine. The existence of a deep-lying, partially filled 4f shell in the ion is responsible for the RE ions' distinctive features (from Ce^{3+} to Yb^{3+}). La and Lu elements, on the other hand, lack *4f* electrons and cannot, therefore, cause optical excitation and emission processes in the visible range or close by. It is also well known that lanthanides' ionic radius reduces as their atomic number rises. The phenomenon known as lanthanide contraction, which has a negligible impact on luminescence output, results from the poor mutual shielding effect of 4f electrons. The RE ions can be utilized as either a sensitizer (S), activator (A), or co-activator depending on the ionic radii, oxidation state, and solubility in various host lattices [22,52]. A total of 7 (= 2l + 1) orbitals, each of which can hold two electrons, are created when the azimuthal quantum number (l) of 4f orbitals is increased to 3. The distribution of electrons in the ground state is such that the total spin angular momentum (S) is as high as possible. In order to obtain the total angular momentum (J), the spin angular momentum (S) is further coupled with the orbital angular momentum (L) [13,53];

$$J = L + S, \text{ if } 4f \text{ electrons} > 7$$

$$J = L - S, \text{ if } 4f \text{ electrons} < 7$$

$^{2S+1}L_J$ notation is used to indicate an electronic state. where L signifies *S, P, D, F, G, H, I, K, L, M*, …, supportive to L = 0, 1, 2, 3, 4, 5, 6, 7, 8, 9, …. Respectively.

Table 1.1: Electronic configurations of trivalent RE ions in ground state.

Atomic number	**RE^{3+} ions**	***4f* electrons**							**S Σs**	**L Σl**	**J Σ(L+S)**
57	**La^{3+}**								**0**	**0**	**0**
58	**Ce^{3+}**	↑							**1/2**	**3**	**5/2**
59	**Pr^{3+}**	↑	↑						**1**	**5**	**4**
60	**Nd^{3+}**	↑	↑	↑					**3/2**	**6**	**9/2**
61	**Pm^{3+}**	↑	↑	↑	↑				**2**	**6**	**4**
62	**Sm^{3+}**	↑	↑	↑	↑	↑			**5/2**	**5**	**5/2**
63	**Eu^{3+}**	↑	↑	↑	↑	↑	↑		**3**	**3**	**0**
64	**Gd^{3+}**	↑	↑	↑	↑	↑	↑	↑	**7/12**	**0**	**7/2**
65	**Tb^{3+}**	↑↓	↑	↑	↑	↑	↑	↑	**3**	**3**	**6**
66	**Dy^{3+}**	↑↓	↑↓	↑	↑	↑	↑	↑	**5/2**	**5**	**15/2**
67	**Ho^{3+}**	↑↓	↑↓	↑↓	↑	↑	↑	↑	**2**	**6**	**8**
68	**Er^{3+}**	↑↓	↑↓	↑↓	↑↓	↑	↑	↑	**3/2**	**6**	**15/2**
69	**Tm^{3+}**	↑↓	↑↓	↑↓	↑↓	↑↓	↑	↑	**1**	**5**	**6**
70	**Yb^{3+}**	↑↓	↑↓	↑↓	↑↓	↑↓	↑↓	↑	**1/2**	**3**	**7/2**
71	**Lu^{3+}**	↑↓	↑↓	↑↓	↑↓	↑↓	↑↓	↑↓	**0**	**0**	**0**

Rare-earth ions exhibit distinctive optical, magnetic, and luminescent capabilities because of their unusual electron configurations and energy levels. They are helpful in a variety of applications because of their qualities. The essential energy levels of RE ions must be understood in order to comprehend

their luminous characteristics. The energy level may be categorized into three groups: $4f^n$ configurations, $4f^{n-1}$ *-5d* configurations and energy transfer associated involved nearby ions.

1.4.1. Discrete $4f^n – 4f^n$ transitions:

Discrete $4f^n–4f^n$ transitions refer to electronic transitions that occur within the *f* orbitals of rare-earth elements or lanthanides. These elements have partially filled *f* orbitals, which can undergo transitions between different energy levels when they absorb or emit photons. Because the outer $5s^2$ and $5p^6$ electrons protect the *4f* electrons from external electric fields, the *4f* electronic energy levels of lanthanide ions are not much influenced by their surroundings. Transitions within 4f shells are absolutely prohibited since the parity does not change in accordance with Laporte's criterion. The observed prohibited transitions result from the RE ion's contact with the crystal field or with the vibrations of the lattice, which can combine states of various parities into 4f states. Alternatively, such transitions are permitted when spin-orbit interaction takes place. Because the luminescence transition is banned, the luminescence lifetime resulting from *4f -4f* transitions is typically in the millisecond range . There are three ways to comprehend how *4f-4f* transitions should be interpreted.

(i) ***Electric quadrupole transitions:*** When a charge has a quadrupole nature or a zero-dipole moment, an electric quadrupole is created. Even parity follows electric quadrupole transitions, which are considerably weaker than induced ED and MD transitions. There has not yet been any investigative proof of the quadrupole transitions in RE ions. Certain transitions, known as hypersensitive transitions, abide by the quadrupole transitions' selection laws [54].

(ii) ***Induced electric dipole transition:*** Induced electric dipole transitions take place when the activator (RE) ions and the electric field vector component of the incoming source electromagnetic radiation interact. According to the literature review, the majority of the transitions in RE ions are of the induced electric dipole type. Charges moving

linearly are the primary cause of the electric dipole (ED) transition. Due to the odd transformation that follows the ED transition and corresponds to the inversion center, the ED transition has odd parity. According to the Laporte selection rule, intra configurational electric dipole transitions are prohibited but non-centro symmetrical interactions, also known as induced electric dipole transitions, allow for the accommodation of electronic states with opposing parity [55].

(iii) ***Magnetic dipole transitions:*** An induced magnetic dipole (MD) transition takes place when the electromagnetic radiation's magnetic field vector component interacts with activator (RE) ions through a magnetic dipole. When a charge moves along a curved route, it creates a magnetic dipole. When compared to the ED transition, the MD transition is thought to have a low intensity rotating displacement of charge. The fact that spin does not reverse results in even parity for the MD transition. Therefore, the MD operator exhibits consistent transformation features under inversion and is followed by transitions with the same parity [56].

1.4.2. $4f^{n-1} - 5d$ Transitions:

It is possible to explain the formation of the $4f^{n-1}$ - $5d$ levels as the result of an interaction between the $4f^{n-1}$ core and the electron in the 5d orbital. The $4f^{n-1}\,5d$ configurations of RE ions in solids differ significantly from those of free ions due to the high crystal field influence on the *5d* electron. The 5*d* level is separated into many levels that are each around 15,000 to 20,000 cm^{-1} apart as a result of this crystal field. The spectral location of the absorption bands related to a certain *4f -5d* transition also changes significantly from one lattice to the next because of how the crystal field splitting fluctuates. Contrarily, the splitting of *5d* orbitals and *4f -5d* de-excitation are not necessarily necessary for the emission bands to form. The most researched RE ion is Eu^{3+}, which glows as a result of the $4f^{n-1}$-*5d* transition. Since the Eu^{3+} ion often emits broad-band emission as a result of the *f-d* transition, the lowest

excited state of the 4f level is situated at about 28 x 10^3 cm^{-1} and is higher than the $4f^6 5d^1$ level in most crystals. The host crystals have a significant impact on how the emission bands' wavelength location shifts from the near UV to the red area [. Crystal characteristics indicating electron-electron attraction or repulsion have an impact on the luminescence peak energy of the *4f -5d* transition. In comparison to other permitted transitions, the lifetime of the Eu^{3+} is unusually lengthy at 10^{-5}-10^{-6} s [55].

1.4.3. Energy transfer in RE ions:

In this part, a thorough discussion of the energy transfer (ET) in RE ions will be described. The majority of luminescent glasses are made of inorganic glass compositions that have been lightly activated or doped with transition metal ions or RE ions. Either the glass host lattice or the sensitizer absorbs the electromagnetic energy. Radiative emission occurs through activator ions only. As a result, the activator, which produces light ideally in the visible spectrum, has been receiving electromagnetic energy from the sensitizer, which has been sensitizing it. One activator can occasionally transfer a tiny portion of the excitation energy to another activator; however, this is very rare. The energy in the excited states and the transit of electrons in the luminous center to excited states can often be distributed in the following ways [22,57]: The activator can be directly excited to emit a photon of visible light (i), as shown in Fig. 1.4 (a), or indirectly excited to emit a photon of visible light (ii), as shown in Fig. 1.5 (b), via phonon emission or other energy transfer from the sensitizer to the activator.

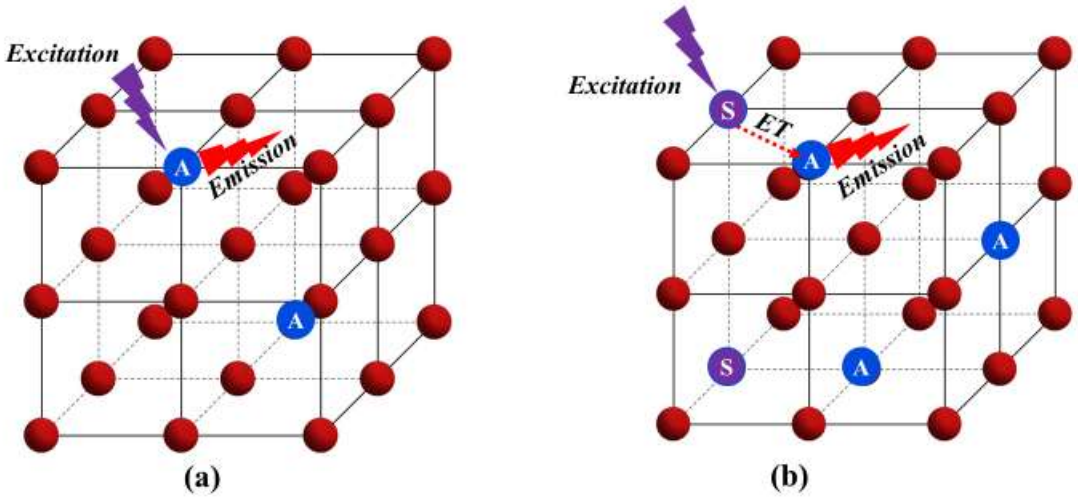

Fig.1.4. *Schematic representation of (a) excitation and emission, (b) excitation, energy transfer and emission in the host lattice.*

The main emission type found in down-conversion luminous materials was Stokes emission. The energy of the photons released during the Stoke emission is lower than the energy of the incident photons. The Stokes shift is the void between the absorption and emission energy bands. Lattice relaxation results in energy loss because the chemical bond's strength changes. Following the adsorption of electromagnetic radiation, ET activities between ions include four fundamental stages [13,58]:

- Sensitizer emission and activator re-absorption by resonance radiative energy transfer
- Sensitizer and activator resonance-related non-radiative transfer.
- Cross-relaxation (CR) between two identical ions.
- Multi-photon assisted energy transfer.

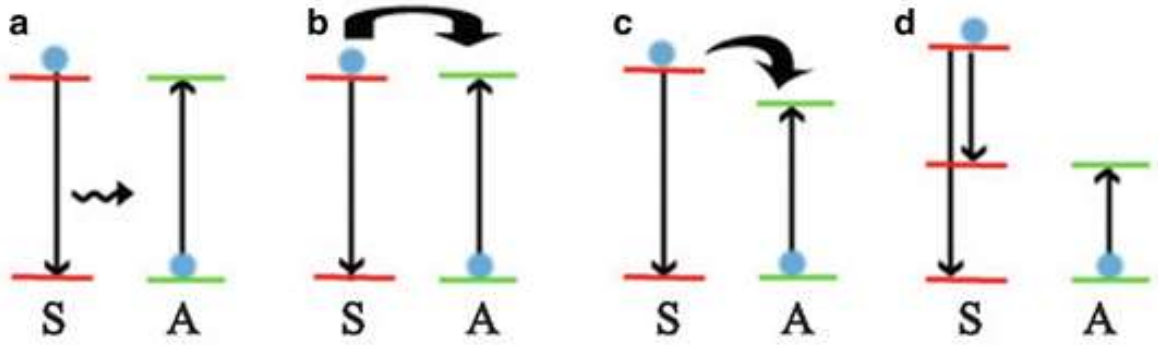

Fig.1.5. *An illustration of the ET processes using a schematic diagram*

Based on how effectively the activator is activated by the sensitizer emission, as shown in Fig. 1.5 (a), radiative energy transfer efficiency may be calculated. The excitation spectrum of the activator and the sensitizer should have a significant amount of overlap in their emission spectra. If primarily radiative energy transfer occurs, the lifetime of the sensitizer fluorescence is not affected by activator concentration. Figure 1.5 (b) shows a non-radiative energy transfer with a considerable decrease in the decay period of the sensitizer fluorescence with increasing activator concentration. The energy transfer process is driven by an energy differential of the same magnitude between the excited states of the

sensitizer and activator. If the gap between the ground and excited states of the sensitizer and activator is considerable, non-resonant ET may be facilitated by a phonon. The sensitizer and activator's potential interactions, distinctive transitions, and the energy differential between them all play a significant role in the ET process in luminous materials. The likelihood of energy transfer is minimal for phonon-assisted non-radiative transitions, which are illustrated in Fig. 1.5(c), if the two ions are in different excited states. The phrase "cross-relaxation" describes all types of down conversion energy transfer between similar, next-to-each-other luminous centers or ions. Cross-relaxation is a simple possible energy level scheme that occurs when the first ion, which is initially in an excited state, trades energy with the second ion, which is initially in the ground state. This results in both ions lying to some intermediate states simultaneously within the energy between the two initial states.

1.5. Judd-Ofelt (J-O) theory:

A model known as J-O theory describes the intensity of electron transitions that occur in the 4f shell of RE ions in solids/solutions as a result of the process of electromagnetic radiation absorption or emission. In 1962, George S. Ofelt and Brian R. Judd [59] both separately introduced the hypothesis. With just a few parameters, this theory offers a straightforward tool for calculating the probable outcome of the absorption and radiation emission process. The following equation may be used to calculate the oscillator strength (f_{exp}) parameter of RE ions as it was measured .

$$f_{exp} = f_{ED} + f_{MD} \tag{1.1}$$

It is made very apparent that both the magnetic and electric dipole oscillator strengths are included in the experimental oscillator strength of RE ions. In an absorption band with energy v (cm^{-1}), the total oscillator strength is written as [60]:

$$f_{exp}(\psi_j, \psi_{j'}) = \left[\frac{8\pi^2 mcv}{3h(2J+1)}\right]\left[\frac{n(n^2+2)}{9n} S_{ED}(\psi_j, \psi_{j'}) + nS_{MD}(\psi_j, \psi_{j'})\right] \tag{1.2}$$

Here, $\frac{n(n^2+2)}{9n}$ represents the dipole-dipole correction term , for the Lorentzian local field corresponding to dipole-dipole correction for the recorded absorption and h stands for Planck's constant. The degeneracy of the ground state is $(2J+1)$, where J is the quantity that indicates total angular momentum. Around 1% of the strengths of the electric dipole oscillator are used to measure the intensity of magnetic dipole transitions. Since electric dipole oscillator strengths are almost equal, the overall experimental oscillator strength is also nearly equal [60].

$$f_{exp} = f_{ED} \tag{1.3}$$

The experimental oscillator strengths

$$f_{exp}(\psi_j, \psi_{j'}) = f_{cal}(\psi_j, \psi_{j'}) = \left[\frac{8\pi^2 mcv}{3h(2J+1)}\right]\left[\frac{(n^2+2)^2}{9n} S_{ED}(\psi_j, \psi_{j'})\right] \tag{1.4}$$

Less Square Fitting Process is used to assess how well f_{cal} and f_{exp} and fit together. Using the following formula, one may determine the root mean square deviations[32,61].

$$\delta_{rms} = \left[\frac{\Sigma(f_{exp}-f_{cal})^2}{p}\right]^{\frac{1}{2}} \tag{1.5}$$

where the total number of energy levels used in the fitting process is denoted by the letter p. Three RE ion intensity parameters Ω_2, Ω_4, and Ω_6, have been analyzed using the J-O theory. The covalency between RE and oxygen ions as well as the symmetry surrounding RE ions in the specific host may be determined using the J-O intensity characteristics, which are of great relevance. In addition to giving information regarding the effectiveness and performance of the luminous material, these factors also play a crucial role. Dependent on covalency parameter. The structural modifications and symmetry of the ligand field surrounding the RE ion site are related to Ω_2. On the other hand, the magnitudes of the intensity parameters Ω_4, and Ω_6 affect bulk characteristics like as the medium's stiffness and viscosity, which are both affected by RE ions [62].

1.6. Nephelauxetic effect & oscillator strengths:

Finding additional crucial characteristics like nephelauxetic ratios and bonding parameters makes use of the absorption spectrum data. To understand the type of bonding between RE ions and oxygen ligands in the glass, such parameters are helpful. The existence of the nephelauxetic effect in the titled glasses is caused by partially filled RE ion f-shells in the host matrix. Using the following relation, the nephelauxetic ratio ((β) is determined [63].

$$\beta = \frac{\vartheta_c}{\vartheta_a} \tag{1.6}$$

Where wave number (cm^{-1}) ϑ_c_c is the wave number (cm^{-1}) of a certain transition for the RE ion under consideration and wave number a is the wave number for the same transition for an aqua-ion. The average value $\bar{\beta}$ of is determined once the values of for all of the observed transitions have been determined. Using the following relation, the bonding parameter is then calculated [64,65].

$$\delta = \frac{1-\bar{\beta}}{\bar{\beta}} \tag{1.7}$$

The covalent or ionic link between the RE ion and the ligand anion will depend on whether δ is positive or negative.

The area under the absorption curve may be used to measure the oscillator strength, which is energy of an absorption band of a RE doped host. The oscillator strength notion was initially put out by Ladenburg. Utilizing the following formula, experimental oscillator strengths (f_{exp}) are assessed. [66]

$$f_{exp} = \frac{2.303mc^2}{N\pi e^2} = 4.318 \times 10^{-9} \int \varepsilon(\vartheta) d\vartheta \tag{1.8}$$

In above equation, e, m are the electron's charge and mass, respectively, and $\varepsilon(\vartheta)$ is the molar extinction coefficient. The Avogadro number is N, and the speed of light is c.

1.7. Radiative characteristics of RE ions:

Owing to their distinctive radiative qualities, RE ions are widely employed in a variety of applications, such as optics, lasers, and lighting technology. These ions have unique energy levels that enable effective absorption and emission of light at particular wavelengths. The J-O theory may be used to correlate absorption and emission spectrum data in order to determine the radiative parameters. The radiative transition rate (A_R) of any given excited state $\psi_{j'}$[is used to calculate the intensity of the *f-f* transition of RE ions [67,68].

$$A_R(\psi_j, \psi_{j'}) = \left[\frac{64\pi^4 v^3}{3h(2J+1)}\right]\left[\frac{(n^2+2)^2}{9n} S_{ED}(\psi_j, \psi_{j'}) + nS_{MD}(\psi_j, \psi_{j'})\right] \quad (1.9)$$

Here, v is the energy band gap (cm^{-1}), and n is the refractive index. The electric and magnetic line strengths are S_{ED} and S_{MD}, respectively.

The following equation is used to estimate the total radiative transition (A_T) [50].

$$A_T = \sum_{\psi_{j'}} A_R(\psi_j, \psi_{j'}) \quad (1.10)$$

The following formula represents how long an excited RE ion will radiate (τ_R):

$$\tau_R(\psi_j, \psi_{j'}) = \left[\frac{1}{A_T}\right] \quad (1.11)$$

According to the expression, the fluorescence branching ratio (β_R) from the excited state to a lower lying state is as follows [62]:

$$\beta_R(\psi_j, \psi_{j'}) = A_R(\psi_j, \psi_{j'})\tau_R(\psi_j, \psi_{j'}) \quad (1.12)$$

A crucial measure that shows the material's energy extraction rate is the stimulated emission cross-section, $\sigma_{se}(\psi_j, \psi_{j'})$. It may be written as [69]:

$$\sigma_{se}(\psi_j, \psi_{j'}) = \left[\frac{{\lambda_p}^4}{8\pi c n^2 \Delta\lambda_p}\right] A_R(\psi_j, \psi_{j'}) \quad (1.13)$$

In the above relation, $\Delta\lambda_p$stands for effective emission line width and, $\lambda_p$for peak wavelength.

Another crucial metric is quantum efficiency, which may be measured by comparing the experimental lifetime (τ_{exp}) to the radiative lifetime (τ_R) [62].

$$\eta = \frac{\tau_{exp}}{\tau_R} \tag{1.14}$$

1.8. Excited and de-excitation process of RE ions:

Following sufficient energy, the intra 4f-4f electronic transition of the RE ion triggers the excitation and de-excitation process. The excitation and de-excitation process are illustrated in Fig. 1.6 by a time-resolved intensity spectrum [70].

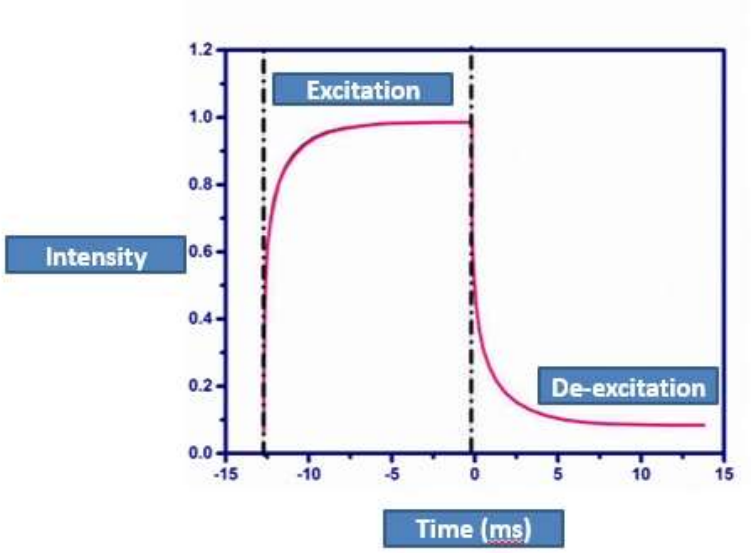

Fig. 1.6. *Excitation and de-excitation process of RE ions.*

The excited RE ion can revert to its ground state via cross relaxation channels, radiative transition, energy exchange between neighboring RE ions, or other means. Since RE ions cannot interact with one another at low RE ion concentrations, the decay curve for intensity against time is fitted with a single exponential function. The equation below can be used to represent the PL intensity [31,71].

$$I_t = I_0 + A_1 \exp\left(-\frac{t}{\tau}\right) \quad (1.15)$$

I_0 in this case represents the PL intensity at time zero. τ displays the lifespan of the excited RE ion, which may be assessed by looking at the logarithmic plot of intensity against time. As seen in Fig. 1.6, the intensity of the excited state gradually diminishes with time as 1/e. The following equation can be used to predict the experimental lifetime of an excited RE ion [72].

$$\tau_{exp} = \frac{\int tI(t)dt}{\int I(t)dt} \quad (1.16)$$

On the other hand, the decay profiles fit the bi-exponential function well at greater RE ion concentrations. Equation may be used to represent the PL intensity for bi-exponential fit [64,73].

$$I_t = I_0 + A_1 \exp\left(-\frac{t}{\tau_1}\right) + A_2 \exp\left(-\frac{t}{\tau_2}\right) \quad (1.17)$$

The following equation is used to calculate the average lifespan (τ_{avg}) in this situation[63,74].

$$\tau_{avg} = \frac{A_1\tau_1^2 + A_1\tau_2^2}{A_1\tau_1 + A_2\tau_2} \quad (1.18)$$

In this case, the lifespan components τ_1, τ_2 are exponential, and A_1, A_2 are fitting constants.

1.9. Inokuti-Hirayama (I-H) model:

The two separate processes by which an ion can relax to the lower energy state after attaining an excited state are widely understood. Before the energy reaches the unexcited acceptor ions, the donor ions in the first mechanism might move it amongst themselves. The second mechanism allows for direct energy transfer from the donor ions to the acceptor ions. When donor and acceptor ions are evenly dispersed throughout the host matrix and the energy movement between donor ions is minimal, the energy transfer that occurred between the donor and acceptor ions is what causes the rapid decay. The I-H model is a good choice in these circumstances to comprehend the main energy transfer process. In this scenario, the luminescence intensity is determined by [64]

$$I_t = I_0 \exp\left\{-\frac{t}{\tau_0} - Q\left(\frac{t}{\tau_0}\right)^{\frac{3}{S}}\right\} \quad (1.19)$$

Here, "t" is the elapsed time following excitation, and $''\tau_0''$ denotes the intrinsic decay period of the donors in the absence of acceptors. The following equation can be used to evaluate "Q," the energy transfer parameter [59]:

$$Q = \frac{4\pi}{3}\Gamma\left(1 - \frac{3}{S}\right) N_0 {R_0}^3 \quad (1.20)$$

In the above relation, N_0 is the acceptor ion concentration, and R_0 is the necessary energy transfer distance. The interactions that make up the mechanism may be categorised as dipole-dipole (S=6, Γ(x)=1.77), dipole-quadrupole (S=8, Γ(x)=1.43) and quadrupole-quadrupole (S=10, Γ(x)=1.43) based on the values of S and gamma function (x). The energy transfer probability W_{ET} and the donor-acceptor interaction parameter C_{DA} are calculated using the following formulas [49,75].

$$C_{DA} = {R_0}^{(S)} {\tau_0}^{-1} \text{ and } W_{ET} = C_{DA} {R_0}^{(S)} \quad (1.21)$$

1.10. Current glass composition importance:

It is reported in the literature that, heavy metal oxide glasses are quite suitable for the development of non-linear optical devices, electro-optic modulators, electro-optic switches, solid-state laser materials and IR technologies because of their high density, refractive index and low phonon energy. Depending on the oxygen-to-phosphorous (O/P) atomic ratio, the phosphate glasses are made up of various structural components. Phosphate glasses have a tetrahedral structure that may be characterized using the notation Q^n (n = 0-3), where n is the number of bridging oxygen atoms in a tetrahedron. Based on the proportion of (O/P) atoms, the phosphate glasses exhibit various structural characteristics. The three structures are ultra-phosphate, meta-phosphate, and polyphosphate, respectively, depending on the O/P atomic ratio. For ultra-phosphate structures, the O/P atomic ratio ranges from 2.5 to 3, and the network is made up of Q^2 and Q^3 structural units. The O/P ratio for the meta-phosphate structure is 3, and the

network is made up of long chains and/or rings of Q^2 structural units. The polyphosphate structure has an O/P atomic ratio larger than 3 and is made up of shorter chains of Q^2 structural units that are terminated by Q^1. Fig.1.6 depicts the many tetrahedral locations that can exist in phosphate glasses [76,77].

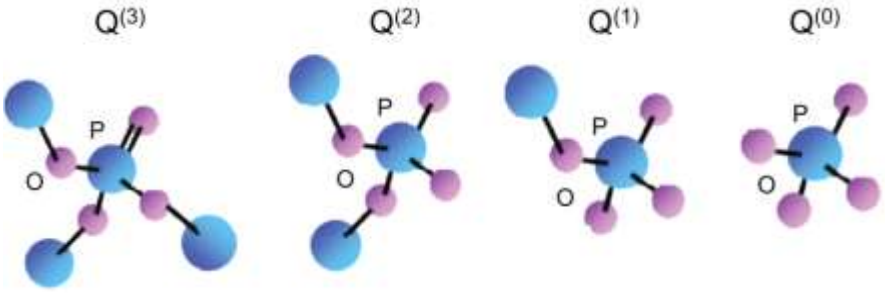

Fig. 1.7*: Many tetrahedral structures of phosphate glass.*

In general, the host glass with relatively low phonon energies can give high quantum efficiency and therefore useful for the designing of a good photonic device . There are several glass formers, including fluorides, phosphates, borates, tellurites, silicates, and borosilicate, that have been created and used to study different spectroscopic characteristics. Due to its unique characteristics, including clear visibility in a broad spectrum, softening, a lower melting point, good thermal stability, high RE solubility, and low dispersion, phosphate is one of the most ideal glass formers [78,79]. Although phosphate glasses have several uses in photonic devices, their hygroscopic nature and weak chemical stability pose certain restrictions. The main focus of the current work is to investigate the benefits of heavy metal oxide glasses that are well suited for photonic devices such as lasers, fiber amplifiers, and light-emitting diodes and have relatively low phonon energies. We looked into these RE-ionized glasses because of the importance of heavy metal oxides in research and technology. To overcome these limitations, network modifiers (BaO, Li_2O) and intermediate (ZnO) have been added to the host glass, which can increase chemical stability and reduce thermal expansions. Moreover, ZnO helps to overcome hygroscopic nature and increases the solubility of RE ions. All the above-discussed characteristic features possessed by the chemical species P_2O_5, Li_2O, BaO and ZnO

prompted us to prepare a glassy system namely barium zinc lithium phosphate (BZLP) glass. Phosphate based glasses doped with RE ions are effective in improving the luminescent characteristics of a materials to have potential applications in the field of optoelectronics. [69,75

. 1.11. Objectives of thesis work:

The main objectives of the present research work are as follows.

- To prepare fine quality optical glasses having relatively less phonon energy and doped with RE ions.
- Physical and optical characterization of such selected glass system doped with RE ions.
- To calculate Oscillator Strengths from the recorded absorption spectral features of RE doped glasses.
- To measure radiative properties of as prepared glasses by using Judd-Ofelt theory.
- To measure the stimulated emission cross-sections, branching ratios and quantum efficiency of doped glasses by correlating absorption spectra data with emission data**.**
- Optimization of glass composition and concentration of doped RE ions for better photonic device applications.

CHAPTER 2

Experimental and Instrumentation Part of the Research Work

The current focuses on the experimental procedure utilized to prepare RE doped glasses as well as the procedures for analyzing the luminescence characteristics of the created glasses. The melt quench method, which is used to synthesize as-prepared glasses, is also thoroughly discussed. In order to study different properties, including thermal, structural, photoluminescent, and colorimetric properties, this chapter describes the use of numerous advanced experimental techniques, including differential scanning calorimetry, thermo gravimetric analysis, X-ray diffraction, Fourier-transform infrared spectroscopy, UV-VIS spectrophotometer, temperature dependent emission study and spectrofluorophotometer.

2.1. Glass synthesis procedure:

The specific preparation steps may vary depending on the intended use of the glass sample and the desired analysis or experiment. For precise glass sample preparation, it is crucial to refer to certain processes, requirements, or methods of experimentation. Some of the procedures described below can be utilized for developing amorphous glass samples [80,81].

- Thermal evaporation
- Melt quenching
- Chemical vapor deposition
- Chemical reaction
- Gel – desiccation
- Glow- discharge decomposition
- Reaction and Shear amorphization
- Sputtering
- Electrolytic deposition

The melt quenching procedure is the simplest and most often utilized of the aforementioned processes.

2.1.1. Melt quenching procedure:

The most popular and traditional way to develop amorphous solids via melt quenching procedure. Using this technique, melts that are abruptly forced to cool can be formed into any desired shape and size. The amorphous solid is prepared by continual hardening of the melt, which is the distinctive characteristic of the melt quench process. Different materials require a varied cooling rate in order to create a glassy state. After removing the melt from the furnace,

it should be quenched promptly before being placed over metals such as copper or brass plates for efficient cooling. According to Fig. 2.1, glass samples have been formed using the melt quenching procedure [82].

- Selection of precursors: A suitable material precursor should be chosen. It could be a pure material and not contaminated.

- Mixing of precursors: If necessary, grind or crush the precursors material into a fine powder in any liquid medium (acetone, ethanol, DI water) to ensure uniform melting and cooling.

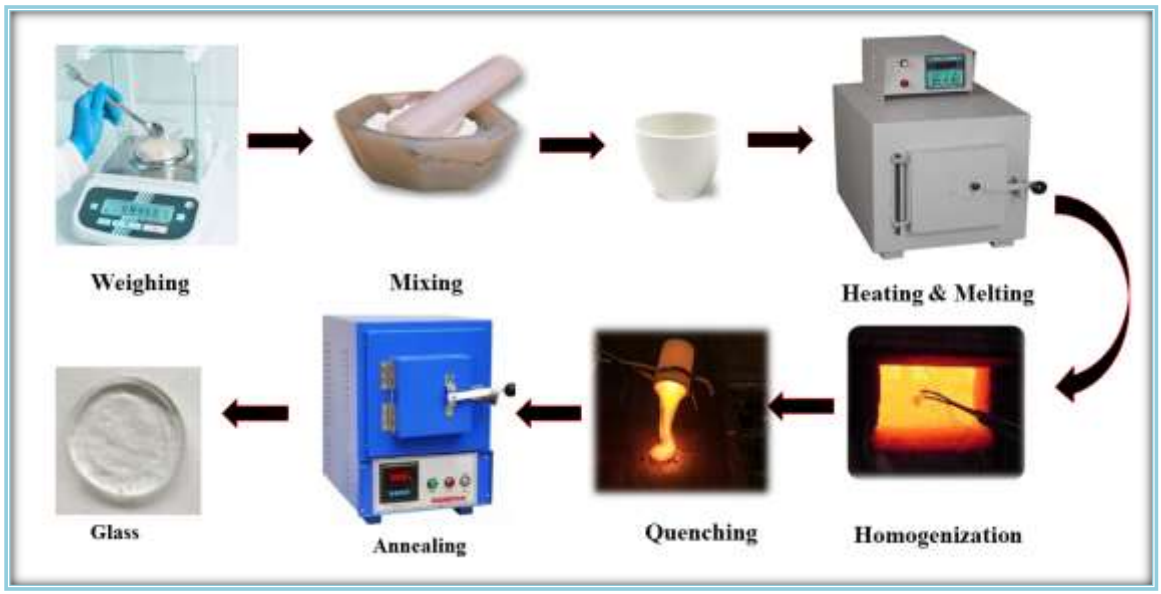

Fig. 2. 1: *Preparation of glass samples by using melt quenching process.*

- Melting: Put the sample in an appropriate container or crucible that can endure high temperatures. The sample should be heated progressively until it reaches its melting point using a heating source like a furnace.

- Homogenization: Keep the sample at its melting point for long enough to achieve homogeneity when it reaches that temperature. If necessary, agitate or stir the sample to encourage even mixing.

- Quenching: After the homogenization step, quickly remove the sample from the heat source and transfer it to a quenching heated metal plat medium. The fast cooling ensures the solidification of the sample in an amorphous or glassy state.

- Annealing: In order to remove thermal stresses, the manufactured samples of glass were annealed in a box furnace, mostly at $1/4^{th}$ of the melting temperature. Allow the sample to cool in the quenching medium until it reaches room temperature.

- Obtaining the glass sample: After cooling, gently take the sample from the furnace and handle it as needed. Depending on your particular experimental needs, either store it in an appropriate container or analyze it. The glass samples that had already been made were then acquired for further characterization and outcome analysis.

2.2. Preparation of glass and physical properties:

2.2.1. Precursor materials:

The oxides raw chemicals have been bought from a number of businesses that could guarantee 99.99% purity, mostly for dopant RE ions. Table 2.1 summarizes the precursor materials used in this thesis, along with their purity and manufacturer:

Table 2.1. List of chemicals and purity along with manufacturer:

S. No.	Chemicals	Purity (%)	Manufacturer
1.	$BaCO_3$	99.90	Fisher Scientific
2.	$LiCO_3$	99.90	Fisher Scientific
3.	$NH_4H_2PO_4$	99.90	Pro analysis Merck
4.	ZnO	99.90	Oualigens
5.	Dy_2O_3	99.99	Sigma Aldrich
6.	Tb_4O_7	99.99	CDH
7.	Pr_6O_{11}	99.99	Sigma Aldrich

The doped and un-doped glass samples have the molar configuration as follows:

(15-*x*) BaO-15ZnO-10Li_2O-60P_2O_5:*x*REO where x value varies between 0.1 to 2.5 mol% depending on the glass system prepared and the kind of doped RE ions.

2.2.2. Glass preparation procedure:

Glass samples with trivalent RE REions doping were manufactured using the melt quenching approach. BZLP glass samples were made using annular grade precursors and 99.9% pure RERE elements. The raw chemical materials were weighed in accordance with the composition calculation. Using an agate mortar and pestle and ethanol as the dispersing medium, the compounds were crushed for one hour. This uniform and smooth chemical mixture was then put into an alumina crucible and heated in a muffle furnace at a rate of 5°C per minute from room temperature to 1150°C, where it was held for an hour. This homogeneous melt mixture

was then removed and quickly quenched between preheated (approximately 320 °C) brass plates to made glass of required shape and thickness. To remove air bubbles and thermal strains, the prepared glass was annealed at 320°C for 3 hours. Finally, BZLP doped and un-doped glass samples were ready for the physical, structural, optical and other characterizations.

2.2.3. Physical properties:

Spectroscopic investigation is dependent on various physical parameters like thickness, density, refractive index, and RE ion concentration. The aforementioned physical parameters are needed to calculate experimental oscillator strength (f_{exp}), which can then be used to evaluate intensity parameters and radiative parameters and providing knowledge about the utility of as-prepared glass.

(I) Thickness: Screw gauge is the tool used to measure the thickness of BZLP glass samples. Least count of the screw gauge is 0.001 cm. Every set of BZLP glasses has the same thickness, which is 2.7 ± 0.01 mm.

(II) Density: By using the Archimedes principle, density (d) of BZLP glasses is estimated with an accuracy of ± 0.0001 g using water as the immersion liquid. For calculating density, the following equation is used[83,84]:

$$d = \frac{W_1}{W_1 - W_2} \tag{2.1}$$

Where, W_1 and W_2 is the weight of glass in air and water respectively.

(III) Refractive index: The refractive indices (n_d) of BZLP glasses are calculated using Brewster's angle method with a He-Ne laser (6328 X 10^{-10} m).

(IV) Concentration of RE ion: The following equation was used to calculate the amount of RE ions (x) (mole liter^{-1}) present

$$x = \frac{m_{RE}}{m_T} \times \frac{d}{MW} \times 100 \quad (2.2)$$

here, MW is the molecular weight of the RE salt and m_{RE} is the mass of the RE salt. m_T is the total weight of the chemical composition. The unit is transformed from mole liter^{-1} to cm^3 by multiplying x by Avogadro's number (N).

These four physical properties are then used to calculate other physical parameters such as Avogadro molecular weight $(\bar{M})$ (g), mean atomic volume (g/cm^3/atom), molar volume (Vm) (cm^3/mol), dielectric constant (ϵ), optical dielectric constant, molar refractivity, reflection losses, polaron radius, interionic distance, molecular electronic polarizability and field strength of RE ions doped BZLP glasses by using the following expression as given in literature :

$$\text{Dielectric constant, } \epsilon = {n_d}^2 \quad (2.3)$$

$$\text{Optical dielectric constant, } \epsilon - 1 = {n_d}^2 - 1 = P\frac{\delta t}{\delta P} \quad (2.4)$$

$$\text{Molar refractivity, } R_M = \left[\frac{({n_d}^2-1)}{({n_d}^2+1)}\right]^2 \frac{\bar{M}}{d} \quad (2.5)$$

$$\text{Reflection loss, } R = \frac{(n_d-1)^2}{(n_d+1)^2} \quad (2.6)$$

$$\text{Polaron radius, } r_P = \frac{1}{2(\pi/6n)^{\frac{1}{3}}} \quad (2.7)$$

$$\text{Interionic distance, } r_i = \left(\frac{1}{N}\right)^{1/3} \quad (2.8)$$

Molecular dielectric polarizability factor (α), $\alpha = \frac{1}{\frac{4\pi N}{3}}\left[\frac{({n_d}^2-1)}{({n_d}^2+1)}\right]$ (2.9)

Field strength, $F = \frac{Z}{r_p^2}$ (2.10)

Where, the oxidation number of cations i, the ionic ratio with respect to total number of oxides, basicity moderating parameter and the Pauli electronegativity are represented by Z_i, r_i, γ_i and x_i respectively. Various physical parameters listed above are represented in respective chapters.

2.3. Characterization techniques:

Characterization techniques are the procedures and equipment used to examine and comprehend a material's characteristics, composition, structure, and behavior. These methods help in the development of novel materials or the enhancement of current ones by offering insightful information on the properties and functionality of materials. Extensive systematic characterization procedures are required to investigate the different structural, chemical, optical, and luminous characteristics of RE doped BZLP glasses. In this part, the characterization tools' basic operating principles have been briefly explained.

2.3.1. Thermal analysis:

Thermal analysis techniques, including differential scanning calorimetry (DSC) and thermogravimetric analysis (TGA), involve subjecting materials to controlled heating or cooling while measuring changes in temperature, heat flow, weight, or other properties. This is useful in figuring out a material's thermal stability, phase transitions, thermal behavior and kinetics of breakdown.

As a function of temperature or time, DSC, a thermal analysis method, evaluates the heat flow into or out of a sample. As a sample is heated or cooled, it gives information on the physical

and chemical processes taking place inside of it. In DSC, the heating or cooling conditions for a sample and a reference material are the same. Phase changes, melting points, crystallization, and other thermal events may all be identified by comparing the heat flow between the sample and the reference, which records any differences. DSC can be applicable for determining the melting points, phase transitions, thermal stability and decomposition kinetics, analysis of glass transitions and crystallinity.

TGA is a method for analyzing weight changes in samples that are heated or cooled under precise temperature control. It offers details on the composition, deterioration, and thermal stability of materials. In TGA, a sample is constantly weighed while being heated or cooled at a steady pace. Indicating thermal events such as breakdown, oxidation, desorption, or changes in moisture content, the weight gain or loss is tracked as a function of temperature or time. TGA is useful for the determination of thermal stability and degradation kinetics, analysis of decomposition and weight loss etc. The DSC TGA was performed by using Setaram Labsys Evo instrument as visible in Fig. 2.2.

***Fig. 2.2**: DSC/TGA simultaneous instrument (SETARAM, Labsys Evo)*

2.3.2. X-Ray diffraction:

A non-destructive method known as X-ray crystallography is used to determine a crystal's atomic and molecular structure as well as the crystallite size, phase, and internal stress of tiny crystalline areas. In order to examine the crystal structure of materials, X-ray diffraction (XRD) is a widely used method in material science. XRD works on the principle of Bragg's law for diffraction. Constructive interference in between these waves is satisfied by the Bragg's equation and is represented in Fig 2.3 (a) [85]:

$$2d\ sin\theta\ = n\lambda$$

Glass, on the other hand, lacks a regular and recurring crystalline structure since it is an amorphous substance. Hence the glassy and amorphous nature can be confirmed via XRD profile. Un-doped glass sample have been analyzed by using the X-ray diffractometer apparatus (Bruker D8 Advance) as shown in Fig 2.3 (b). The recorded XRD profile for an un-doped BZLP glass consists of huge hump rather than sharp peaks which confirms the amorphous nature of the titled glass.

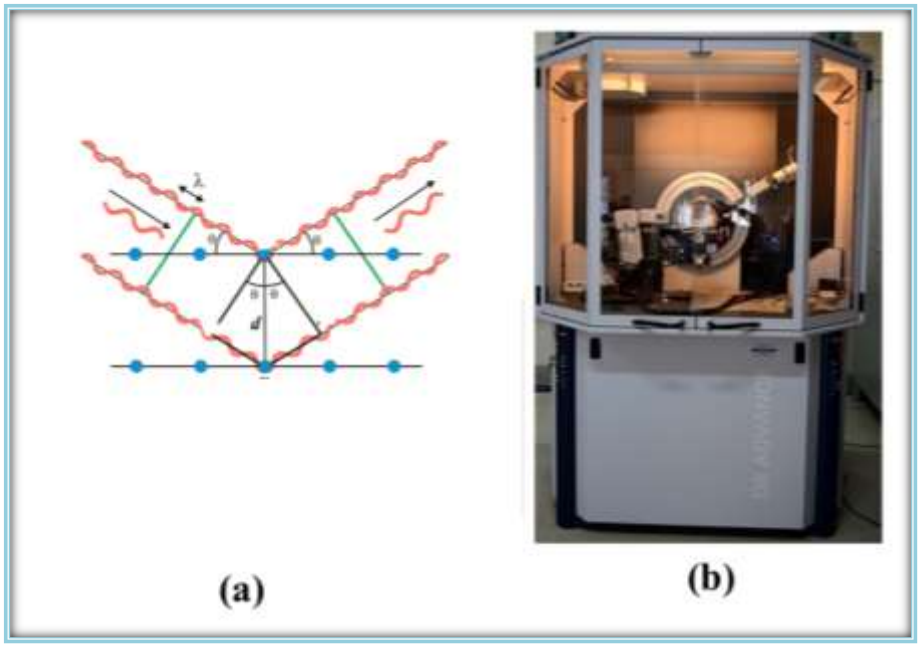

Fig. 2. 3: *(a) Brags law for diffraction (b) X-ray diffractometer instrument (Bruker D8 Advance).*

2.3.3. Fourier transmission infrared spectroscopy (FT-IR):

An equipment called an FT-IR Spectrometer is used to identify absorption peaks in the near-to-far infrared spectral band. One of the multiplex types of spectroscopic techniques that collects all wavelengths simultaneously is FT-IR spectroscopy. To determine vibrational groups and bonding in compounds, FT-IR is frequently utilized. Additionally, it may categorize the atomic conformations of networks that constitute glass. The molecules vibrate in two different ways, stretching and bending [88]. Stretching causes a change in the distance between two nearby atoms but not in their angle. However, as an object bends, the atom's location in relation to the bond axis changes. When a molecule is exposed to IR radiation, the amplitude of a certain frequency of vibration rises in direct proportion.

Fig. 2. 4: *Perkin Elmer's frontier FT-IR spectrometer*

A beam splitter, a detector, a fixed mirror, and a moving mirror make up the FT-IR. By using a beam splitter, IR radiation from the source was separated into two equal beams. In order to reach the fixed mirror, one portion of the beam is transmitted via the beam splitter, and in order to reach the moving mirror, the other portion is reflected off the beam splitter. Both stationary and mobile mirrors were used to reflect these transmitted and reflected beams back to the beam splitter. After several iterations, the detector ultimately picks up one beam that is travelling through the sample, while the second beam returns to the source. In most cases, wave numbers (cm^{-1}) or wavelengths (λ, nm) are used to represent the places of FT-IR absorption. The quantity of waves per length is indicated by the wave number [89]. As a result, wave numbers and the energy of IR absorption are both linearly proportional to frequency

[88]. The Frontier FT-IR spectrometer from Perkin Elmer carried out the FT-IR, as shown in Fig. 2.4. Sample in pellet form was required for the FT-IR spectra recording. In order to create the pallet, KBr powder and glass powder were combined in a ¼ ratio, and the pallet was then crushed using a hydraulic press at a pressure of 2.5 tones.

2.3.4. UV/VIS/NIR Spectrophotometer:

The three distinct electromagnetic radiation phenomena, i.e., transmission, absorption, and reflection, take place when electromagnetic radiation or light impacts anything like a material's surface. Measurements of the samples' transmission, reflectance, and absorption of light were made using a UV/VIS/NIR spectrophotometer. In spectroscopy, a light source that emits light in the UV to NIR range (200 to 1500 nm) impacts the sample, and the light that is transmitted is collected at the other end of the sample. After interacting with them, the sample's optical data is included in the light that was sent. In order to quantify the optical characteristics of diverse organic and inorganic materials, UV-VIS spectroscopy is employed [52].

In UV/VIS spectroscopy, the Beer-Lambert law is used. According to the Beer-Lambert equation, the rate at which the intensity of radiation decreases when the thickness of the absorbing solution is increased or decreased in correlation to the amount of radiation that hits it as well as the concentration of the solution itself. The following is how absorbance (A) is expressed mathematically [90]:

$$A = \log_{10}\left(\frac{I_t}{I_0}\right) \tag{2.3}$$

where, I_o and I_t denotes the incident light intensity and transmitted light intensity, respectively. The formula for the transmittance, T, is $T = I/Io$. Using the following relationship, the absorbance coefficient was determined from the absorbance values. [91]:

$$\alpha(\nu) = \frac{1}{d}\ln\left(\frac{I_0}{I_t}\right) \tag{2.4}$$

here, d represent the thickness of sample, $\alpha(\nu)$ signifies the absorption coefficient.

Fig. 2.5: *Jasco V-770 UV/VIS/NIR spectrophotometer*

A converged beam from the light source enters the monochromator in a UV/VIS/NIR spectrophotometer. Deuterium and tungsten lamps served as the corresponding sources of UV and NIR light. The monochromator's grating scatters the light, which exits via the exit slit. By use of a sector mirror, this light is divided into two light streams, one of which incident on the sample being measured and the other on the reference sample, such as solvent. The sample or reference sample's light is incident on the detector after passing through it. In order to record the spectrum, a detector photomultiplier tube is employed. Software was then used to analyze the captured spectrum and produce a spectrum on a wavelength scale. A UV/VIS/NIR spectrophotometer (Jasco, V-770) is displayed in Fig. 2.5.

2.3.5. Spectrofluorophotometer: photoluminescent studies

A versatile, non-destructive way of examining a material's optical features is photoluminescence spectroscopy. Usually, a laser or UV/visible/NIR radiation beam from source strikes a sample and is absorbed there. The material's surplus energy can be released by emitting light, a process known as luminescence. This luminescence is referred to as "photoluminescence" since the sample is excited by light. Thus, PL is the spontaneous light emission from a substance when it is being excited by light. This light may be captured and subjected to spectral, spatial, and temporal analysis. In actuality, PL spectroscopy provides details on the system under investigation's low-lying energy levels [10,35]. The most frequent radiative transition in semiconductor systems occurs between states in the conduction and valence bands; this energy difference is referred to as the band gap. The electrons and holes that make

up the photo-excited carriers relax towards their respective band edges and recombine by producing light at the band gap's energy. Excitation source light impacts the sample after passing via an emission monochromator. The sample absorbs some of the input light and then emits light in all directions. The absorption monochromator allows some light to pass through and reach the detector [12].

A Xenon lamp is employed as the UV light source because of its continuous emission spectra and virtually constant intensity in the 300-800 nm region. When using a monochromator, collimated light illuminates a diffraction grating and departs at a varied angle depending on the wavelength. The transmitting wavelengths can then be chosen by adjusting the monochromatorBasically, a monochromator selects a certain wavelength of light from a light source (Xenon Lamp) and directs it towards the target sample in a typical PL experiment. The sample's light is captured by lenses, spread out by a second monochromator, and then detected by a photodetector. An A/D (analogue to digital) converter transforms the analogue electrical output produced by the optical detector into a digital signal, which is then processed by software on a computer [92]. The spectrum is shown as a function of the wavelength of the emitted light in terms of the intensity of PL light that is emitting (proportional to the electrical signal created).

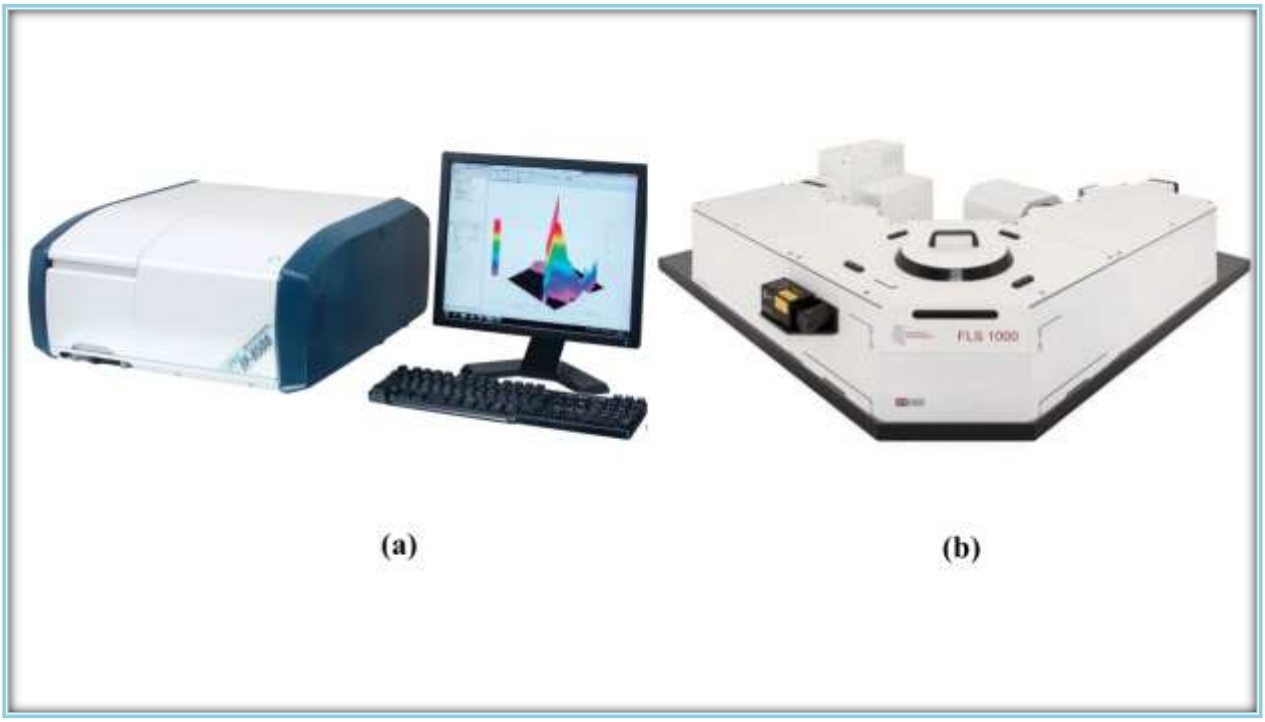

Fig. 2. 6: *(a) Jasco 8300FP spectrofluorophotometer (b) Edinburg, FLS 980 spectrofluorophotometer.*

PL characteristics were recorded by using Jasco 8300FP spectrofluorophotometer and Edinburg, FLS 980 spectrofluorophotometer as shown in Fig. 2.6 (a) & (b) respectively.

Time-Resolved Photoluminescence (TR-PL) is an improvement above the common spectrophotometer. A rapid photodetector is used to capture a sample's emission as a function of time following stimulation, and a pulse light source is used to excite it. This technique may be used to track material quality, identify spectrum emissions with distinct emissive states, or research energy transfer from one ingredient to an alternative in mixed composites or samples. The photoluminescent characteristics' inherent property of recorded lifespan can shed light on the species' excited state dynamics. TR-PL is one of the top options for researching decay time or lifespan, which are terms used to describe the quick and slow electrical deactivation processes that cause photon emission. The surrounding molecular environment and interactions with other molecules may have an impact on its lifespan [31,93]. The local chemical environment may therefore be learned about or response processes can be understood via lifetime changes. As shown in Fig. 2.6 (b), lifetime profiles were captured using an Edinburgh Instruments

(FLS980) Spectrofluorophotometer. Here, a microsecond xenon flash light was employed as the excitation source.

2.3.6. Temperature dependent PL (TD-PL) emission studies:

TDPL studies refer to investigations that examine the changes in the emission properties of a material or system as a function of temperature. By studying the temperature dependence of emission properties, researchers can gain insights the thermal stability of as prepared glass samples. This information is crucial for optimizing the performance of devices, understanding energy transfer mechanisms, designing sensors, and exploring fundamental phenomena related to light-matter interactions [94–96].

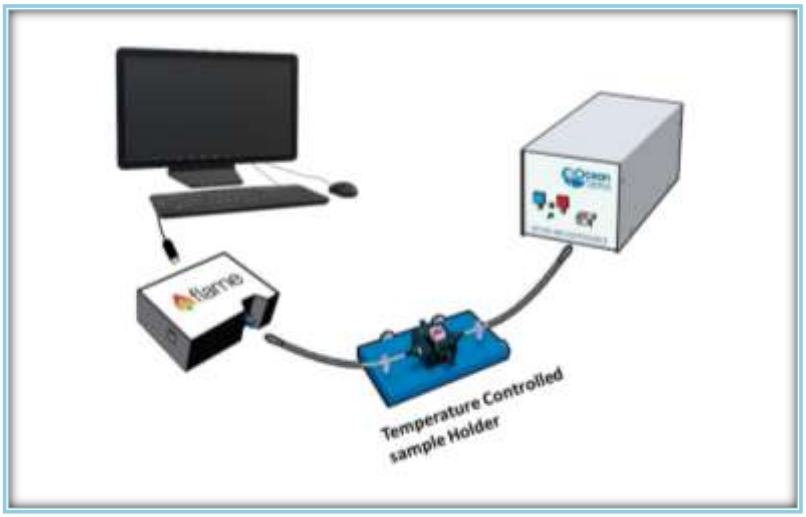

Fig. 2.7: *Schematic representation of Temperature-dependent spectrofluorophotometer.*

CHAPTER 3

Photoluminescence downshifting studies of thermally stable Dy^{3+} ions doped phosphate glasses for photonic device applications

Trivalent dysprosium (Dy^{3+}) activated barium zinc lithium phosphate (BZLP) glasses were prepared by employing melt quench routes. To understand the possible applicability of prepared glasses in photonic device applications, numerous structural, optical, and radiative characteristics have been explored in detail. The non-crystalline character of BZLP glass has been confirmed with the help of an X-ray diffraction pattern. The titled glasses doped with Dy^{3+} ions show several absorption peaks in 330-2000 nm range with an indirect optical band gap of 3.41-3.76 eV. The Judd-Ofelt (J-O) theory was employed on the absorption profiles and estimated various radiative parameters for the Dy^{3+} ions activated BZLP glasses. The Dy^{3+} ions activated glasses exhibit intense excitation at 350 nm and three sharp visible emissions at blue ($^4F_{9/2}\rightarrow{}^6H_{15/2}$), yellow ($^4F_{9/2}\rightarrow{}^6H_{13/2}$), and red ($^4F_{9/2}\rightarrow{}^6H_{11/2}$). To ascertain the lasing potentialities of BZLP glasses, the stimulated emission cross-section and branching ratios have been assessed by correlating the emission spectral information with the radiative parameters calculated from the absorption spectral features. The colorimetric properties show the coordinates situated in a bright white region. Temperature-dependent photoluminescence (TD-PL) spectral features recorded revealed the thermal stability of as-prepared glasses. The explored distinctive features for Dy^{3+} ions activated BZLP glasses suggested the superiority and direct utility of the as-prepared glasses in advanced photonic device applications such as lasers and w-LEDs.

3.1. Introduction

Recently, enormous research has been focused on the non-crystalline glasses activated with RE ions owing to their excellent features such as high transparency, low manufacturing cost, easy fabrication technique, highly durable, excellent emission properties, and high thermal stability. RE ions activated glasses have direct utility in numerous areas such as solid-state lasers, optical fibers, sensors, light converters, and other optoelectronic devices [97]. The spectroscopic investigations for instance absorption, PL excitation, PL emission, PL decay, and TD-PL features recorded for the RE ions doped glasses explore the utility of the host glass matrix for the aforementioned various photonic devices applications. The spectral features of the active ions (RE ions) doped into a host matrix can be varied by appropriate choice of host matrix composition or by varying the RE ion concentration in a host. RE ions doped glasses have distinct optical properties in various host glasses like phosphate, borate, silicate, telluride and chalcogenides from the perspective of their applications in solid-state lasers [98–100]. To enhance the lasing properties, the glass host can be formed by using a good former added with intermediates and network modifiers [101,102]. For the best optical and lasing properties, the selection of host glass with various RE ions is a still difficult task [103]. To increase the stimulated emission cross-section and quantum efficiency, host glass with low phonon energy is very much essential. A host glass with relatively less phonon energies can increase radiative properties by suppressing non-radiatve decay process [104].

In quite recent times w-LEDs replace traditional fluorescent and incandescent lamps. These diodes serve many purposes, including excellent durability, less power consumption, and a longer life span [105]. For the commercial availability of w-LEDs, phosphors activated by the blue LED chip to emit green and red lights alternately are usually employed. The majority of

current research, on the other hand, is focused on white emission by UV excitation without the usage of an LED chip. RE doped glasses provide many advantages, including decreased manufacturing costs, a straightforward manufacturing process, and no halo effect [106].

There are various glass formers like fluorides, phosphates, borates, tellurites, silicates, borosilicate etc. The researchers working in the field of glass science & technology have prepared variety of glasses using the above mentioned glass formers along with network formers and studied their spectroscopic properties. Among various glass formers, phosphate is one of the suitable glass formers owing to distinctive properties like clear visibility in the wide-ranging spectrum, softening, less melting temperature, high thermal stability, high RE ion solubility and low dispersion [107]. Phosphate glasses possess various applications in photonic devices but it has some limitations because of its hygroscopic nature and poor chemical stability [108].. All the above-discussed characteristic features in chapter 1 possessed by the chemical species P_2O_5, Li_2O, BaO and ZnO prompted us to prepare a glassy system namely barium zinc lithium phosphate (BZLP) glass. Phosphate based glasses doped with RE ions are effective in improving the luminescent characteristics of a materials to have potential applications in the field of optoelectronics [109–112].

Dy^{3+} is one of the very attractive RE ions for fabricating visible solid-state devices as its emission takes place in the visible region due to f-f transitions. In general, Dy^{3+} doped materials have two major peaks in blue and yellow regions, and if their intensity ratio is appropriate, then Dy^{3+} ions doped materials show a white light. The Y/B ratio can be enhanced by changing Dy^{3+} ions concentration and excitation wavelength, which further gives magnificent emission from glassy materials in the visible region [113–117]. Recently, S. Tian et al. investigated Silicate-clad Dy^{3+} doped multi-component phosphate glass core glass fiber for yellow laser applications.

The sample with 1 mol.% Dy_2O_3 (2.6 wt.%) doping concentration exhibits the most intensive yellow emission and its internal quantum efficiency was determined to be 39.27% [118]. P. Babu et al. prepared Dy^{3+} ions doped zinc oxyfluorotelluride glasses. The CIE coordinates of as-prepared T20ZofNDy1.0 glass are very nearer to the white light region, showing their applications in w-LEDs [119]. R.J. Amjad and his co-workers synthesized Dy^{3+} doped PbO–ZnO–B_2O_3–P_2O_5 glasses for white light-emitting materials and solid-state laser applications [120].

In the present research work, BZLP glasses doped with varying concentration of Dy^{3+} ions were prepared by using melt quench route. Various spectroscopic characterizations were performed to on Dy^{3+} ions doped BZLP glasses to explore its structural, optical absorption, PL properties and thermal stability. The J-O theory has been applied to the measured absorption bands (called oscillator strengths) useful in assessing various radiative properties for the prominent fluorescent levels of Dy^{3+} ions in the titled glasses. Further, the absorption and emission properties are correlated to understand the lasing potentialities of the titled glasses. TD-PL spectral features are recorded to understand the thermal stability of the titled glasses. Colorimetric studies were also conducted on the titled glasses to understand the usage of the titled glasses for lighting industry as epoxy-free w-LEDs.

3.2. Experimental procedure and characterization:

BZLP glasses doped by varying concentration of Dy^{3+} ions in accordance with the molar composition $60P_2O_5$- (15-x)BaO -15ZnO -$10Li_2O$-xDy_2O_3 (x = 0, 0.1, 0.5, 1.0, 1.5 and 2.0 mol% named as PDY0, PDY1, PDY2, PDY3, PDY4 and PDY5 glasses, respectively) were prepared via melt quench approach. The process used to synthesize these phosphate glasses has

been depicted in Fig. 2.1 in chapter 2. Further, all the glasses were characterized through various techniques to check their suitability for photonic devices.

3.3. Results & discussion:

3.3.1. Structural analysis:

The XRD pattern recorded for an un-doped BZLP glass in angular range (10-70 degrees) has been depicted in Fig. 3.1. It shows a wideband rather than distinguish sharp peaks, which indicates the non-crystalline character of BZLP glass.

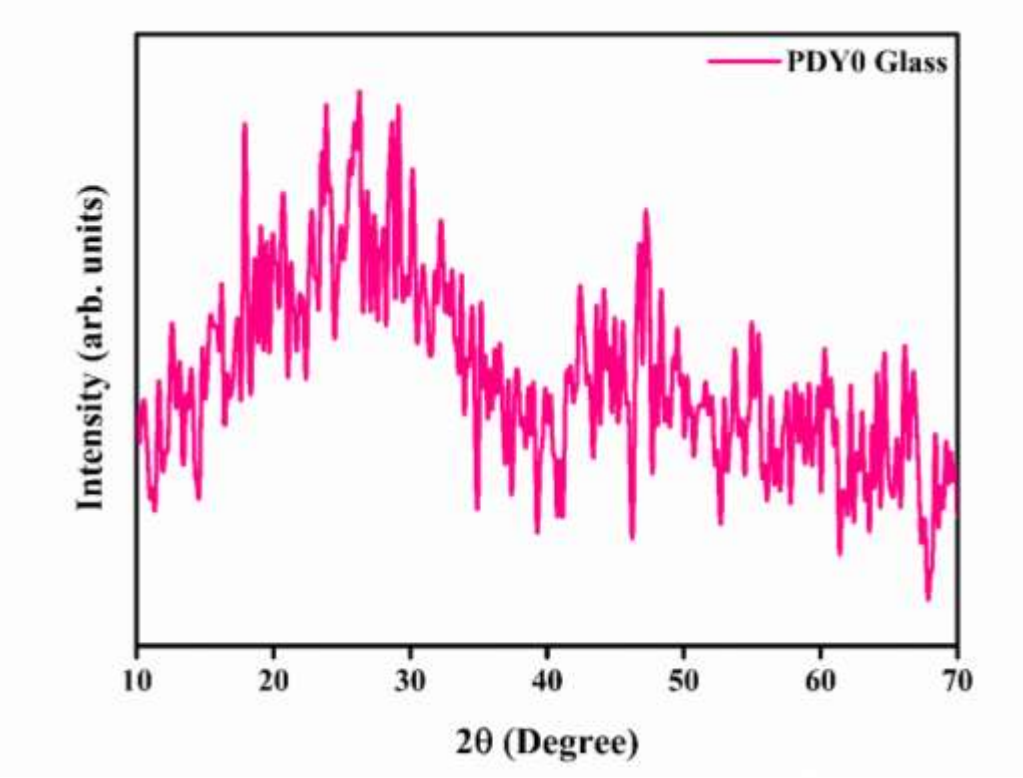

Fig. 3.1: *XRD pattern of an un-doped BZLP glass.*

3.3.2. Physical properties:

Several physical and optical characteristics for BZLP glasses were assessed using the relevant mathematical expressions given in the chapter 2 and shown in Table 3.1 It is noted for BZLP glasses, as the Dy^{3+} ions concentration is increasing from PDY1 (0.1 mol%) to PDY5 (2.0

mol%), substantial quantities such as density, mean atomic weight, molar volume, molar reflection, and field strength are increasing, while others such as refractive index, optical dielectric constant, reflection loss (R%), polaron radius, mutually distance between atoms (r_i), and electronic polarizability are reducing. Densities for BZLP glasses increases because the molecular weight of host compounds i.e., P_2O_5 (141.94 g/mol), ZnO (81.37 g/mol), BaO (153.33g/mol) and Li_2O (29.88g/mol) is lower than that of Dy_2O_3 (372.9 g/mol) which reveals the degree of structural closeness in BZLP glasses [121,122].

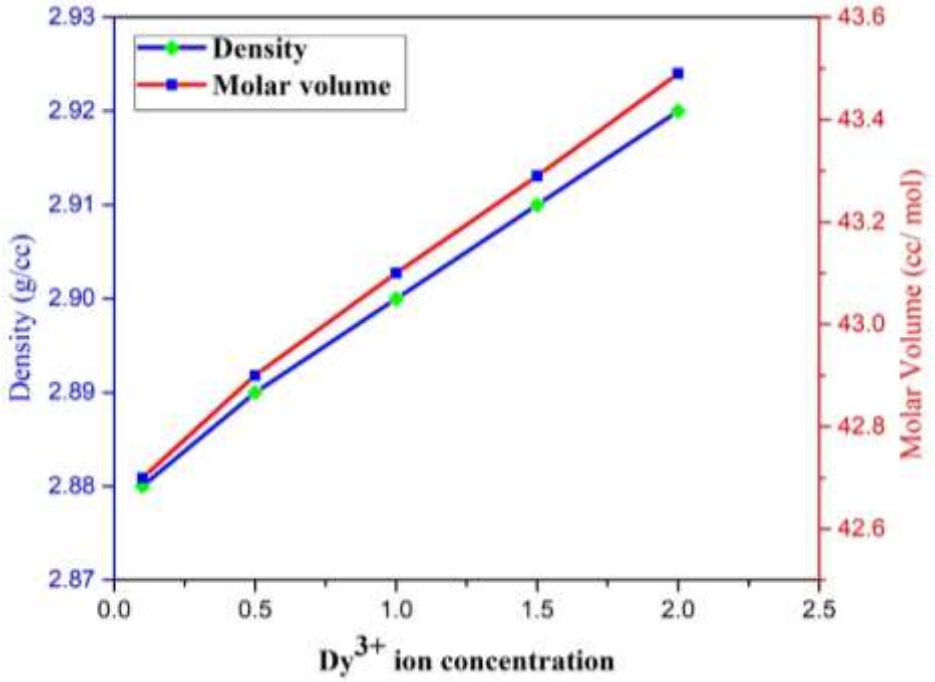

Fig . 3.2(a): *Density and molar volume variation with Dy^{3+} ions concentration in BZLP glasses.*

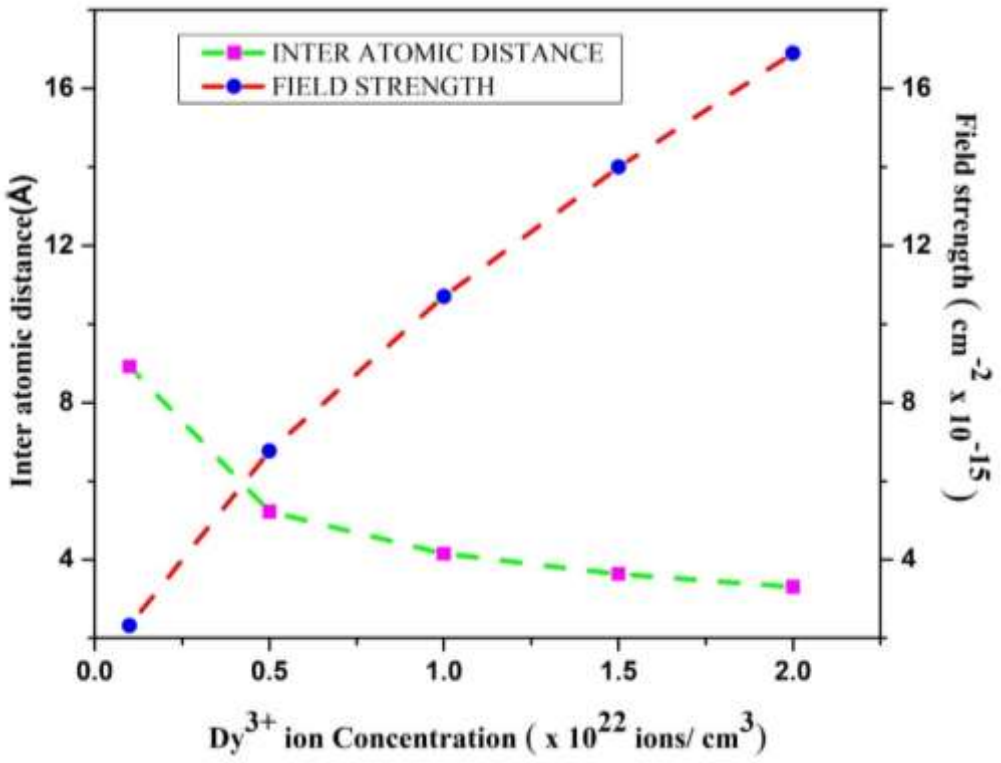

Fig . 3.2(b): *Variation of inter atomic distance and Field strength with Dy^{3+} ions concentration in BZLP glasses.*

The average molecular weight of BZLP glasses is also escalating due to the addition of Dy_2O_3 in the host glass. The variation of density and molar volume alongwith varying Dy^{3+} ion concentration in BZLP glasses is represented in Fig 3.2 (a). From Fig 3.2 (a), it is conspicuous that density and molar volume are surging as the concentration of Dy^{3+} ions increase. With increase in Dy^{3+} ions concentration, the number of dysprosium ions per unit volume also increases in host glass which intern leads to increase in molar volume and other physical properties. Furthermore, in the present work, alkaline earth oxide (Li_2O) is added to enhance the stability of glass network by bridging oxygen atoms with Dy^{3+} ions. The inter atomic distance decreases as the concentration of Dy^{3+} ions increase for the prepared glasses. The decrease in inter atomic distance results in the surge of Field strength. The interatomic distance and field strength shows inverse relationship with increase in the concentration of Dy^{3+} ions in

BZLP glass as shown in Fig 3.2(b). Comparatively, low values of Field strength for BZLP glasses represents the high solubility of Dy^{3+}ions in the host glass. Molecular electronic polarizability is another important physical property which relates optical, chemical and dielectric properties like UV absorption, ionic reflection and chemical stability. BZLP glasses with relatively low values of molecular electronic polarizability helps in increasing its stability.

Table 3.1 Various physical properties of Dy^{3+} ions in BZLP glasses.

S. No	Physical Property	PDY1	PDY2	PDY3	PDY4	PDY5
1	Refractive index (n_d)	1.60	1.60	1.59	1.599	1.59
2	Density (gm/cm^3)	2.88	2.89	2.90	2.91	2.92
3	Average molecular weight	123	124	125	126	127
4	Dy^{3+} ion concentration, N(10^{22} ions/cm^3)	0.14	0.70	1.39	2.08	2.77
5	Molar Volume (cc/mol)	42.70	42.90	43.10	43.29	43.49
6	Mean atomic volume (g/cm^3/atom)	8.36	8.38	8.39	8.41	8.42
7	Dielectric constant (ϵ)	2.56	2.56	2.55	2.55	2.55
8	Optical dielectric constant ($\epsilon - 1$)	1.56	1.56	1.55	1.55	1.55
9	Reflection losses (R %)	5.32	5.32	5.32	5.32	5.32
10	Molar refraction (R_m) (cm^{-3})	14.59	14.67	14.73	14.80	14.86
11	Polaron radius (r_p) (Å)	3.59	2.10	1.67	1.46	1.33
12	Inter-atomic distance (r_i) (Å)	8.92	5.22	4.15	3.63	3.30

13	Molecular electronic polarizability (10^{-23} cm^3)	5.79	1.16	0.58	0.39	0.29
14	Field Strength F ($X10^{15}cm^{-2}$)	2.32	6.77	10.7	14.0	16.9

3.3.3. Vibrational spectroscopy:

FT-IR spectrum recorded for an un-doped BZLP glass (PDY0) within 400-4000 cm^{-1} range has been depicted in Fig. 3.3. The FT-IR spectrum displayed in Fig. 3.3 show several peaks situated at 490, 789, 909, 1097,1290,1648, 2855, 2922 and 3465 cm^{-1}. The band at 490 cm^{-1} may be assigned due to bending of PO_2 vibrations and also tetrahedral bond stretching of Zn-O [123]. Other bands located at 789 cm^{-1} and 909 cm^{-1} may be attributed due to symmetric stretching (υ_s) and asymmetric stretching, (υ_{as}) of PO_2 connection of Q_1 tetrahedral and Q_2 tetrahedral respectively with non-bridging oxygen atoms [108,124]. The band at 1097 cm^{-1} may be due to asymmetric stretching of Q_2 tetrahedral vibrating in PO mode, υ_{as} ($P\text{-}O^-$) and may be resembled as linkage of P-O-Zn stretching band [125]. The band at 1290 cm^{-1} is ascribed due to stretching vibrations of P-O bonds in PO_4 units. The band at 1648 cm^{-1} is ascribed due to O-H bending vibrations integrated because of air present in making of KBr pellets for FT-IR characterization [126]. The band at 2855 cm^{-1} represents the presence of carbon contaminants [127]. The band observed at 2922 and 3465 cm^{-1} are on account of asymmetric and symmetric vibrations of the H_2O molecules respectively [128].

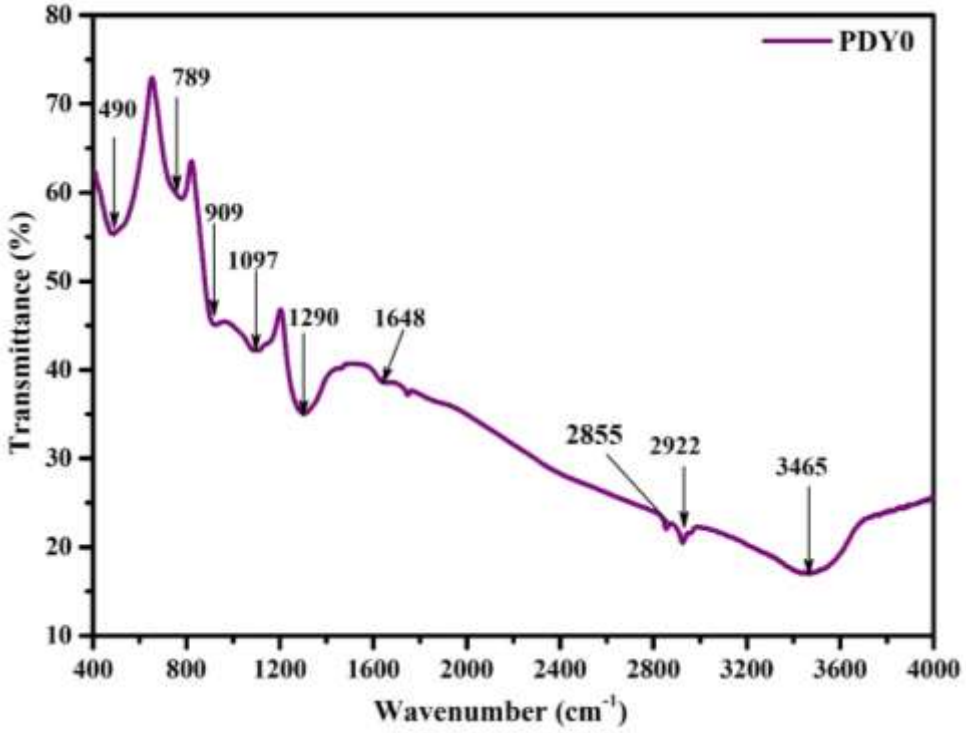

Fig. 3.3: *FT-IR spectrum of an un-doped BZLP glass.*

3.3.4. Absorption spectral analysis:

Absorption spectra of Dy^{3+} ions doped BZLP glasses recorded from 330-1850 nm wavelength range in UV-vis-NIR region is shown in Fig. 3.4. The spectra depicted in Fig. 3.4shows a series of dysprosium absorption peaks observed in UV, Visible, and NIR regions arising from its ground ($^6H_{15/2}$) to numerous higher energy states such as $^6P_{7/2}$, $^4I_{11/2}$ + $^6P_{3/2}$, $^4M_{19/2}$ + $^4K_{17/2}$, $^4G_{11/2}$, $^4I_{15/2}$, $^4F_{9/2}$,$^6F_{3/2}$, $^6F_{5/2}$, $^6F_{7/2}$, $^6F_{9/2}$ + $^6H_{7/2}$, $^6F_{11/2}$ +$^6H_{9/2}$ and $^6H_{11/2}$ at wavelengths of 351, 364, 386, 425, 452, 487, 753, 803, 900, 1095, 1278 and 1685 nm, respectively [129]. From Fig. 3.4**,** it is conspicuous that, the absorption bands observed in NIR region (spin allowed) are relatively stronger than the once observed in visible region (forbidden). Among various absorption transitions observed in NIR region, the one pertaining to $^6H_{15/2}$ to $^6F_{11/2}$ + $^6H_{9/2}$ detected at 1278 nm follows spin allowed rule $|\Delta S| = 0$, $|\Delta L| \leq 2$ and $|\Delta J| \leq 2$ and is highly intense than the other transitions.

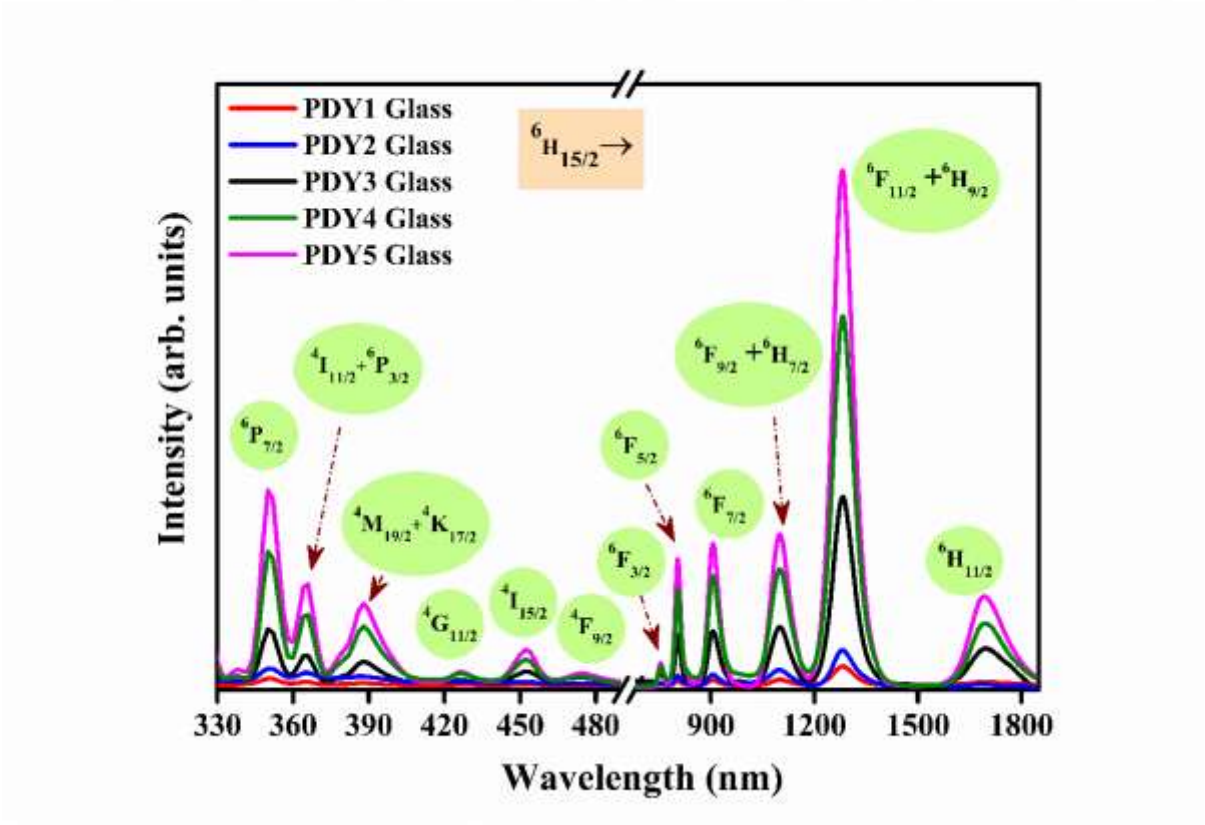

Fig. 3.4: *Absorption spectra of Dy^{3+} ions doped BZLP glasses in UV-vis- NIR region.*

The indirect optical band gap for Dy^{3+} ions activated BZLP glasses were assessed as per recorded absorption spectra with the help of relation given by Davis and Mott as follows [108]:

$$\alpha h\nu = B\left(h\nu - E_{opt}\right)^{n} \tag{3.1}$$

In the above relation, α denotes the absorption coefficient, $h\nu$ represents the incident photon energy, B signifies the band tailing parameter, E_{opt} indicates the energy bandgap. The value of parameter n describes the type of transition having values where n = ½ and n = 2 for direct and indirect allowed transitions, respectively. The E_{opt} values were acquired for indirect and direct optical transition using Tauc's plot by extrapolating the linear portion of the plot $(\alpha h\nu)^n$ versus $(h\nu)$ with n =1/2 and n= 2 [as presented in Fig 3.5 (a) & (b)] respectively. The estimated indirect E_{opt} Values were found to be 3.64, 3.53, 3.41, 3.56 and 3.76 eV for PDY1, PDY2,

PDY3, PDY4 and PDY5 glasses, respectively. Similarly the values for direct E_{opt}were 4.28, 4.33. 4.35,4.16 and 4.83 eV for respective glasses.

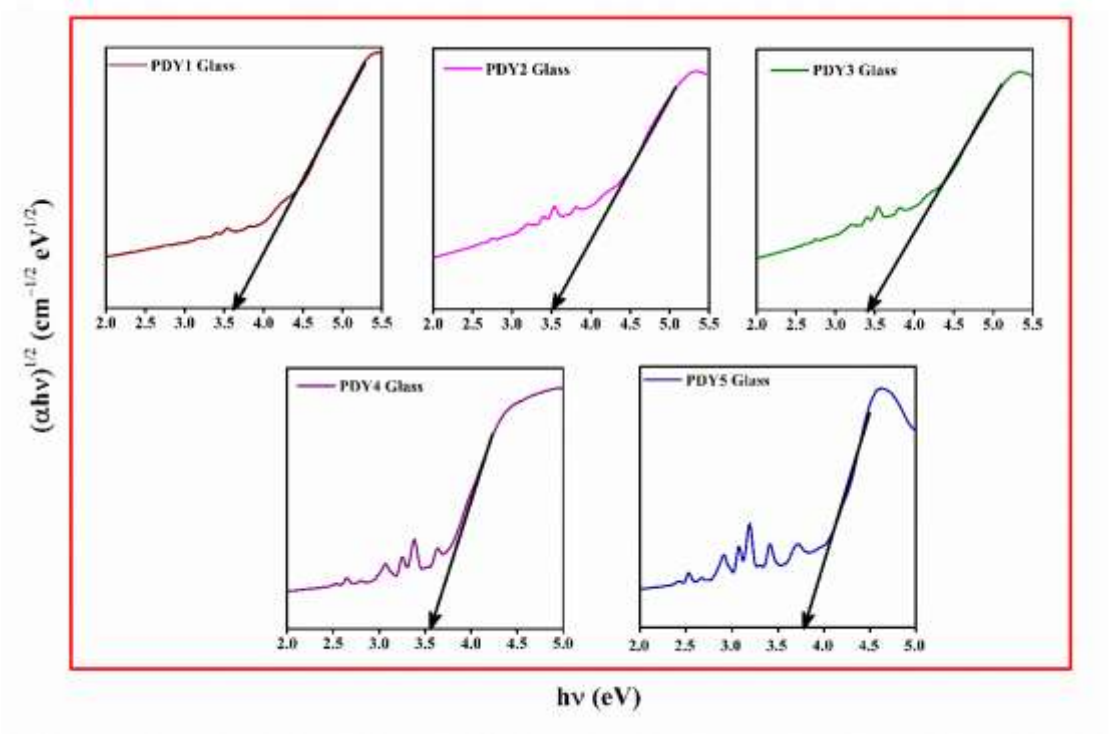

Fig. 3.5: (a) *Indirect bandgap plot for Dy^{3+} ions doped BZLP glasses.*

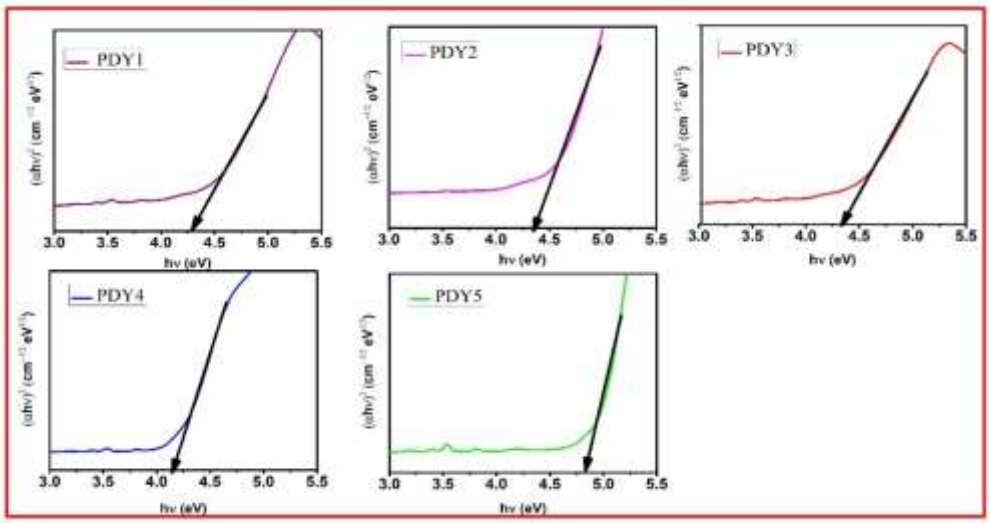

Fig. 3.5 (b): *Direct bandgap plot for Dy^{3+} ions doped BZLP glasses.*

Furthermore, in most of glassy materials, the fundamental absorption edges is identified by the degree of exponential tail. These absorption edges may arise due to inter-band transitions included tails of the localized states and followed by the Urbach rule [130]

The Urbach rule is explained by the following formula:

$$\alpha(\vartheta) = Cexp\left(\frac{h\vartheta}{\Delta E}\right) \tag{3.2}$$

Where C is constant, ΔE is the Urbach energy represents the width of band tails of localized states.The Urbach energies are evaluated by plotting a graph between ln ($\alpha h\vartheta$) versus $h\vartheta$ and then taking the inverse of the slope of plotted graph as shown in Fig 3.5 (c). The values of ΔE are decreasing (0.324, 0.316, 0.283, 0.280 and 0.239 eV) with increase in the concentration of the doped RE ion concentration from 0.1 to 2.0 mol%. Relatively lower values of ΔE indicates the minium defect present in host galss network.

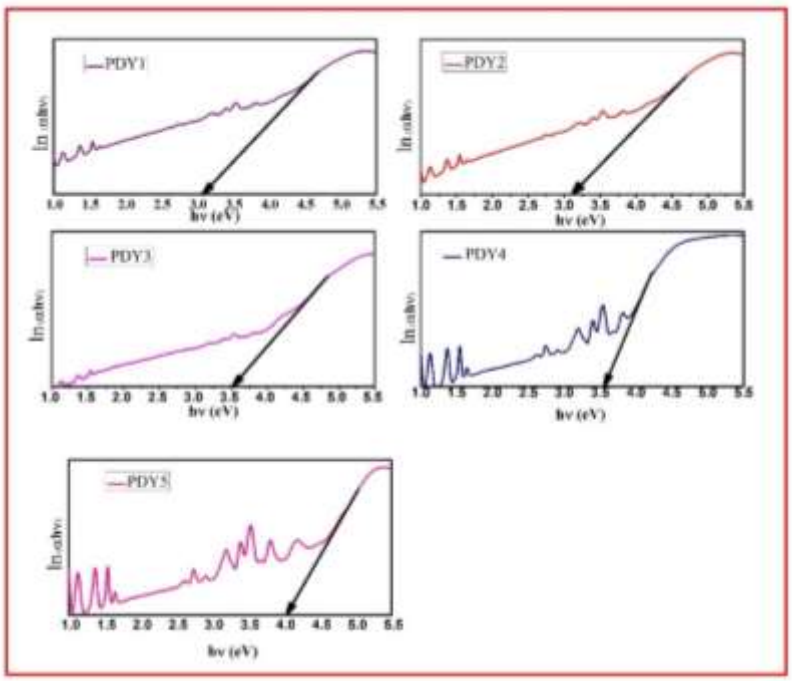

Fig. 3.5 (c): *Urbach energy plot for Dy^{3+} ions doped BZLP glasses.*

The nephelauxetic effect, an estimation of the covalent character of transition metal-ligand interaction in BZLP glass matrix will appear as of partially filled f shells. Electronic orbitals for 4f configuration are disfigured because Dy^{3+} ions are present in BZLP glass [131]. To get an idea about the bond linking in metal transition ions (Dy^{3+}) and nearby ligands, nephelauxetic ratio (β) and bonding parameters (δ%) were determined by using formula 1.6 & 1.7 given in Chapter 1 and are given in Table 3.2 [132]**.** The bonding nature of ligands around the RE ions is dependent on positive or negative values for δ**.** In Table 3.2**,** it was observed that δ has positive values, which represent covalent bonding is prominent in these glasses.

The experimental oscillator strength (f_{exp}) is a key parameter, which was used to know the radiative properties of BZLP glasses. The value of f_{exp} and f_{cal} were calculated using the equation 1.8 and 1.4 respectively given in chapter 1 and are shown in Table 3.2 along with bonding parameters and refractive index [133–135].

Table 3.2 Experimental (f_{exp}) (x10^{-6}), calculated (f_{cal}) (x10^{-6}) oscillator strengths, r.m.s deviation (δ_{rms}), nephelauxetic ratio ($\bar{\beta}$), bonding parameters (δ), and refractive index (n_d) for Dy^{3+} ions in BZLP glasses.

Transitions from $^6H_{5/2}\rightarrow$	**PDY1**		**PDY2**		**PDY3**		**PDY4**		**PDY5**	
	f_{exp}	**f_{cal}**	**f_{exp}**	**f_{cal}**	**f_{exp}**	**f_{cal}**	**f_{exp}**	**f_{cal}**	**f_{exp}**	**f_{cal}**
$^6P_{7/2}$	-	-	0.21	1.73	0.3	1.92	1.17	2.70	0.92	2.396
$^4I_{11/2} + {}^6P_{3/2}$	-	-	0.17	0.04	0.25	0.07	0.65	0.09	0.24	0.069
$^4M_{19/2} + {}^4K_{17//2}$	0.67	0.36	0.68	0.26	0.86	0.33	0.95	0.37	0.61	0.325
$^4G_{11/2}$	-	-	-	-	0.04	0.05	0.14	0.07	0.06	0.065
$^4I_{15/2}$	0.46	0.26	0.52	0.21	0.54	0.26	0.62	0.28	0.31	0.247
$^4F_{9/2}$	0.41	0.05	0.42	0.02	0.46	0.04	0.55	0.05	0.2	0.040
$^6F_{3/2}$	-	-	0.1	0.02	0.11	0.03	0.12	0.04	0.09	0.032
$^6F_{5/2}$	0.43	0.29	0.44	0.11	0.51	0.19	0.74	0.22	0.5	0.172
$^6F_{7/2}$	0.55	0.66	0.8	0.38	1.08	0.55	1.18	0.68	1.07	0.555
$^6F_{9/2}+{}^6H_{7/2}$	0.51	0.46	0.96	0.39	1.05	0.49	1.16	0.65	1.05	0.556
$^6F_{11/2}+{}^6H_{9/2}$	4.16	4.16	4.56	4.40	5	4.82	5.41	5.23	4.92	4.758
$^6H_{11/2}$	-	-	0.11	0.71	0.17	0.84	0.21	0.91	0.18	0.805
δ_{rms} (x 10^{-6})	±0.25		±0.55		±0.60		±0.62		±0.52	
n_d	1.600		1.600		1.599		1.599		1.599	
$\bar{\beta}$	0.996		0.995		0.994		0.994		0.993	
δ	0.38		0.49		0.53		0.59		0.61	

J-O theory is employed to compute the intensity parameters (Ω_2, Ω_4, Ω_6) through a method of least-squares fit, as per the formula given in the literature [134]. To measure the quality fit

between f_{exp} & f_{cal}, the rms deviation indicated by δ_{rms} can be estimated by using equation 1.5 given in chapter 1.

Comparatively less value of δ_{rms} is attained to justify the J-O theory in calculating J-O parameters and to know radiative properties of BZLP glasses. The J-O parameters (Ω_2, $\Omega 4$, $\Omega 6$) were computed by the method of least squares fit and were represented in Table 3.3 and compared with other glasses reported in literature [136–145]. Intensity parameters imitate a similar trend ($\Omega_2 > \Omega_4 > \Omega_6$) for BZLP glasses as given in the literature for other glasses [146–152].

Table 3.3 Judd-Ofelt parameters ($\Omega_\lambda \times 10^{-20} cm^2$) of Dy^{3+} ions in BZLP glasses along with various reported host glasses.

Glass System	$\boldsymbol{\Omega_2}$	$\boldsymbol{\Omega_4}$	$\boldsymbol{\Omega_6}$	Trend	References
PDY1	10.63	0.89	0.069	$\boldsymbol{\Omega_2 > \Omega_4 > \Omega_6}$	Present work
PDY2	11.24	1.18	0.27	$\boldsymbol{\Omega_2 > \Omega_4 > \Omega_6}$	Present work
PDY3	12.24	1.30	0.46	$\boldsymbol{\Omega_2 > \Omega_4 > \Omega_6}$	Present work
PDY4	12.87	1.83	0.53	$\boldsymbol{\Omega_2 > \Omega_4 > \Omega_6}$	Present work
PDY5	11.78	1.63	0.40	$\boldsymbol{\Omega_2 > \Omega_4 > \Omega_6}$	Present work
Lead Borosilicate	11.43	4.38	3.82	$\boldsymbol{\Omega_2 > \Omega_4 > \Omega_6}$	[148]

SKNPLDy1.0 (PW)	10.02	4.84	2.70	$\boldsymbol{\Omega_2 > \Omega_4 > \Omega_6}$	[149]
PZDy1.0	7.30	1.14	0.86	$\boldsymbol{\Omega_2 > \Omega_4 > \Omega_6}$	[150]
KPKlCaFDy	13.30	3.38	2.83	$\boldsymbol{\Omega_2 > \Omega_4 > \Omega_6}$	[151]
TeWLiK	12.70	8.202	1.827	$\boldsymbol{\Omega_2 > \Omega_4 > \Omega_6}$	[152]

The intensity parameter (Ω_2) presents the highest value for all BZLP glasses, which represents covalent character for metal-ligand and asymmetric of BZLP ions near Dy^{3+} ions. For BZLP glasses intensity of transition $^6H_{15/2}$ to $^6F_{11/2}$ + $^6H_{9/2}$ increases as Ω_2 increases, and vice versa. The prepared glasses show a value of Ω_2 rises from PDY1 to PDY4 glasses and drops for PDY5 glass. Among various prepared glasses, PDY4 glass has highest intensity for the hypersensitive transition and the lowest for PDY5 glass, which represents a higher symmetrical crystal structure of Dy^{3+} ions for PDY4 glass. Radiative parameters were calculated from intensity parameters such as A_R (radiative probability), β_R (luminescence branching ratio),τ_R (radiative lifetimes) as tabulated in Table 3.4. Required expressions for evaluating radiative properties were used from published literature [153].

Table 3.4 Transition probability (A_R) (s^{-1}), luminescence branching ratio (β_R), total transition probability (A_T) (s^{-1}) and radiative lifetime (τ_R) (μs) for the observed emission transitions of Dy^{3+} ions in BZLP glass.

Sample name	Transition	A_R	A_T	β_R	τ_R
PDY1	$^4F_{9/2} \rightarrow {}^6H_{11/2}$	16.49	1094.61	0.0151	913
	$^4F_{9/2} \rightarrow {}^6H_{13/2}$	824.28		0.7530	
	$^4F_{9/2} \rightarrow {}^6H_{15/2}$	109.91		0.1004	
PDY2	$^4F_{9/2} \rightarrow {}^6H_{11/2}$	36.02	1202.90	0.0299	
	$^4F_{9/2} \rightarrow {}^6H_{13/2}$	896.93		0.7456	831
	$^4F_{9/2} \rightarrow {}^6H_{15/2}$	116.89		0.0972	
PDY3	$^4F_{9/2} \rightarrow {}^6H_{11/2}$	52.30	1332.17	0.0393	750
	$^4F_{9/2} \rightarrow {}^6H_{13/2}$	991.13		0.7440	
	$^4F_{9/2} \rightarrow {}^6H_{15/2}$	126.79		0.0952	
PDY4	$^4F_{9/2} \rightarrow {}^6H_{11/2}$	64.15	1428.17	0.0449	700
	$^4F_{9/2} \rightarrow {}^6H_{13/2}$	1057.46		0.7404	
	$^4F_{9/2} \rightarrow {}^6H_{15/2}$	133.65		0.0936	
PDY5	$^4F_{9/2} \rightarrow {}^6H_{11/2}$	51.99	1297.93	0.0401	770
	$^4F_{9/2} \rightarrow {}^6H_{13/2}$	959.92		0.7396	
	$^4F_{9/2} \rightarrow {}^6H_{15/2}$	123.00		0.0948	

3.3.5. PL excitation, PL emission and radiative properties analysis:

PL properties of Dy^{3+} ion activated BZLP glasses have been recorded at room temperature. The recorded PL excitation spectrum recorded for PDY3 glass (1% mol Dy^{3+} ions) exhibits several peaks in range 300 -500 nm via monitoring the emission wavelength at 575 nm as illustrated in Fig. 3.6. The spectrum consists several excitation peaks at wavelength 322, 337, 350, 362, 386,

425, 449 and 473 nm, which arises due to transition from the lower energy level ($^6H_{15/2}$) to several higher energy states $^6P_{3/2}$, $^4I_{9/2}$, $^6P_{7/2}$, $^6P_{5/2}$, $^4I_{13/2}$, $^4G_{11/2}$, $^4H_{15/2}$ and $^4F_{9/2}$, of Dy^{3+} ions, respectively. The dominant transition was noticed at wavelength 350 nm, which is opted for recording the PL emission spectra for Dy^{3+} ions activated BZLP glasses.

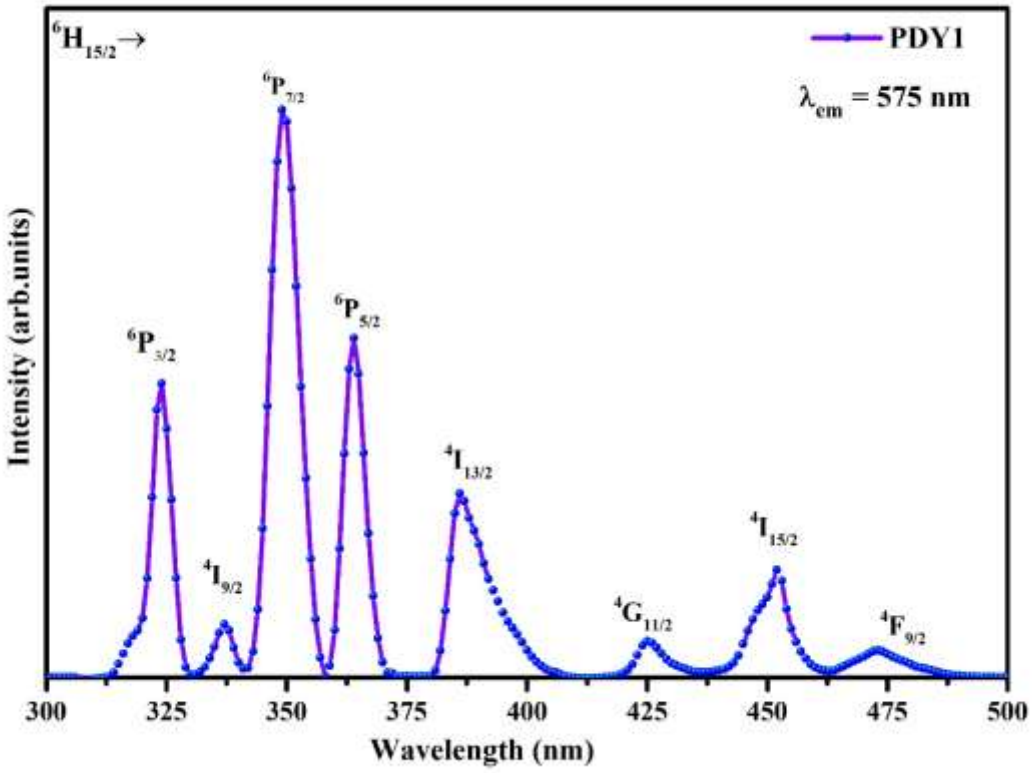

Fig.3.6: *Excitation spectrum of 1.0 mol% of Dy^{3+} ions in BZLP glasses under 575 nm emission wavelength*

The emission spectra recorded for Dy^{3+} ions activated BZLP glasses at an excitation wavelength of 350 nm were depicted in Fig.3.7. The PL spectra for all doped glasses have shown three peaks at 483, 575 and 663 nm due to transition from higher energy state $^4F_{9/2}$ to lower energy states at $^6H_{15/2}$, $^6H_{13/2}$ and $^6H_{11/2,}$ respectively. Amid these PL peaks, transition ($^4F_{9/2} \rightarrow {}^6H_{13/2}$)

was the most prominent as compared with other two transitions. The intense transition ($^4F_{9/2} \rightarrow {}^6H_{13/2}$) was electric dipole in nature, extremely affected by nearby Dy^{3+} ions and followed selection rule $\Delta L = \pm 2$, $\Delta S = 0$, $\Delta J = 0$ or ± 2. The ($^4F_{9/2} \rightarrow {}^6H_{15/2}$) transition was magnetic dipole (MD) in nature, which following $\Delta J = 0$ or ± 1 selection rules & insensitive to the glass host environment.

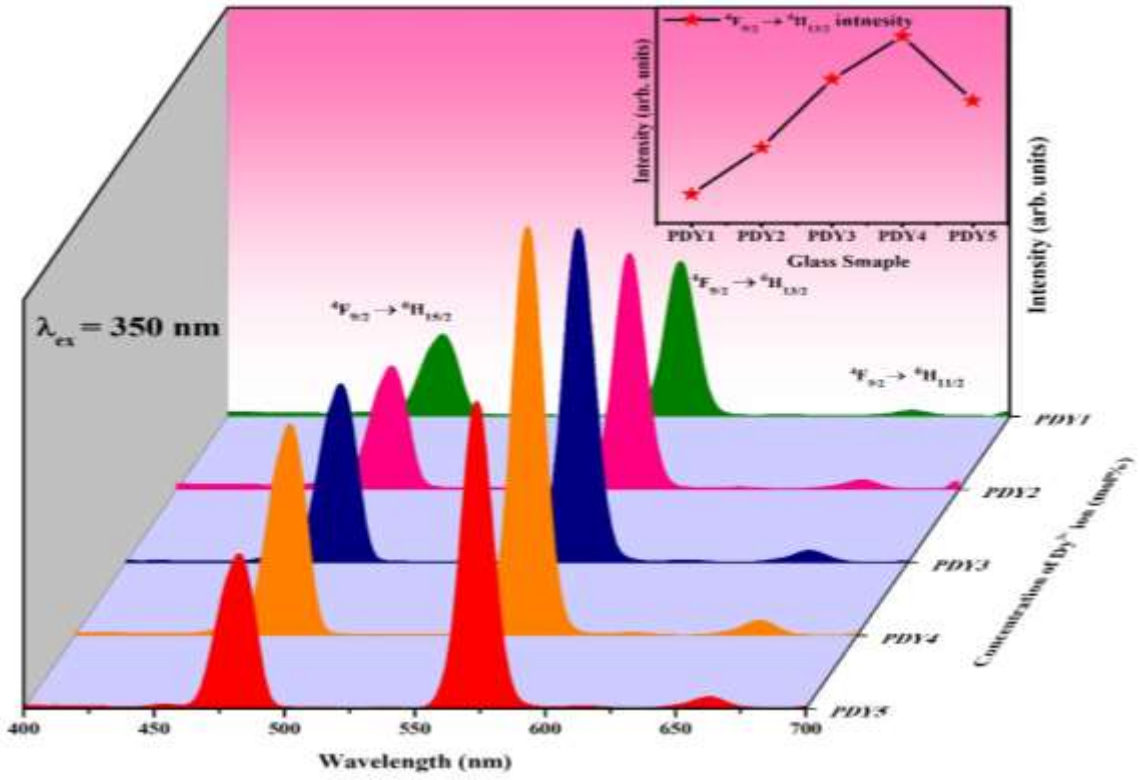

Fig. 3.7: *Emission spectra of Dy^{3+} ions in BZLP glasses monitored at 350 nm excitation wavelength. The inset plot shows the relative intensity variation of a most intense peak with different Dy-doped BZLP glasses.*

The yellow to blue (Y/B) intensity ratio is used to measure the rate of deformation in the glass matrix surrounded by Dy^{3+} ions and is also known as the asymmetry ratio. The ratio between yellow and blue PL peaks has been utilized as a tool to observe the configuration of radiant glass. The asymmetry ratio of RE i.e. (Dy^{3+}) ions that change with the configuration of glass.

The Y/B ratio is calculated for all the prepared glasses with the help of PL spectra and is tabulated in Table 3.7 In present studies, the Y/B ratio for all prepared glasses is greater than 1. From the inset plot of Fig.3.7**,** it can be perceived that the intensity of emission spectra gradually rises from PDY1 to PDY4 glass as the concentration changes from 0.1 to 1.5 mol% of Dy^{3+} ions and reduces for PDY5 glass. This decrement in intensity beyond 1.5 mol% of the doped ion is due to concentration quenching that took place by resonant energy transfer (RET) and mutual interactions between Dy^{3+}- Dy^{3+} ions that describes the self-quenching mechanism [8].

An energy level diagram depicted in Fig. 3.8 explains all processes such as excitation, emission, RET, and CR channels. Due to the small energy gap in the higher excited states above $^4F_{9/2}$, the non-radiative transitions take place and are therefore known as radiation-less relaxation energy levels. Such non-radiative relaxations ultimately populate the $^4F_{9/2}$ energy state and consequently radiative emissions starts occurring from $^4F_{9/2}$ energy state to $^6H_{15/2,}{}^6H_{13/2}$ and $^6H_{11/2}$ lower levels producing intense peaks at blue, yellow, and red color of the visible spectrum, respectively. The energy gap between $^4F_{9/2}$ and $^6F_{3/2}$ is sufficiently large (~6600 cm^{-1}) than the phonon energy of the host glass (~1300 cm^{-1}), and this leads to achieve intense luminous radiative transitions as shown in Fig.3.8 [154]. Fig. 3.8 also depicted the resonance energy transfer ($^4F_{9/2}+{}^6H_{15/2} \leftrightarrow {}^6H_{15/2} +{}^4F_{9/2}$) and possible cross-relaxation channels, CRC-1, CRC-2 and CRC-3 for as prepared glasses [137,155–158].

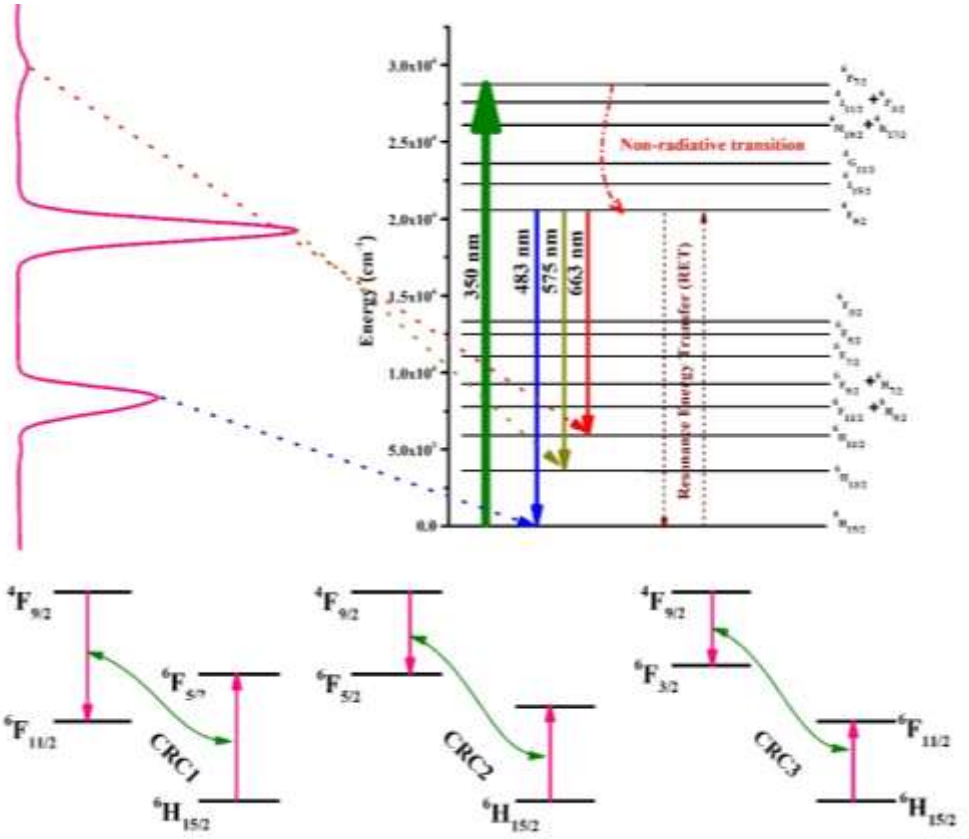

Fig. 3.8: *Partial energy level diagram showing absorption, excitation, emission and cross-relaxation mechanism for Dy^{3+} ions in BZLP glasses.*

To understand more about the utility of the titled glasses for laser and optoelectronic device applications, the PL spectra for Dy^{3+} doped BZLP glasses has been further used to estimate some radiative parameters like luminescence branching ratio (β_R), radiative transition probability (A_R), total transition probability (A_T) and radiative lifetime (τ_R) using relevant formulas that are given in the literature [159]. Stimulated emission cross-section (σ_{se}) is an important parameter used to know more about the lasing potentiality of a host matrix can be calculated by employing equation 1.13 in chapter 1. Radiative parameters A_R, β_R, and A_T calculated for Dy^{3+} doped BZLP glasses are tabulated in Table 3.4. Branching ratio is another crucial parameter for the designing of a laser. The higher value of $\beta_R \geq 0.5$ specifies the probability of achieving more stimulated emission for a particular transition. An important

parameter was the high value of stimulated cross section for obtaining high gain and identifying laser transitions of Dy^{3+} ions in host glass for various CW laser applications. Moreover, higher values of σ_{se} x $\Delta\lambda p$ (gain bandwidth) and σ_{se} x τ_R (optical gain parameters) have characteristics of good optical fiber and were listed in Table 3.5. The value of σ_{se} and β_R were highest for PDY4 glass related with $^4F_{9/2} \rightarrow {}^6H_{13/2}$ transition and similar to other reported values [160,161]. Further, it is observed that various radiative parameters as mentioned above have the highest values for PDY4 glass for its relatively intense transition $^4F_{9/2} \rightarrow {}^6H_{13/2,}$ which makes this glass suitable in solid-state lighting and lasing applications.

Table 3.5. Emission peak wavelength (λ_P)(nm), effective bandwidths ($\Delta\lambda_P$)(nm), measured and experimental branching ratios (β_R & β_{exp}), stimulated emission cross-sections (σ_{se}) (cm^2), gain bandwidth ($\sigma_{se} \times \Delta\lambda_P$) ($cm^3$) and optical gain parameter ($\sigma_{se} \times \tau_R$) ($cm^2$ s) parameters for the emission transitions for Dy^{3+} ions in BZLP glasses.

Spectral parameters	**PDY1**	**PDY2**	**PDY3**	**PDY4**	**PDY5**
$^4F_{9/2} \rightarrow {}^6H_{15/2}$					
λ_P	663	663	663	663	663
$\Delta\lambda p$	14.53	15.16	15.29	15.45	15.93
β_R	0.01	0.02	0.03	0.04	0.04
β_{exp}	0.02	0.02	0.02	0.02	0.02
σ_{se}	1.13	2.37	3.42	4.15	3.26
$\sigma_{se} \times \Delta\lambda_P$	1.65	3.60	5.23	6.42	5.20
$\sigma_{se} \times \tau_R$	1.03	1.97	2.56	2.91	2.51
$^4F_{9/2} \rightarrow {}^6H_{13/2}$					
λ_P	575	575	575	575	575

Δλp	13.22	13.18	13.33	13.36	13.37
β_R	0.75	0.74	0.74	0.74	0.73
β_{exp}	0.56	0.56	0.59	0.60	0.59
σ_{se}	35.32	38.53	42.10	44.84	40.66
$\sigma_{se} \times \Delta\lambda_P$	46.70	50.82	56.15	59.92	54.39
$\sigma_{se} \times \tau_R$	32.24	32.02	31.58	31.39	31.31
$^4F_{9/2} \rightarrow {}^6H_{11/2}$					
λ_P	483	483	483	483	483
Δλp	12.30	11.67	12.05	11.90	11.97
β_R	0.10	0.09	0.09	0.09	0.09
β_{exp}	0.35	0.35	0.36	0.34	0.34
σ_{se}	2.51	2.82	2.96	3.16	2.89
$\sigma_{se} \times \Delta\lambda_P$	3.10	3.29	3.57	3.77	3.47
$\sigma_{se} \times \tau_R$	2.30	2.34	2.22	2.21	2.23

3.3.6. Colorimetric properties:

The Commission International de I'Eclairage (CIE) coordinates were evaluated for Dy^{3+} activated BZLP glasses using PL spectra under wavelength 350 nm. CIE coordinates for PDY1 to PDY5 BZLP glasses were tabulated in Table 3.6. The CIE coordinates for optimizing glass i.e., PDY4 glass is (0.362, 0.391) as indicated in Fig. 3.9, which is placed in a white zone and nearby with a standard white light point (0.33, 0.33).

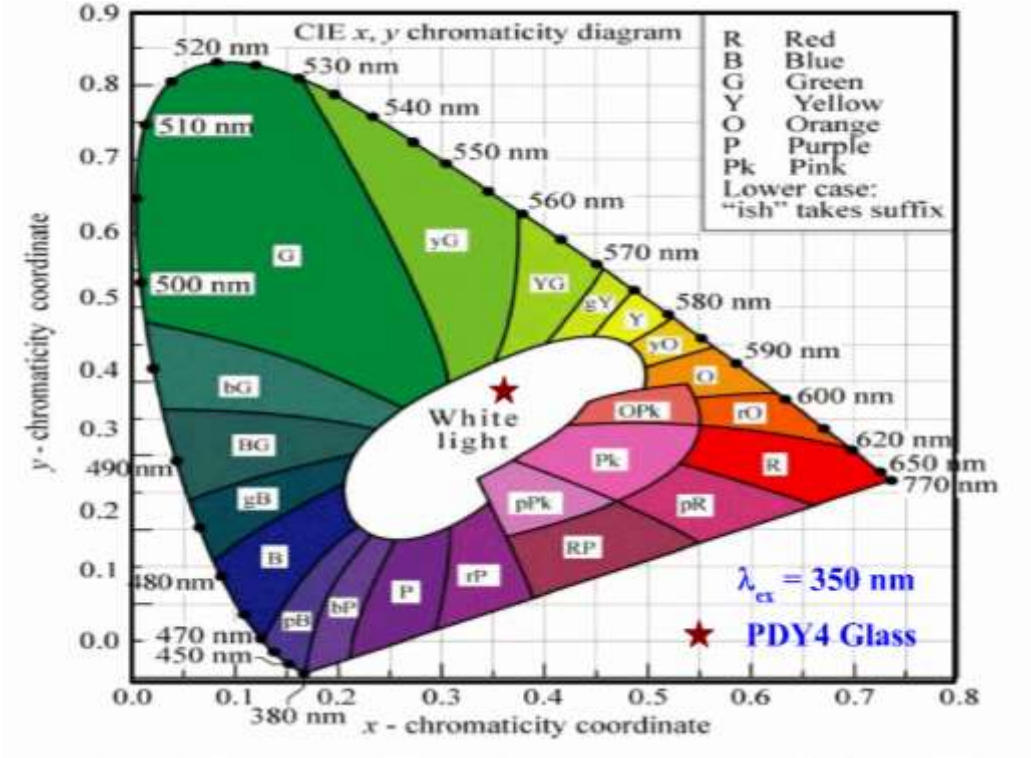

Fig. 3.9: *CIE chromaticity coordinates of 1.5 mol% Dy^{3+} ions in BZLP glass.*

One of the important parameters known as correlated color temperatures (CCT) is used to get familiar with the trait of emission. Moreover, it is specified as a black body Planckian radiator temperature, the color emitted by the Planckian radiator is nearly similar to the color emitted by the white light source. CCT is evaluated using the McCamy formula with the help of chromaticity coordinates in this manner:

$$CCT = -449\ n^3 + 3525\ n^2 - 6823.3n + 5520.33 \quad (3.3)$$

where, $n = \frac{(x-x_e)}{(y-y_e)}$ is inverse slope line and (x_e, y_e) (= 0.332, 0.186) is epicenter [162,163]. CCT values were evaluated for differing concentrations of Dy^{3+} doped BZLP glasses and represented in Table 3.6. The calculated values of are observed in the range 4000K–5000K specifically lie in the bright white region, which makes them reliable for visible lasers and lighting applications.

Table 3.6. CIE coordinates of Dy^{3+} ions in BZLP glasses

Name of the sample	CIE co-ordinates		CCT(K)
	X **co-ordinate**	***Y*** **co-ordinate**	
PDY1	0.354	0.412	4609
PDY2	0.356	0.40	4588
PDY3	0.361	0.394	4525
PDY4	0.362	0.391	4474
PDY5	0.372	0.414	4453

3.3.7. PL decay spectral analysis:

The PL radiative decay curves for highly intense peak $^4F_{9/2} \rightarrow {}^6H_{13/2}$ observed at 575 nm emission under 350 nm excitation were shown in Fig. 3.10. For the different concentration of Dy^{3+} ions, the PL decay profile curves are recognized as exponential in nature. The experimental lifetimes (τ_{exp}) for all the as prepared glasses were estimated by using the observed PL decay curves and tabulated in Table 3.7 along with radiative lifetime (τ_R) values. From Table 3.7, it has been noticed that the τ_{exp} values are smaller than τ_R. The variation in the observed data arises because of phonon energy transfer by the donors and interlinked between Dy^{3+} ions with OH vibrational bands available in prepared glasses [164].

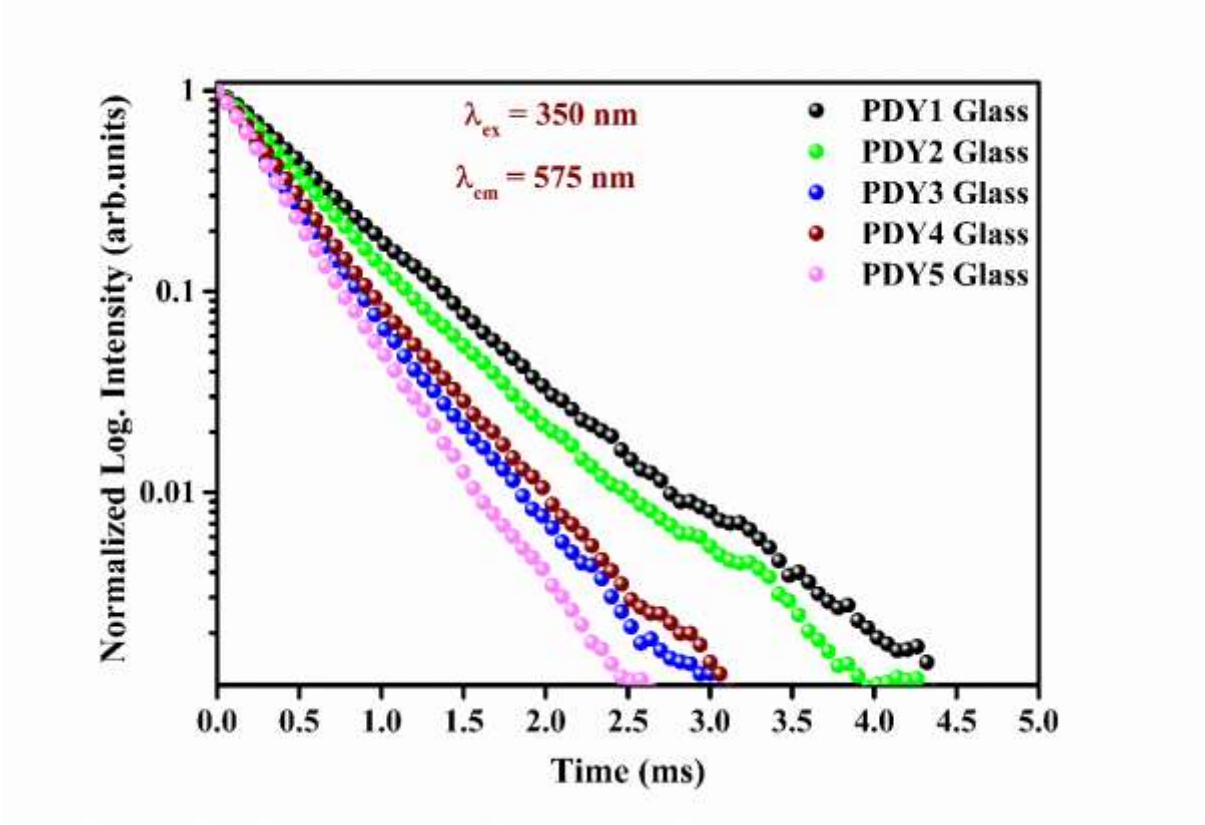

Fig. 3.10: *Decay profile of Dy^{3+} ions in BZLP glasses for $^4F_{9/2} \rightarrow {}^6H_{13/2}$ (575 nm) transition under 350 nm excitation wavelength.*

One more important parameter useful in understanding the lasing potentiality of the as prepared glasses is quantum efficiency (ɳ), which is defined as the ratio for output photons to input photons. Practically such ɳ value can be evaluated for the glasses under study by using the expression 1.14 given in chapter 1.

The calculated values of ɳ for all the titled glasses are given in Table 3.7. From the data appearing in Table 3.7, it is conspicuous that among all the glasses investigated in the present work, PDY4 glass is best suited for lasing action at 575 nm as it has relatively high ɳ value in

comparison with other glasses. The non-radiative energy transfer (W_{NR}) can be calculated by using the following formula:

$$W_{NR} = \frac{1}{\tau_{exp}} - \frac{1}{\tau_R} \quad (3.4)$$

The estimated W_{NR} values for the titled glasses are depicted in Table 3.7. Among all the titled glasses, PDY4 glass perceives relatively least W_{NR} value indicating its superiority in achieving more radiative emissions that other glasses. Glasses having relatively less W_{NR} values are more liable and prone to show high stimulated cross-section and quantum efficiency, which are essential for getting potential lasing action.

Table 3.7 Experimental lifetime (τ_{exp}) (μs), radiative lifetime (τ_R) (μs), quantum efficiency (η), Y/B ratio and non-radiative decay rates (W_{NR}) (s^{-1}), for Dy^{3+} ions in BZLP glasses.

Sample	τ_{exp} (μs)	τ_R (μs)	η (%)	Y/B	W_{NR}
PDY1	584	913	63	1.73	617
PDY2	565	831	67	1.88	566
PDY3	555	750	74	1.80	468
PDY4	536	700	77	1.86	437
PDY5	489	770	63	1.92	746

3.3.8. Temperature dependent PL (TD-PL) studies:

In the process of understanding the thermal stability of the optimized glass (PDY4), the TD-PL spectra has been recorded for it 575 nm under λ_{ex} = 350 nm and is shown in Fig. 3.11. The data plotted in Fig. 3.11 reveals that the PL intensity of Dy^{3+} ions in PDY4 glass is diminishing as

the temperature rises from room temperature (27 °C) to 200 °C. The PL intensity of all the peaks were reduced due to the thermal quenching on the luminescent characteristics. Clear analysis of the data shown in Fig.3.11 allows us to contemplate that PDY4 glass at 150 °C retains 85.34% of its intensity in comparison to its initial intensity. Further this values falls down to 75.49% at 200 °C. This data obtained from TD-PL spectra reveals that the optimized glass is having relatively high thermal stability.

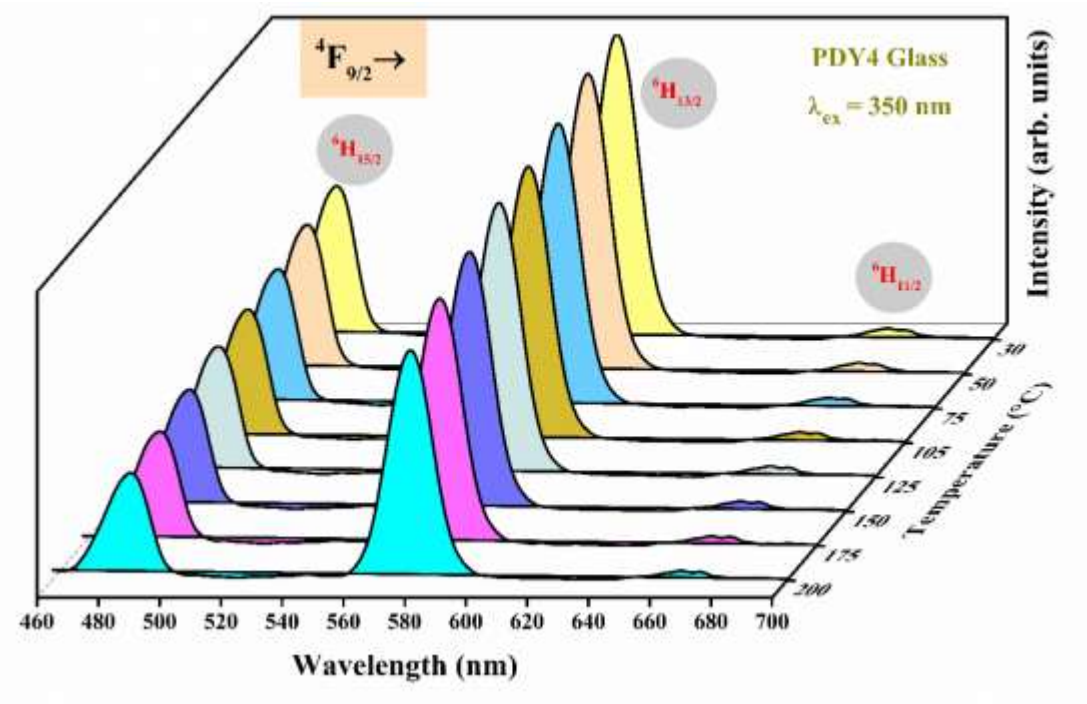

***Fig. 3.11**. Temperature-dependent PL spectra for 1.5 mol% Dy^{3+} ions in BZLP glass.*

Furthermore, the activation energy (ΔE_a) for the optimized glass has been evaluated using the expression given by the Arrhenius equation [165]:

$$I_T = \frac{I_0}{1+C\ exp\left(-\frac{\Delta E}{K_B T}\right)} \tag{3.5}$$

as per the expression I_0 and I_T indicate the PL intensity at room temperature and T (K) temperature, respectively. C signifies a constant and K_B signifies the Boltzmann constant. The linearly fitted graph between $\ln((I_0/I_T)-1)$ with $1/K_BT$ plot gives the slope value, which is equal

to the activation energy for the prepared glass as presented in Fig. 3.12. The ΔE value is found to be 0.159 eV for PDY4 glass which is less than the value already reported literature [166]. Thus, the TD-PL spectral data obtained for PDY4 glass showcases its superior nature in exhibiting excellent thermal stability.

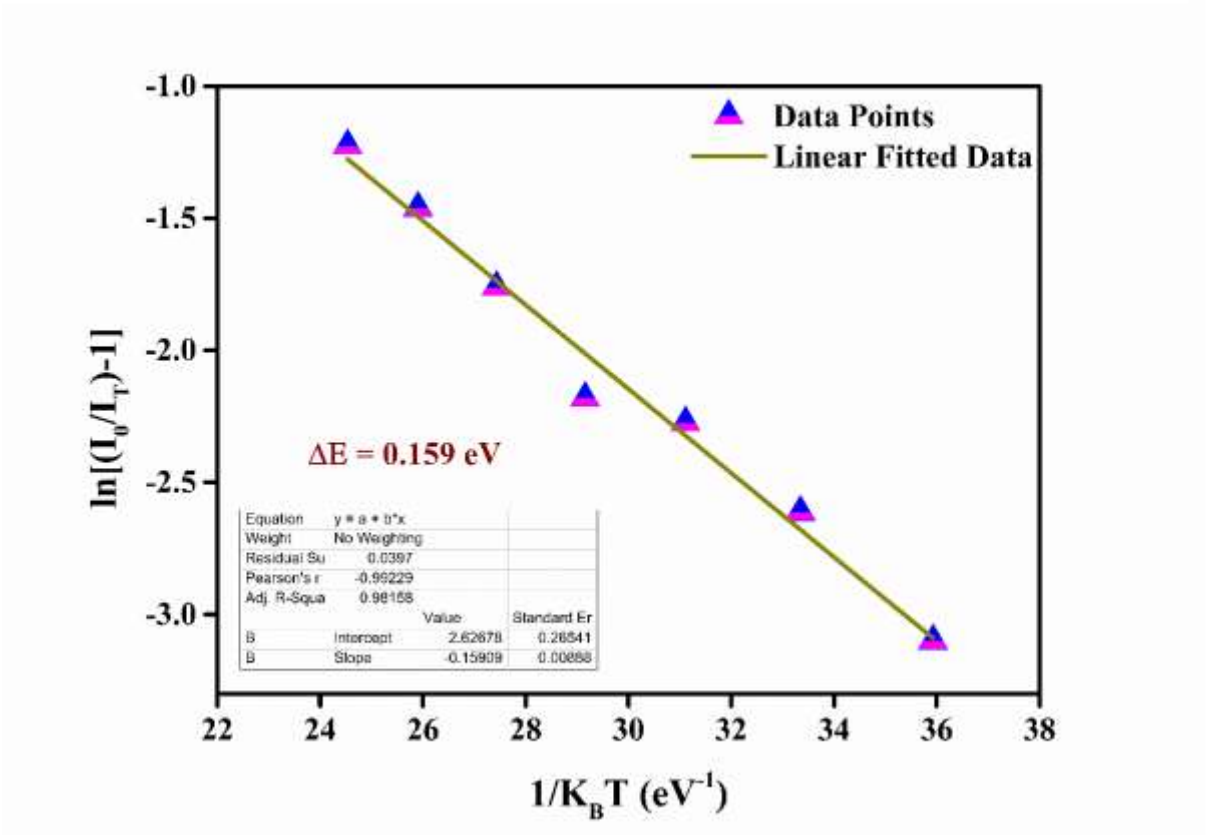

Fig. 3.12*. Graph between ln[(I$_o$/I$_T$)-1] and (1/K$_B$T) for 1.5 mol% Dy^{3+} ions in BZLP glass.*

3.4. Conclusions:

BZLP glasses with varying Dy^{3+} ions concentrations were prepared via melt quenching routes and studied their numerous spectroscopic characteristics to know its applicability in the visible photonic device applications. The non-crystalline nature of the un-doped BZLP glass is confirmed by the XRD pattern. From the FT-IR spectral recording several vibration bands were noticed in the as prepared un-doped BZLP glass and confirms the formation of various bonds.

Dy^{3+} activated BZLP glasses are effectively absorbing UV, visible and NIR radiation having the optical bandgap in the 3.64 - 3.76 eV range. Radiative properties of distinguished glowing levels of Dy^{3+} ions in BZLP glasses were measured through J–O parameters. The PL spectra of BZLP glasses reveal three sharp peaks, out of which yellow emission (575 nm) was the more intense as compared with blue, and red emission under 350 nm excitation wavelength. The decay curves show the exponential in nature. The calculated CIE coordinates are in good approximation with standard white light points (0.33, 0.33) of equal energy and lie in the visible region. The values of CCT of BZLP glasses fall in the bright white light and make them suitable for w-LEDs. Relatively high activation energy obtained for PDY4 glass from the recorded TD-PL spectrum reveasls excellent thermal stability for it. From the various calculated radiative parameters especially quantum efficiency and stimulated emission cross-section, it was summarized that among various Dy^{3+} activated BZLP glasses, PDY4 glass (BZLP glass with 1.5 mol% of Dy^{3+} ion concentration) is quite suitable for the fabrication of visible photonic devices such as yellow lasers and w-LEDs.

CHAPTER 4

Down-shifting photoluminescent properties of Tb^{3+} doped phosphate glasses for intense green-emitting devices applications

Tb^{3+} doped BZLP glasses were prepared via melt-quenching route and investigated thoroughly using spectroscopic techniques such as XRD, UV-VIS absorption and PL to explore their utility in visible photonic device applications. The information pertaining glass transition temperature, melting temperature and thermal stability were understood by using recording the differential scanning calorimetry (DSC) spectrum for an un-doped BZLP glass. The total weight loss during the glass composition melting process was analyzed using thermo gravimetric curves. The UV spectral information recorded for the titled glasses reveal the optical bandgap falling in the range from 4.57 to 4.19 eV. The prepared Tb^{3+} doped BZLP glasses exhibit intense green emission along with relatively less intense blue, yellow and red peaks under 373 nm excitation. In the resultant PL spectra, the emission intensity increases with the activator concentration of Tb^{3+} ions from 0.5 to 5.0 mol%. The estimated CIE chromaticity coordinates falling in the green region reveals the aptness of the titled glasses as a green constituent in visible photonic devices. The PL decay curves show the bi-exponential behaviour with an average decay time of 2-3 ms. The temperature-dependent PL profile shows fewer changes in spectra and has a relatively high activation energy value, confirming the high thermal stability. Various results obtained for Tb^{3+}doped BZLP glasses finally reveal their usage as a green emitter needed to fabricate w-LEDs and other green emitting photonic device applications.

4.1. Introduction:

Over the last few decades, the fabrication of rare-earth (RE) activated inorganic glasses have received lot of attention because of their significant role in the advancement of photonic devices and their applications[24,36,167,168]. Furthermore, RE doped glasses have specific properties such as high luminous efficiency, thermal resistance, chemical stability, extended durability, low production cost, and many more, which can position them as a critical player in the field of science and technology [64,168]. These different properties of RE doped glasses are required in many sectors and multiple advantageous applications to build sophisticated display devices, variable power lasers, solar cells, optical fibers, waveguides, optical memory systems, advanced lighting devices, sensors, and so on [40,46,169,170]. Modern lighting devices, such as white light emitting diodes (w-LEDs), are replacing traditional and long-lasting illuminating systems. The RE doped glasses are one of the utmost promising materials for fabricating w-LEDs since they can overcome the disadvantages of phosphor materials, do not require organic epoxy resins, and have no aging effects. [171]. Furthermore, the RE activated glasses act as an appropriate wavelength converters as well as an encapsulant in the fabrication of w-LEDs [172]. The luminescent features of the RE doped glasses depend not only on the RE ions but also on the host matrix that provides a crystal field environment to the RE ions. As a result, selecting a glass host matrix is equally important along with the choice of a particular RE ion for the designated applications. Out of many host glass matrices, the phosphate glass host offers outstanding features such as high thermal stability, reduced melting point, thermal resistance, chemical durability, high transparency and many more. These unique properties of phosphate glasses motivated us to explore more about them [173–176]. An alkaline oxide, such as BaO, can be used as a network modifier in phosphate glass formers, forming non bridging oxygen groups and lowering the melting temperature of the glass host [177,178,179]. Adding alkali

oxides helps to minimize the non-radiative losses that lead to the enhancement of the luminescence characteristics. Furthermore, alkali oxides such as lithium oxide added to a phosphate glass increases the transition temperature. The only setback with phosphate glasses is its hygroscopic nature which can be mitigated considerably by adding zinc oxide to it. Addition of ZnO can modify P-O-P to P-O-Zn bonds and improves moisture resistant characteristics [36,180]. All the aforementioned special characteristic features owned by the constituent chemical substances such as BaO, ZnO, Li_2O and P_2O_5 motivated us to synthesize barium zinc lithium phosphate (BZLP) glass system doped with distinct RE ions to understand the suitability of the BZLP host glass for numerous photonic device applications.

The desired luminescence characteristics of Lanthanide ions in tri/divalent states show the different energy states in UV to the IR region of the electromagnetic spectrum, making available a broad range and producing visible lasers and other photonic device applications. In lanthanides ions, mostly a sharp excitation and sharp radiative emission ($f - f$ transitions) were perceived due to the partially filled $4f$ shells shielded by $5s^2 5p^6$ orbitals [181]. The highest effective green emitting PL ingredient among the RE ions was found when the host was activated with Tb^{3+} ions. The PL properties of Tb^{3+} ions in the host were determined by $^5D_4 \rightarrow {}^7F_j$ transitions, which were affected by the amount of Tb^{3+} ions doped, the composition of the surrounding host, and the pumping wavelength [181,182]. Long lifetime, high quantum efficiency, and narrow emission spectral width can make Tb^{3+} ions contained molecules more suitable for many distinctive applications such as biological probes, green color components in displays, sensors, thermos luminescent dosimeters, field emission displays, and other photonic devices [183-185]. Many researchers have recently investigated Tb^{3+} doped glasses for luminous device applications.

Due to the distinctive optical characteristics and direct applicability of RE induced glassy systems in diversified areas, Tb^{3+} doped BZLP glasses have been prepared and studied for its spectroscopic properties. UV-vis absorption, luminescence properties and lifetime profiles were used to distinguish the suitability of the Tb^{3+} incorporated BZLP glass for appropriate w-LEDs and luminescent devices applications.

4.2. Experimental section:

4.2.1. Synthesis:

Tb^{3+} ion doped BZLP glass samples have been synthesized using melt quenching process with molar composition given below:

$$60P_2O_5\text{-}15ZnO\text{-}(15\text{-}m)\ BaO\ \text{-}10Li_2O: mTb_4O_7$$

where m = 0.5, 1.0, 1.5, 2.0, 2.5, 3.0, 3.5, 4.0, 4.5 and 5.0 mol% in BZLP glasses abbreviated as $PZBaLTb_{0.5}$, $PZBaLTb_{1.0}$, $PZBaLTb_{1.5}$, $PZBaLTb_{2.0}$, $PZBaLTb_{2.5}$, $PZBaLTb_{3.0}$, $PZBaLTb_{3.5}$, $PZBaLTb_{4.0}$, $PZBaLTb_{4.5}$ and $PZBaLTb_{5.0}$ respectively. Here m signifies the doping content of Tb^{3+} ions.

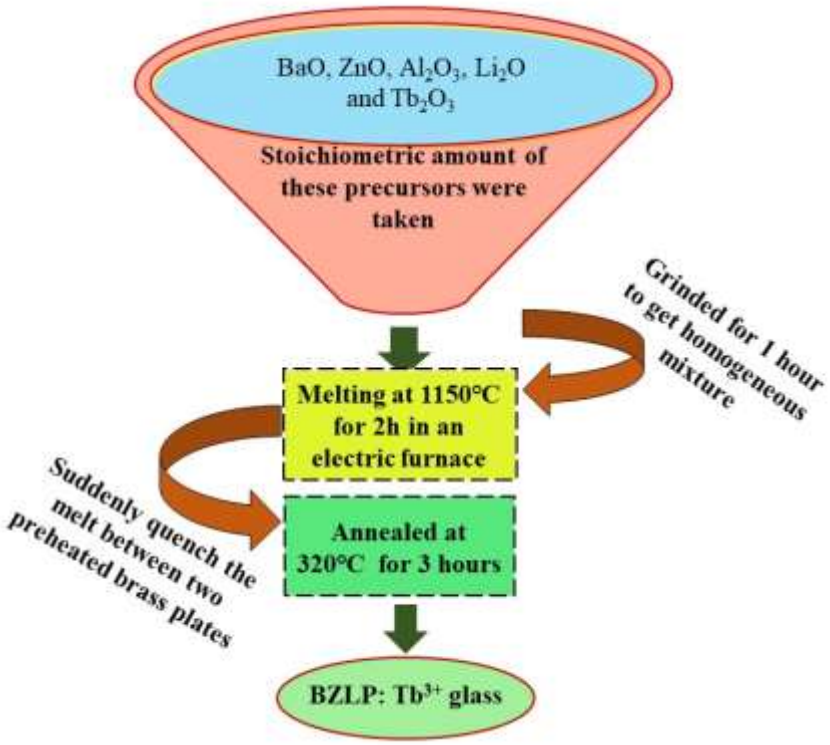

Fig.4.1: *Schematic diagram of a melt-quenching technique*

Fig. 4.1 indicates the steps followed to prepare the aforementioned glasses through most commonly used melt quenching technique. The transparent and uniformed glasses were obtained and ready for further characterizations at ambient temperature.

4.2.2. Characterization:

The density of the as-prepared glasses has been calculated using Archimedes' principle in the distilled water medium. DSC-TGA data were recorded in the range of 50-1300°C by DSC/TGA real-time instrument (SETARAM, Labsys Evo). XRD has been done to confirm the glassy nature of the titled glasses (D8 advance, Bruker). The absorption spectral studies have been done via spectrophotometer (JASCO, V-770). Photoluminescence excitation and emission spectra were recorded via Spectro fluorophotometer (JASCO, 8300 FP) at 300 K. The lifetime measurements were investigated via spectrophotometer (Horiba, Fluorolog-3). The

temperature-dependent PL (TD-PL) studies have been performed using a spectrophotometer (FLAME- S-XR1-ES, Ocean optics) with a heating sample assembly.

4.3. Results and discussion:

4.3.1. DSC/TGA analysis

The DSC curve for the un-doped BZLP glass has been plotted in the range of 50-1300°C, as presented in Fig.4.2. It contains various endo as well as exothermic peaks. The values of glass melting, peak crystallization, onset crystallization and transition temperature were found to be T_m = 1193 ℃, T_p = 226 ℃, T_c = 179 ℃, and T_g = 157 ℃, respectively. The thermal stability of the as-prepared glass composition can be analyzed on the basis of temperature difference (ΔT) and thermal stability parameter (S). These two critical parameters can be estimated by using the following expressions [182,183].

$$\Delta T = T_p - T_g \tag{4.1}$$

$$S = \frac{(T_p - T_c)(T_c - T_g)}{T_g} \tag{4.2}$$

The ΔT value signifies the range of temperature where the material can endure crystallization through any type of heat treatment. Here it was found to be 69℃ which is relatively higher than the other reported values [183]. Such a significant value reveals that the as-prepared glass is thermally stable. Furthermore, the value of S was found to be 6.58. Also, the endothermic peak observed at 1193°C indicating the melting temperature of the glass composition, which is used for glass preparation. Based on the observed values of ΔT and S, the un-doped BZLP glass may be considered a good host for photonic device applications. The two stages of weight loss in TGA curve plotted for an un-doped BZLP host glass and shown in Fig 4.3. The first weight loss was observed between 50-600°C and the corresponding loss was found to be 21.38 %, owing to water molecules and ammonia.

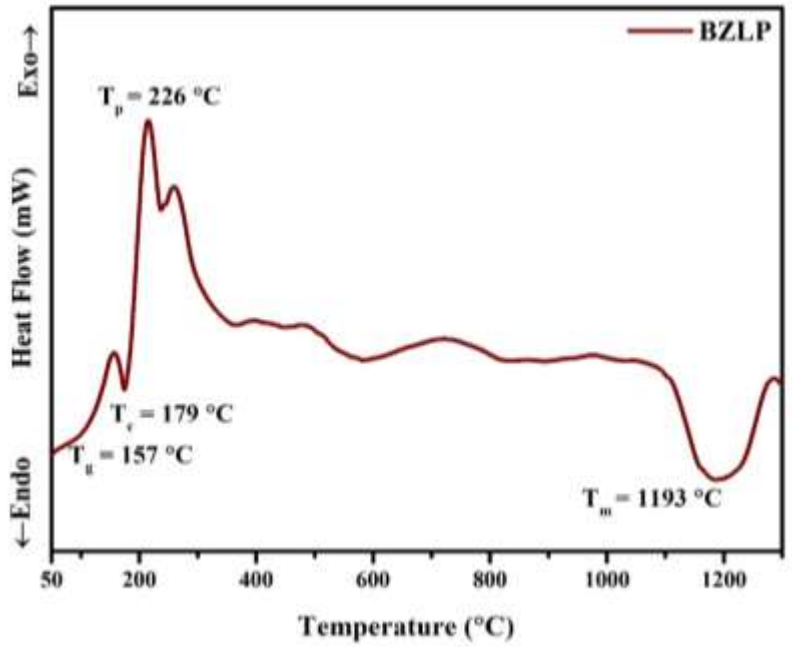

Fig. 4.2: *DSC curve for un-doped BZLP glass.*

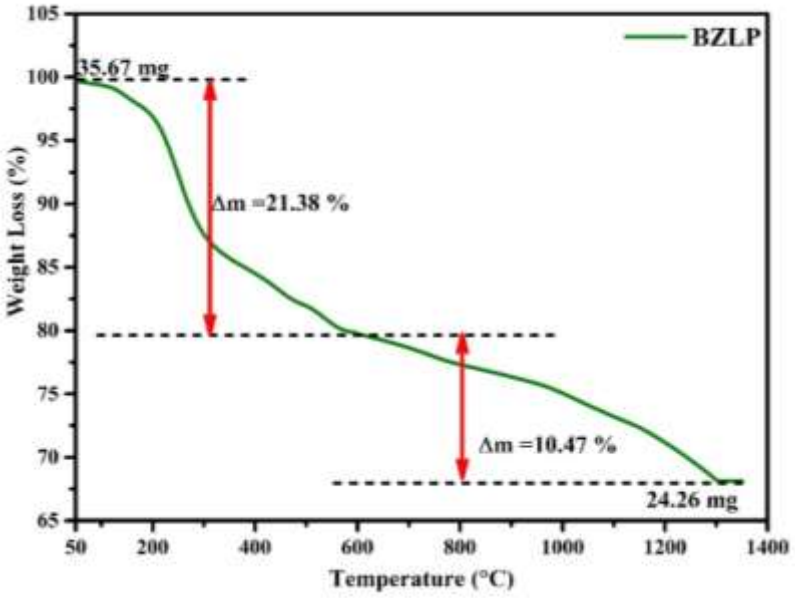

Fig. 4.3: *TGA curve for un-doped BZLP glass.*

It means the reaction happening is an exothermic reaction. This is in the correlation with the outcomes of the DSC curve. The second stage of the weight loss at 600°C ascribed because of the release and decomposition of CO_2 gas, which was found to be 10.47 %. Initially, we have taken a sample amount is 35.67 mg, which is homogeneously mixed. After heating it to 1300 °C, the remaining sample is 24.26 mg. Hence, a total of 68.15 % of the weight remained after the preparation of BZLP glass.

4.3.2. Physical properties:

The density of Tb^{3+} doped BZLP glasses was determined based on the experimental approach. Several physical parameters were estimated including average molecular weight, molar reflection and refraction losses (R), dielectric constant (ϵ), electronic polarizability (e) and optical electronegativity (χ_{opt}) by following the expressions from already published papers [184]. The increase in Tb^{3+} ions concentration increases the value of refractive index (n) and density (d) in BZLP glasses. A heavy weight of Tb_4O_7 responsible for an increase in the molecular weight of the glass samples, which could explain the increase in density. By linking the oxygen atom to Tb^{3+} ions in BZLP glasses, the incorporation of Li_2O in our host matrix produces non-bridging oxygen's and helps to improve the network stability. In addition, the inter-ionic radius (r_i) and the polaron radius (r_p) of the as-synthesized BZLP glasses decrease with the Tb^{3+} ion content. All these physical parameters have been depicted in Table 4.1.

Table 4.1. Physical parameters of Tb^{3+} doped BZLP glasses.

Physical Property	PZBaL $Tb_{0.5}$	PZBaL $Tb_{1.0}$	PZBaL $Tb_{2.0}$	PZBaL $Tb_{3.0}$	PZBaL $Tb_{4.0}$	PZBaL $Tb_{5.0}$
Refractive index (n_d)	2.06	2.12	2.13	2.13	2.14	2.14
Density (gm/cm^3)	3.02	3.04	3.20	3.21	3.26	3.33
Average molecular weight	211.51	214.47	220.41	226.35	232.30	238.24
Tb^{3+}ion concentration N (10^{22} ions/cm^3)	0.4278	0.8691	1.7254	2.5424	3.3276	4.0823
Polaron radius (r_p) (Å)	2.4836	1.9602	1.5467	1.3703	1.2453	1.1705
Inter-atomic distance (r_i) (Å)	61.6329	48.6232	38.736	34.0098	31.1092	29.0502
Optical band gap (eV)	4.57	4.38	4.32	4.27	4.21	4.19
Dielectric constant (Ɛ)	4.2759	4.4106	4.4549	4.4926	4.5387	4.5538
Optical dielectric constant (Ɛ-1)	3.2759	3.4106	3.4549	3.4926	3.5387	3.5538
Molar refraction (R_m) (cm^{-3})	18.493	19.098	19.382	19.656	19.723	19.784
Reflection losses (R %)	6.883	7.418	7.487	7.522	7.582	7.698

The increase in field strength (F) signifies that the bond strength between Tb and O is increasing, and tri-borate units are converting into tetra-borate units [185]. With an increase in Tb^{3+} ions concentration, some more parameters such ε and R are also increasing. The variation in all these physical parameters tells the behaviour of the as-prepared glass with change in concentration of RE ions.

4.3.3. Structural analysis:

XRD was performed to confirm the glassy nature of the titled glasses. The XRD patterns investigated for all (un-doped as well as doped) glasses are the same, so we have shown the XRD pattern of $PZBaLTb_{5.0}$ glass only in Fig. 4.4. It has only a large hump about an angle of 28ºC without any solid crystalline peak, which discloses the non-crystalline and glassy characteristics of the as-prepared glasses.

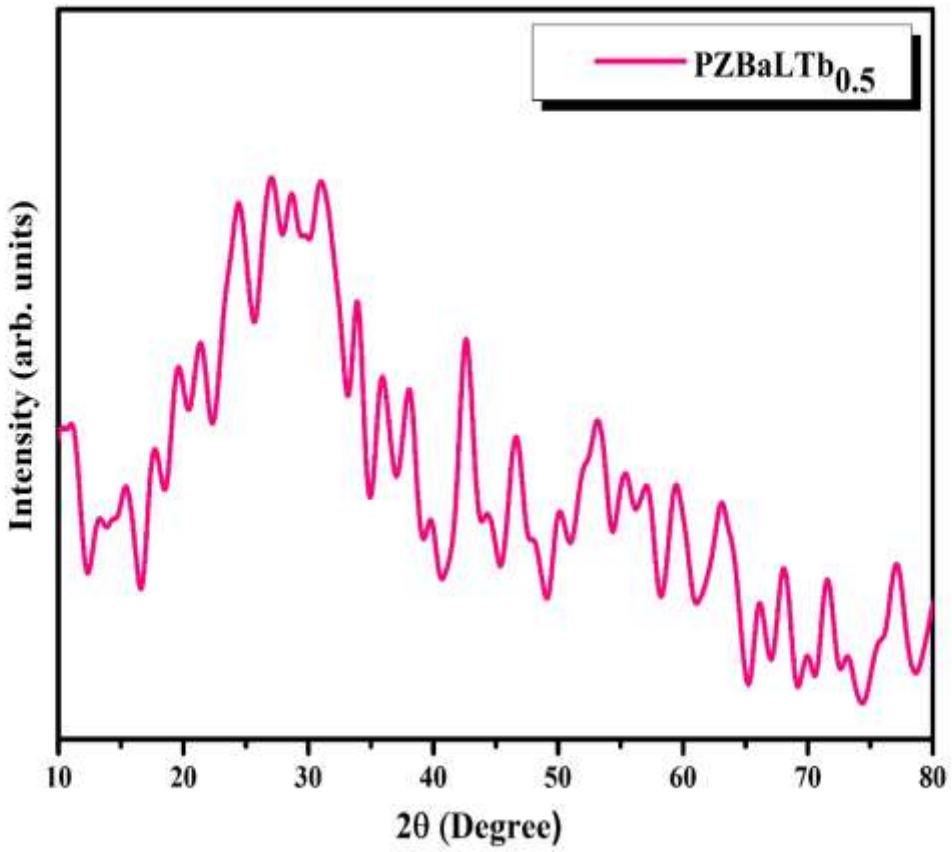

Fig. 4.4: *XRD pattern of 5.0 mol% Tb^{3+} doped BZLP glass ($PZBaLTb_{5.0}$).*

4.3.4. Absorption properties of glass:

Fig. 4.5 illustrates the absorption spectra recorded for Tb^{3+} doped BZLP glasses in the range of 250-500 nm. It consists eight peaks at 284, 302, 318, 339, 350, 370, 379 and 484 nm related to f-f transitions of Tb^{3+} ions based on the Carnall report [186]. The electric dipole-induced transitions followed the selection rule $|J| \leq 6$, whereas the magnetic dipole-induced transition followed $|J|=0, +1$.

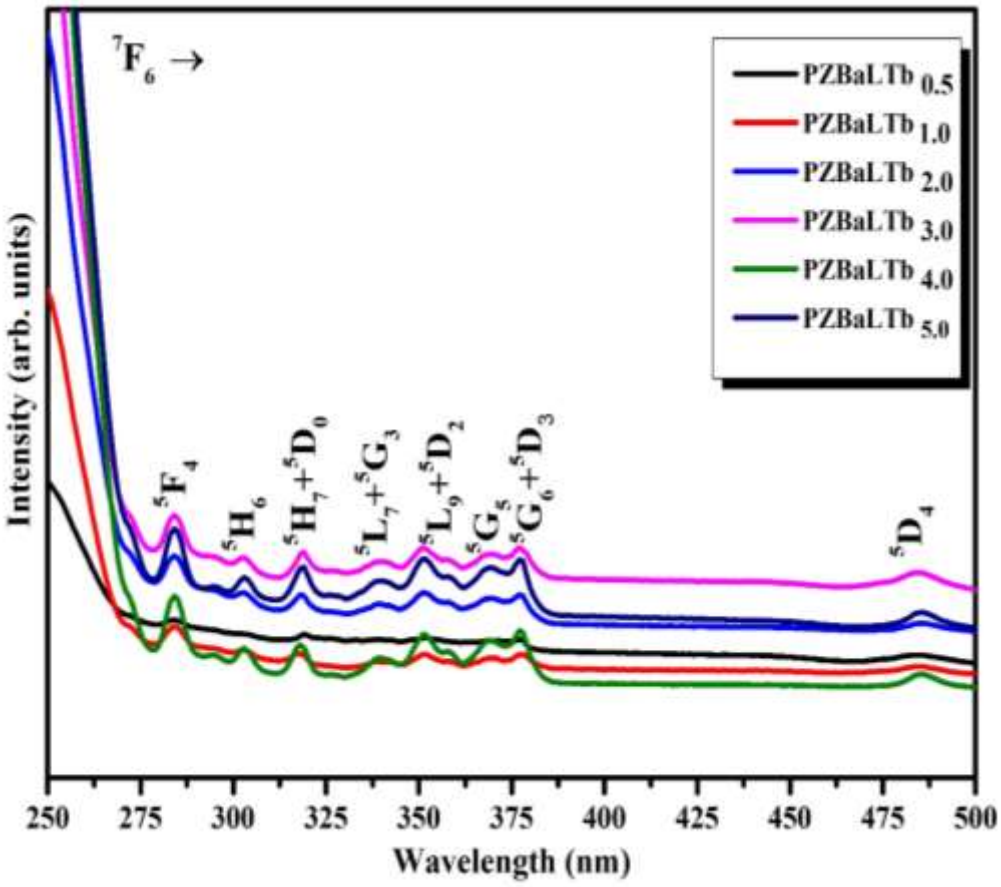

***Fig. 4.5**: Absorption spectra of Tb^{3+} doped BZLP glass with variable concentration of Tb^{3+} ions.*

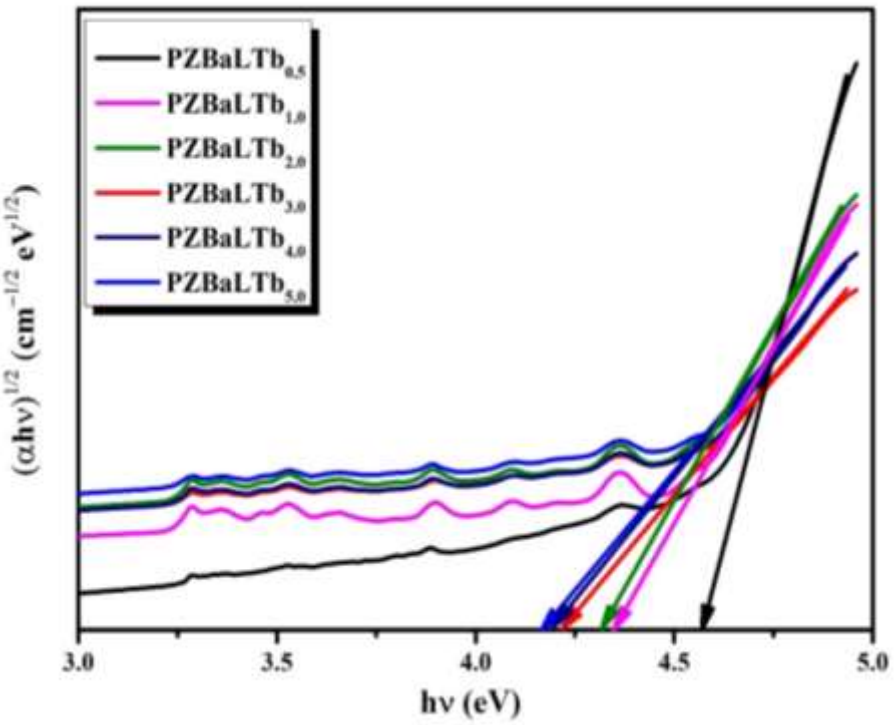

***Fig. 4.6**: Indirect optical bandgap Tauc plot of Tb^{3+} doped BZLP glasses.*

Using the absorption spectra, the optical band gap of Tb^{3+} doped glasses was estimated by employing the relation 3.1 given in chapter 3 [187]:

. The $\alpha(\nu)$ was estimated by using the expression [188]:

$$\alpha(\nu) = \left(\frac{1}{d}\right) ln\left(\frac{I_0}{I_T}\right) \tag{4.1}$$

Here d is glass thickness and the absorbance represents by the factor $ln\ (I_0/I_T)$. The E_{opt} values for Tb^{3+} doped glasses were evaluated for indirectly allowed transitions via Tauc's plot, as presented in Fig. 4.6. These values were found in the range of 4.57 – 4.19 eV and placed in Table 4.1.

4.3.5. PL analysis:

PL excitation spectra of the as-prepared glasses were recorded in 250-500 nm range by fixing emission wavelength at 545 nm. The excitation spectrum in Fig. 4.7, exhibits many excitation peaks. The excitation peaks were detected at 284, 302, 318, 339, 350, 368, 375, and 485 pertaining the transitions from ground level ($^7F_6$) to various energy levels $^5F_4$, $^5H_6$, $^5H_7$ + $^5D_0$, $^5L_7$ + $^5G_3$, $^5L_9$ + $^5D_2$, $^5G_5$, $^5G_6$ +$^5D_3$, and $^5D_4$ of Tb^{3+} ions, respectively [189,190]. The dominant excitation peak was observed at 373 nm corresponding to the transition from the lowest energy state $^7F_6$ ($4f^8$) to the higher spin–allowed excited state $^5H_6$ ($4f^75d^1$) of the Tb^{3+} ion. Hence, the as-prepared glasses have been effectively excited by that n-UV excitation source. Further, this excitation wavelength (373 nm) was chosen to record the PL emission spectra of Tb^{3+} doped BZLP glasses.

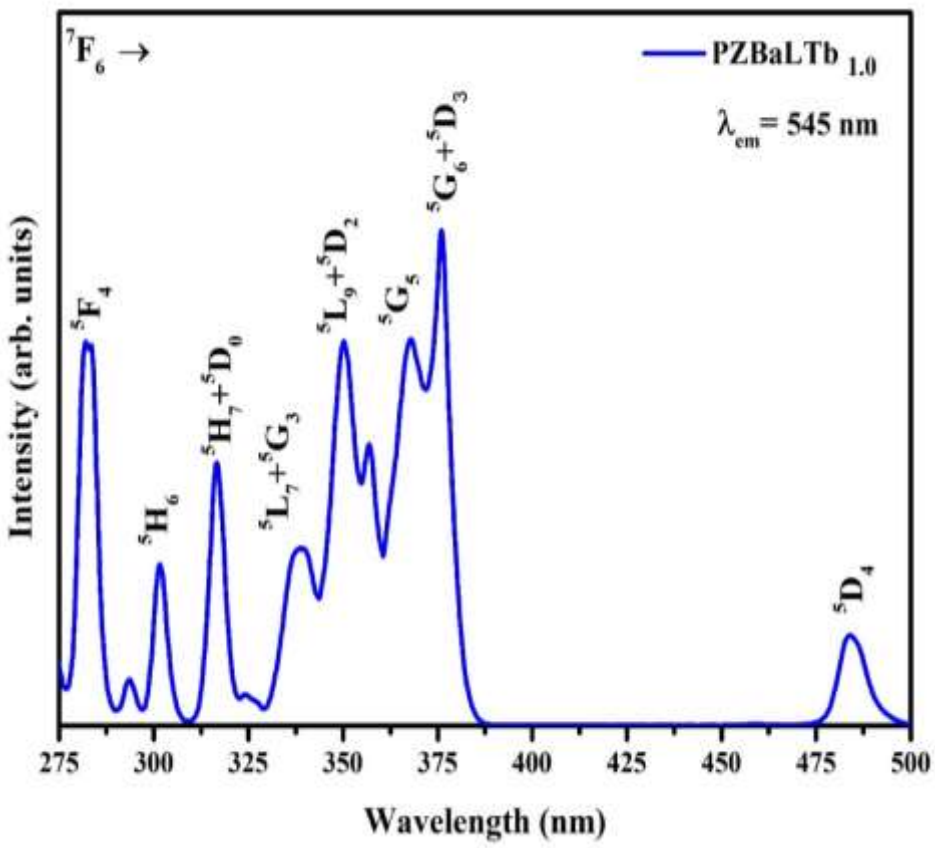

Fig. 4.7: *The excitation spectrum of the PZBaLTb$_{1.0}$ glass with monitoring the emission wavelength at 545 nm.*

The PL spectra of BZLP glasses doped with the varying concentration of Tb^{3+} ions under 373 nm excitation wavelength shown in Fig. 4.8. The resulting PL profile exhibits several peaks in the range of 450 to 700 nm. The blue, green, yellow and red emission peaks were situated at 490, 542, 585 and 620 nm due to the characteristic transitions $^5D_4 \rightarrow {}^7F_6, {}^7F_5$ $^7F_4$ and $^7F_3$ of Tb^{3+} ions, respectively. The blue emission peak related to the $^5D_4 \rightarrow {}^7F_6$ transition followed the selection rule $\Delta J = \pm 1$ rule and magnetic dipole in nature. The green emission peak arises due to the $^5D_4 \rightarrow {}^7F_5$ transition following the Laporte-forbidden selection rule, which is the most intense among all the emission peaks [191-194]. In the resultant PL spectra, the emission intensity changed with a surge in the doping concentration of Tb^{3+} ions in BZLP glasses. The

emission intensity intensifies with an increase in activator concentration of Tb^{3+} ions from 0.5 to 5.0 mol%. No concentration quenching was observed up to 5.0 mol% of Tb^{3+} ions in BZLP glasses.

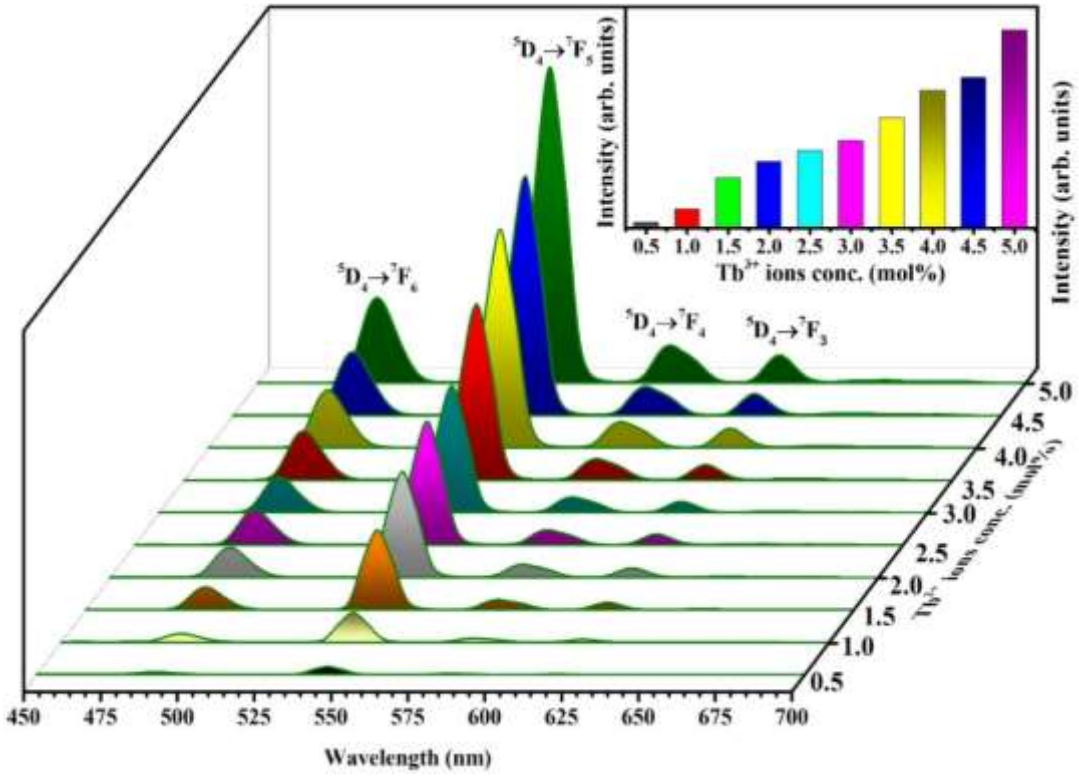

Fig. 4.8: *PL spectra of Tb^{3+} doped BZLP glasses with the doping concertation varying from 0.5 to 5.0 mol% at 373 nm excitation wavelength. The inset plot shows the variation of the emission intensity with Tb^{3+} ions concentration.*

This is another key feature of the BZLP glass host having high RE solubility and can be suitable for photonic applications. The ratio between blue ($^5D_4 \rightarrow ^7F_6$) and green ($^5D_4 \rightarrow ^7F_5$) emission peaks defines the center of symmetry around the Tb^{3+} ions in BZLP glasses. Hence the green color (G) to blue color (B) ratio was evaluated, which was reckoned to be more than four and varies with activator ions content. The high value of the G/B ratio recommends no center of symmetry around the Tb^{3+} ions in BZLP glasses [192].

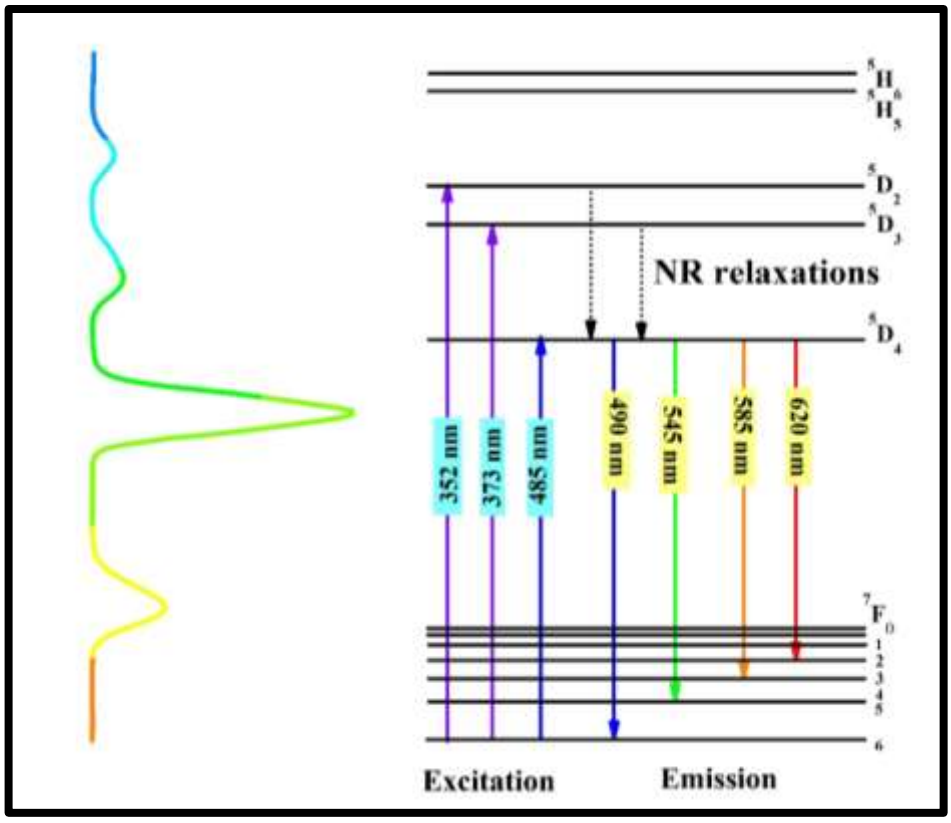

***Fig. 4.9**: Partial energy level diagram of Tb^{3+} doped BZLP glass.*

Fig. 4.9 illustrated the partial energy level of Tb^{3+} doped BZLP glasses, which clarified the excitation, radiative and non-radiative transitions mechanism involved. It is represented that Tb^{3+} ions were excited at 373 nm wavelength and populated the energy level. The occupied $^5D_3$ excited energy level may release the energy in two ways, initially some non-radiative relaxation up to the $^5D_4$ level. Finally, radiative emission occurs from the $^5D_4$ to $^7F_{6\text{-}3}$ levels of Tb^{3+} ions in BZLP glasses, giving visible blue, green, yellow and red light in the range of 450 to 700 nm [176].

4.3.6. Colorimetric study:

The recorded emission profiles under 373 nm excitation for Tb^{3+} doped BZLP glasses were used to evaluate chromaticity color coordinates. The chromaticity coordinates for all glasses were tabulated in Table 4.2. All the evaluated coordinates were situated in the green region of

the CIE diagram. The chromaticity coordinates for PZBaLTb$_{5.0}$ glass (0.309, 0.597) as shown in Fig. 4.10, closely match the green emitting component by the European Broadcasting Union illuminant (0.290, 0.600). The CCT was evaluated with the help of the formula 3.3 given in chapter 3 Click or tap here to enter text.:

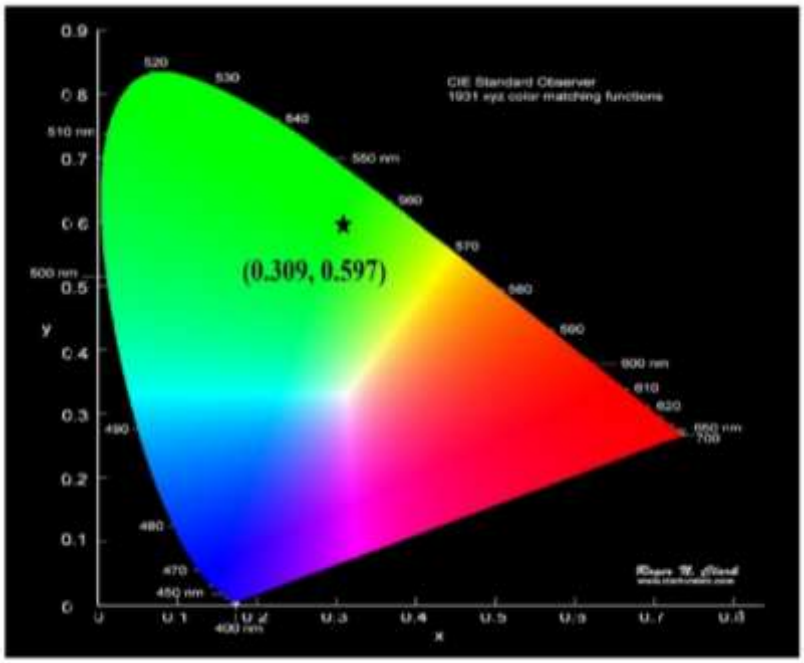

Fig. 4.10: *CIE chromaticity coordinates of PZBaLTb$_{5.0}$ glass.*

Table 4.2. CIE coordinates (*x*, *y*), CCT (K), color purity (%) and lifetime (ms) of Tb^{3+} doped BZLP glasses.

. The emitted light can be considered as a cool green light because CCT values are greater than 5000K as placed in Table4 2. Based on chromaticity coordinates, the color purity has been evaluated for all glasses by using the following expression [186,195-196]:

Glass	Chromaticity coordinates		CCT (K)	Color Purity (%)	Lifetime (ms)
	x	y			
PZBaLTb$_{0.5}$	0.302	0.499	6201	69 %	2.893
PZBaLTb$_{1.0}$	0.308	0.562	5972	71 %	2.851
PZBaLTb$_{2.0}$	0.307	0.576	5971	73 %	2.828
PZBaLTb$_{3.0}$	0.307	0.586	5949	74 %	2.793
PZBaLTb$_{4.0}$	0.310	0.593	5902	77 %	2.757
PZBaLTb$_{5.0}$	0.309	0.597	5917	79 %	2.724

$$Color\ Purity = \sqrt{\frac{(x-x_{ee})^2+(y-y_{ee})^2}{(x_d-x_{ee})^2+(y_d-y_{ee})^2}} \quad (4.2)$$

here, (x, y), (x_d, y_d) and $(x_{ee},\ y_{ee})$ specify the CIE coordinates of glass, dominate wavelength point and standard white point, respectively. The calculated color purity for prepared glasses is listed in table 4.2. The color purity for PZBaLTb$_{5.0}$ glass was found to be 79%. The result described above favors that Tb^{3+} doped BZLP glasses are very effective green emitting constituents for developing w-LEDs and other photonic devices.

4.3.7. Decay profile analysis:

PL decay curves of Tb^{3+} doped BLZP glasses were recorded from the $^5D_4$ level via monitoring the emission of 542 nm at 373 nm excitation, as illustrated in Fig 4 11. The recorded PL decay curves at room temperature for all the glasses show the exponential behaviour. The decay curves of the as-prepared glasses were found to best fit with the bi-exponential equations and average decay time can be calculated by using relation 1.17 & 1.18 given in chapter 1 [196]. The average decay time for the series of Tb^{3+} doped glasses was listed in table 4. 2, which shows the minor disparity with changes in doping concertation. The average lifetime value for the PZBaLTb$_{0.5}$ glass is 2.893 ms, which was reduced to 2.724 ms for the PZBaLTb$_{5.0}$ glass.

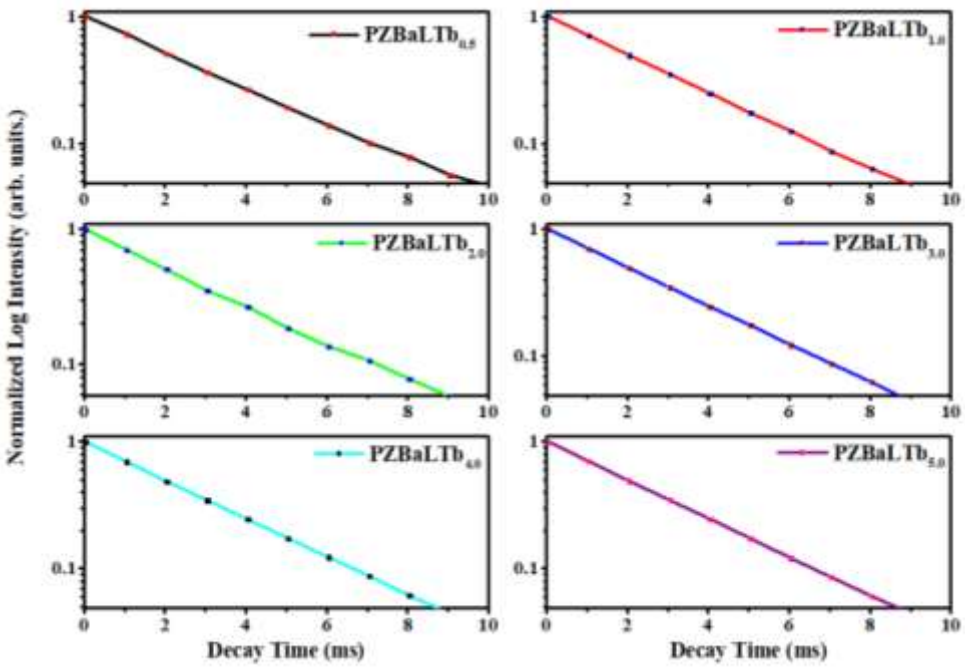

Fig.4.11: *Decay curves of* Tb^{3+} *doped BZLP glasses at 373 nm excitation and emission at 545* nm.

4.3.8. Temperature-dependent PL characteristics:

To investigate the luminescence features and thermal stability of the as-prepared glasses, the TDPL spectra were recorded at different temperatures under 373 nm excitation. TDPL spectra of $PZBaLTb_{5.0}$ glass are shown in Fig. 4.12. The TDPL spectra reveal a slightly falling intensity with temperature rise. It may be described as thermal energy increasing with temperature. It supported the electrons to pass the point of ground and excited level, emitting energy through the non-radiative transition process.

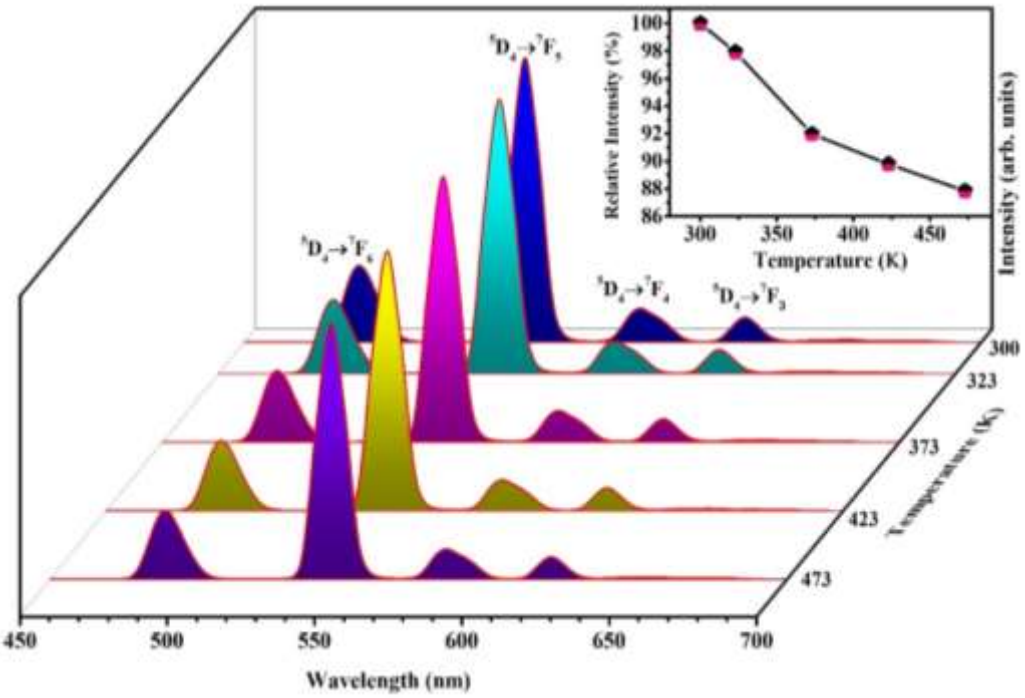

Fig.4.12: *TDPL spectra of PZBaLTb$_{5.0}$ glass with the upsurge in temperature from 300 to 473 K at the excitation wavelength of 373 nm. The inset plot shows the decrease in relative emission intensity with the surge in temperature from 300 to 473 K.*

The thermal stability can be considered a direct measure of activation energy. Arrhenius equation was used as given in 3.5 in chapter 3.The graph between $ln[(I_o/I_T) - 1]$ and $(1/K_BT)$ was plotted and fitted with a linear equation as shown in Fig.4. 13. Using the plotted graphs, the estimated activation energy is 0.161 eV. This high value of ΔE value proposes the high thermal stability of the present glass system, which supports the utility of the as-prepared glasses.

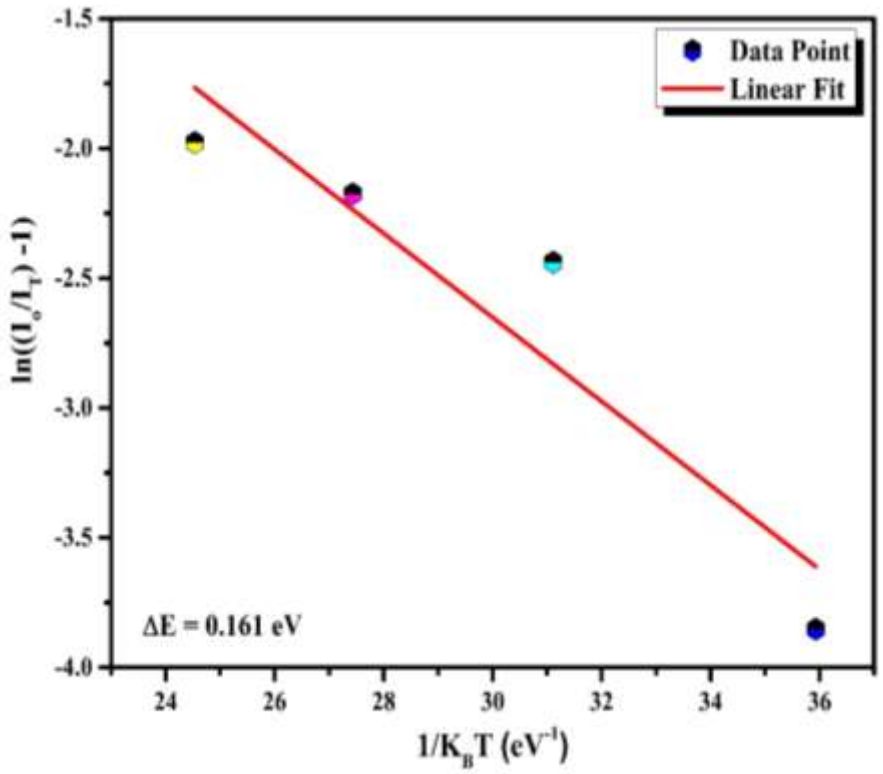

Fig. 4.13: *Variation of ln[(I_o/I_T)-1] with ($1/K_BT$) for $PZBaLTb_{5.0}$ glass.*

4.4. Conclusions:

In this work, the Tb^{3+} doped BZLP glasses have been synthesized using the melt-quenching technique. We have characterized the titled glasses through several techniques, analyzed and then summarized them as:

- The XRD pattern recorded for Tb^{3+} doped glasses confirmed their glassy nature.
- UV- vis spectra were employed to estimate the energy band gap for Tb^{3+} doped BZLP glasses via Tauc's plot, which is found in the range of 4.57-4.19 eV.
- The dominant emission attributed to the $^5D_4 \rightarrow {}^7F_5$ transition gave the intense green emission at 542 nm under 373 nm excitation wavelength.

- All the evaluated coordinates were situated in the green region of the CIE diagram. The chromaticity coordinates for $PZBaLTb_{5.0}$ glass (0.309, 0.597) matched with green emitting standard data.
- The PL decay profiles of Tb^{3+} doped BZLP glasses are found bi-exponential in nature.
- A significantly slighter decrease in emission intensity with rising temperature and the high activation energy value (0.161 eV) suggests that the prepared glasses have good thermal stability.

The above-mentioned characteristics indicate the suitability of Tb^{3+} doped BZLP glasses for green color emitting components useful in various photonic device applications such as display devices and w-LEDs.

CHAPTER 5

Spectroscopic Studies of Pr^{3+} doped Red Emitting BaO-ZnO-Li_2O-P_2O_5 Glasses For Luminescent Devices Applications

Pr^{3+} doped BaO-ZnO- Li_2O-P_2O_5 (BZLP) glass samples synthesised through melt quenching route were studied. The x-ray diffraction (XRD) confirms the amorphous non-crystalline nature of un-doped and doped BZLP glass. Absorption spectra show several bands in ultraviolet, visible and infrared regions. The absorption data was used in Judd-Ofelt (J-O) theory to evaluate various radiative parameters. Three peaks are visible in the photoluminescence (PL) emission spectra with the strongest peak positioned at 604 nm for which stimulated emission cross section and quantum efficiency has been assessed . The CIE color coordinates of the samples lie in the red region. The decay time values for 604 nm emission decreased with increased Pr^{3+} concentration. The luminescence intensity decreased to 88.12% and 82.61% of maximum value at 423 K and 473 K respectively showing high thermal stability. These BZLP glasses can work as an effective deep red-emitting component for w-LEDs and other photonic applications.

5.1. Introduction:

Lighting is one of the most fundamental & essential parts of our everyday lives. A variety of electricity-based artificial lighting technologies are available and are being used for indoor/outdoor illumination and lighting industries, complexes, and other areas [197,198,]. Solid-state lighting (SSL) technology is one of the advanced artificial lighting technologies. It is eco-friendly in nature and more efficient thereby saving enormous energy in various sectors [199,200]. The white light emitting diodes (w-LEDs) are most widely researched amongst all SSL devices. w-LEDs are developed by mixing a yellow color emitting phosphor d with an inorganic compound (epoxy resin) and coated over a blue InGaN chip [201]. This technique has some shortcomings like less color rendering index, inappropriate correlated color temperature and a halo-effect owing to absence of a red color component. To overcome the drawbacks as mentioned above, numerous other approaches were explored and published [199,202]. These approaches involved usage of inorganic phosphors having less thermal stability, which reduced efficiency and performance of illuminating devices [203]. Therefore, a suitable glass doped with an appropriate lanthanide/ transition metal ion is the best replacement for a phosphor. So, in this work, thermally stable red-emitting inorganic glasses were synthesized and explored for lighting applications.

Inorganic oxide glass formers like phosphates are used to prepare excellent glasses for use in numerous applications due to eco-friendliness, high transparency, ease of synthesis, low preparation cost, better mechanical and thermal stability etc. [204,205]. Also, high transparency in ultraviolet (UV) to infrared (IR) regions and high rare-earth solubility make phosphates a superior glass host material for photonic applications as compared with borate and silicate glasses [206,207]. But phosphate glass is hygroscopic in nature, which restricts the utility of

phosphate glass for many applications in various fields. The hygroscopic nature of phosphate glasses can be tackled by adding ZnO, which constitutes P-O-Zn bonds and makes the glass moisture resistant 208,209,]. Also, the addition of ZnO offers superior characteristics like direct bandgap, non-toxicity, less cost, non-hygroscopic and large exciton binding energy [208]. Alkaline earth metal oxide can work as an active network modifier, which can disrupt the glass network thereby leading to creation of non-bridging oxygen groups and bringing down the melting temperature of glass compositions [73,177]. The addition of alkali oxide in glass compositions may reduce the non-radiative losses, heighten the stability of host matrix. Addition of lithium oxide to the host leads to the intensification of transition temperature and lowering of thermal expansion coefficient [179]. With aforementioned characteristics in minds, we were able to synthesize BZLP glass that is highly transparent, moisture-resistant, has less phonon energy, is thermally and mechanically stable with excellent optical characteristics.

Lanthanide ions exhibit a ladder like energy level structure in the ultraviolet (UV) to infra-red (IR) range which is extremely useful for lasing and other photonic device applications [209,210]. The radiative emissions in the lanthanide ions are due to the f-f transitions of 4f shells that are screened by the $5s^2/5p^6$ orbitals [179,211]. Europium, praseodymium and samarium ions in trivalent states produce radiative emission in orange/red regions via pumped by UV/near-UV/blue radiations [79]. Among these lanthanides, Pr^{3+} ions can effectively absorb blue emission emanating from blue LED chips and has significant fluorescence emission in the conspicuous deep-red range of the electromagnetic spectrum. [212,213].

In this work, various optical and morphological characteristics of highly transparent Pr^{3+} doped BZLP glass samples have been examined in detail. Absorption data was used to determine the bandgap of the as prepared glass. Photoluminescence (PL) excitation and emission studies were

conducted on the glass samples. Under 445 nm excitation, the glasses show a sharp band centered at 604 nm. Decay curves for 604 nm emission were plotted as well. Temperature dependent PL studies were performed to check whether or not the samples are thermally stable. The aim of performing all the aforementioned studies was to check the applicability of Pr^{3+} glass in w-LEDs and SSL applications.

5.2. Experimental work and characterizations:

5.2.1. Preparation of glass

Trivalent praseodymium (Pr^{3+}) doped glass samples were synthesized by employing melt quenching route. The doped and un-doped glass samples have the molar configuration as follows:

$$(15\text{-}x)\ BaO\text{-}15ZnO\text{-}10Li_2O\text{-}60P_2O_5\text{:}xPr_6O_{11}$$

In the above-mentioned molar composition, *x* represents the amount of Pr^{3+} ions in BZLP glasses. In this study, x varies as 0.0, 0.01, 0.05 0.1, 0.5, 1.0, 1.5, 2.0 & 2.5 mol% and the glasses have been assigned names as BZLP, BZLP:0.01Pr, BZLP:0.05Pr, BZLP:0.1Pr, BZLP:0.5Pr, BZLP:1.0Pr, BZLP:1.5Pr, BZLP:2.0Pr and BZLP:2.5Pr respectively. The detailed synthesis procedure for the preparation of glass has been explained in 2.2 chapter 2.

5.2.2. Characterization techniques:

The physical characteristics for Pr^{3+} doped BZLP glass samples such as density and refractive index and other related parameters were assessed using Archimedes principle (H_2O used as a contribution medium) and He-Ne laser (650 nm). Diffraction patterns of un-doped and Pr^{3+} doped BZLP glass samples were recorded at room temperature (300 K) via Bruker D8 Advance X-Ray diffractometer attached with a Ni filter and Cu (K_α) radiation source in $20° \leq 2\theta \leq 70°$ range. Using a spectrophotometer JASCO, V 670, optical absorption spectral investigations

were measured in the UV to near-infrared (NIR) range. The spectral luminescence studies for Pr^{3+} doped BZLP glass samples were carried out via spectrofluorophotometer JASCO 8300FL at 300 K. Decay profile for Pr^{3+} doped BZLP glass samples were recorded via spectrometer Edinburg, FLS980 coupled with a microsecond Xenon flash lamp. Temperature-dependent photoluminescence (TD-PL) features were observed with spectrophotometer FLAME- S-XR1-ES, Ocean optics and sample holder attached with heating assembly.

5.3. Results and discussion:

5.3.1. Physical properties of Pr^{3+} doped BZLP glass samples

The density and refractive index of the samples were calculated using Archimedes' principle and Brewster's angle method respectively [187]. Other related physical parameters were also calculated using formulae from relevant articles in literature and have presented in Table 5.1 [214].

The physical parameters for Pr^{3+} doped BZLP glass samples showed variation with an increase in Pr^{3+} ions concentration due to altered environment around the Pr^{3+} ions. The values of parameters like molar refraction, average molecular weight, optical dielectric constant, molar refraction and reflection losses were seen to be increasing with increase in the Pr^{3+} ions concentration in BZLP glass samples whereas polaron radius and interatomic distance decreased with increasing Pr^{3+} ions.

Table 5.1 Physical Properties of Pr^{3+} doped BZLP glasses.

Physical Property	**BZLP: 0.01Pr**	**BZLP: 0.05Pr**	**BZLP: 0.10Pr**	**BZLP: 0.50Pr**	**BZLP: 1.00Pr**	**BZLP: 1.50Pr**	**BZLP: 2.00Pr**	**BZLP: 2.5Pr**
Refractive index (n_d)	1.78	1.81	1.84	1.86	1.89	1.93	1.94	1.96
Density (gm/cm^3)	2.99	3.09	3.14	3.18	3.20	3.22	3.26	3.28

Average molecular weight	208.61	208.96	209.39	212.86	217.20	221.54	225.89	230.23
Pr^{3+} ion concentration N (10^{22} ions/cm^3)	0.008	0.04	0.09	0.45	0.88	1.32	1.73	2.14
Polaron radius (r_p) (Å)	9.10	5.27	4.16	2.43	1.94	1.70	1.55	1.44
Inter-atomic distance (r_i) (Å)	22.60	13.09	10.33	6.05	4.82	4.23	3.85	3.59
Optical band gap (eV)	3.57	3.51	3.48	3.64	3.92	3.94	4.02	4.07
Dielectric constant (Ɛ)	3.16	3.27	3.38	3.45	3.57	3.72	3.76	3.84
Optical dielectric constant (Ɛ-1)	2.16	2.27	2.38	2.45	2.57	2.72	2.76	2.84
Molar refraction (R_m) (cm^{-3})	29.18	29.14	29.45	30.10	31.30	32.67	33.19	34.09
Reflection losses (R %)	4.25	4.51	4.78	4.96	5.23	5.59	5.69	5.87

5.3.2. Glass structural analysis:

Diffraction patterns for BZLP and BZLP:0.1Pr glass samples have been recorded at room temperature and shown in Fig. 5.1. The spectra shows a broad ranging hump and absence of any sharp peaks thereby confirming the amorphous nature of the glass.. Also, the doping of Pr^{3+} ions in BZLP glass does not affect the amorphous properties of the doped glasses.

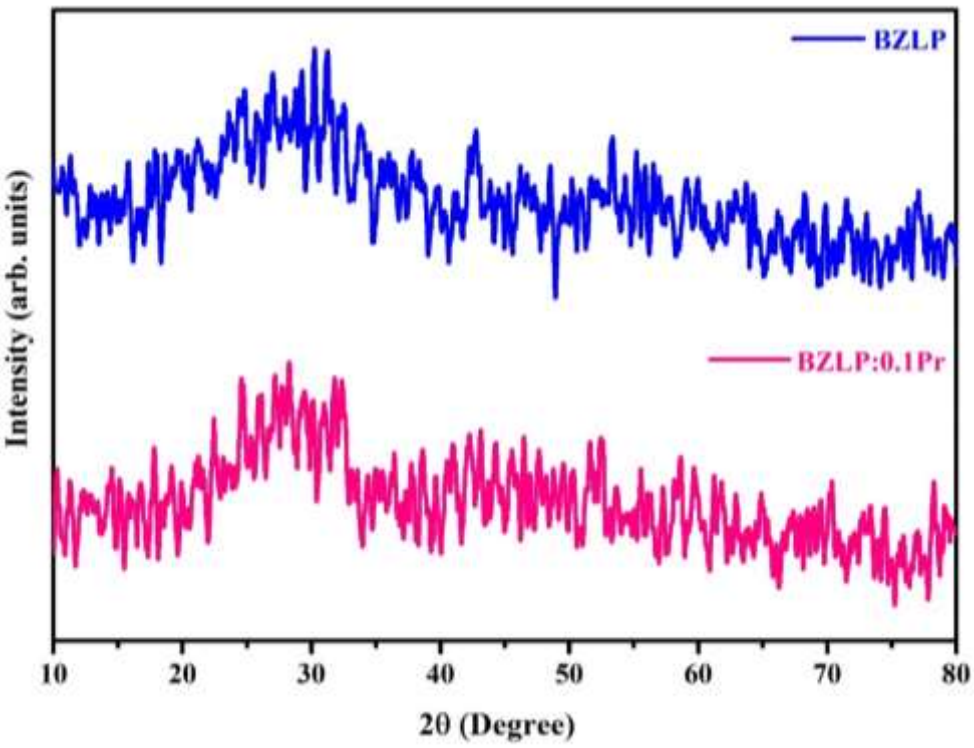

Fig. 5.1. *XRD patterns recorded for BZLP and BZLP:0.1Pr glasses.*

5.3.3. Absorption properties of glass:

Fig.5.2 shows the absorption spectra from UV to IR region for BZLP glasses doped with Pr^{3+} ions that were measured at room temperature. The absorption profile exhibits numerous peaks in 300 to 2000 nm wavelength range. In the spectra, three peaks related to $^3H_4 \rightarrow {}^3P_{2,\ 1,\ 0}$ transitions and one peak related to $^3H_4 \rightarrow {}^1D_2$ transition is present in the visible range and the residual three peaks were related to $^3H_4 \rightarrow {}^1G_4$, $^3F_{4,3,2}$ transitions present in NIR region [215]. These transitions are in agreement with Carnall's work [216]. The absorption intensity increased with increase in the concentration of Pr^{3+} ions. . The $^3H_4 \rightarrow {}^3P_2$ transition is hypersensitive in nature $[|\Delta S| = 0, |\Delta L| \leq 2\ and\ |\Delta J| \leq 2]$ which predominantly depends upon on the neighbourhood of Pr^{3+} ions and correspondingly affect the J-O intensity parameters[217]. The hypersensitive transition's peak position is shifted towards shorter wavelengths as depicted in Fig. 5.2 when the concentration of Pr^{3+} ions rises. This change in shift arises due to

nephelauxetic effect [218]. For the mentioned band positions in absorption spectra, nephelauxetic ratio ($\overline{\beta}$) and bonding parameters (δ) were assessed for Pr^{3+} doepd BZLP glasses by employing expression in literature [219,220] . Bonding parameters can represent the covalent or ionic character of as-prepared glasses by having +ve or -ve values respectively. Table 5.2, shows that the bonding parameter values are positive, indicating the covalent character of as prepared glasses. This covalent nature increases in the as prepared glasses as the concentration of Pr^{3+} ions rises.

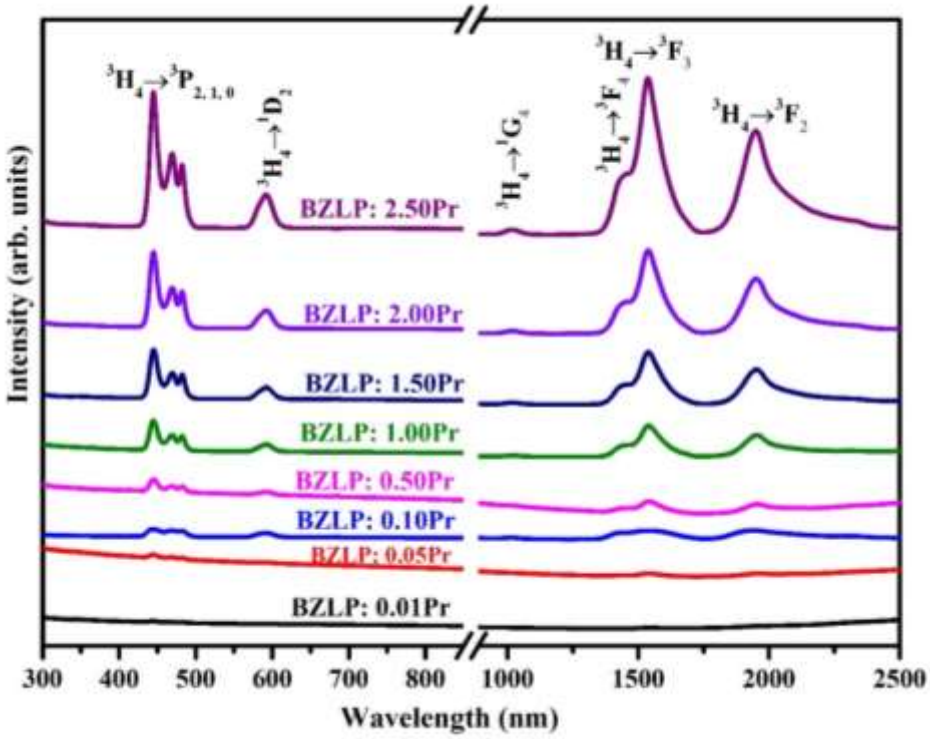

Fig. 5.2*. Absorption spectra of doped BZLP glasses with varying concentrations of Pr^{3+} from 0.01 to 2.5 mol%.*

An essential parameter, the experimental oscillator strength (fexp), has been evaluated by relation 1.8 given in chapter 1 .

Table 5.2. Experimental (f_{exp}) ($x10^{-6}$), calculated (f_{cal}) ($x10^{-6}$) oscillator strengths, r.m.s deviation (δ_{rms}), nephelauxetic ratio ($\bar{\beta}$), and bonding parameters (δ) for Pr^{3+} ions in BZLP glasses.

$^3H_4$ →	BZLP: 0.01Pr		BZLP: 0.05Pr		BZLP: 0.1Pr		BZLP: 0.5Pr		BZLP: 1.0Pr		BZLP: 1.5Pr		BZLP: 2.0Pr		BZLP: 2.5Pr	
	fcal	fexp	fexp	fcal	fexp	fcal	fexp	fcal	fexp	fcal	fexp	fcal	fexp	fcal	fexp	fcal
$^3F_2$	4.76	4.73	5.79	5.76	9.73	9.72	5.74	5.75	4.21	4.22	4.09	4.11	3.95	3.98	3.73	3.76
$^3F_3$	6.05	6.31	6.83	7.18	10.4	10.3	6.89	6.50	5.55	5.22	5.12	4.70	4.67	3.99	4.56	3.83
$^3F_4$	-	-	3.5	3.64	3.65	5.05	1.87	3.18	1.63	2.55	1.43	2.30	0.37	1.65	0.21	1.56
$^1D_2$	-	-	8.77	1.17	12.8	1.65	5.86	1.04	4	0.84	2.78	0.75	2.67	0.60	2.63	0.581
$^3P_0$	5.72	5.18	6.03	3.94	6.54	5.94	2.36	3.79	1.93	3.15	1.32	2.75	1	3.13	0.78	3.10
$^3P_1$	-	-	2.29	4.01	2.66	6.04	2.3	3.86	2.22	3.21	1.93	2.80	1.81	3.19	1.77	3.16
$^3P_2$	7.61	3.05	7.75	3.71	12.9	5.14	9.28	3.27	5.9	2.65	4.04	2.36	3.88	1.84	3.7	1.76
δ_{rms} (x 10^{-6})	2.29		3.41		5.34		3.06		1.85		1.23		1.55		1.58	
$\bar{\beta}$	0.997		0.995		0.994		0.993		0.998		0.998		0.997		0.997	
δ	0.03		0.05		0.06		0.07		0.12		0.15		0.20		0.21	

The evaluated values had been presented in Table 5.2. The calculated oscillator strength (f_{cal}) and J-O parameters (Ω_2, Ω_4, Ω_6) were estimated through experimental oscillator strength (f_{exp}) . Least square fit method is used to evaluate the calculated oscillator strength for measured

electric dipole transitions within $4f^2$ configuration using following relation 1.4 given in chapter 1. The best fit between f_{exp} and f_{cal} is assessed through the root mean square deviation (δ_{rms}), that can be calculated by employing the formula 1.5 given in chapter 1.

The values of fcal, fexp, and δ_{rms} for BZLP glasses are shown in Table 5.2. Table 5.3 lists the evaluated J-O intensity parameters together with the values of other reported glasses from the literature [221–224]. J-O parameters emulate the uniform trend ($\Omega_4 > \Omega_2 > \Omega_6$) for all reported glass samples. The intensity parameter Ω_2 is a depiction of covalent character of metal ligand bond whereas other two parameters Ω_4 and Ω_6 indicate the rigidity and viscosity of host glass matrix.

Table 5.3 Judd-Ofelt Parameters ($\Omega_\lambda \times 10^{-20} cm^2$) of Pr^{3+} ions in BZLP glasses along with various reported hosts

Glass System	Ω_2	Ω_4	Ω_6	Trend	References
BZLP: 0.01Pr	2.57	5.20	3.05	$\Omega_4 > \Omega_2 > \Omega_6$	Present work
BZLP: 0.05Pr	5.34	5.40	4.47	$\Omega_4 > \Omega_2 > \Omega_6$	Present work
BZLP: 0.1Pr	7.86	9.98	5.88	$\Omega_4 > \Omega_2 > \Omega_6$	Present work
BZLP: 0.5Pr	4.94	5.45	3.67	$\Omega_4 > \Omega_2 > \Omega_6$	Present work
BZLP: 1.0Pr	3.48	4.00	2.87	$\Omega_4 > \Omega_2 > \Omega_6$	Present work
BZLP: 1.5Pr	3.23	3.38	2.50	$\Omega_4 > \Omega_2 > \Omega_6$	Present work
BZLP: 2.0Pr	3.03	3.22	1.61	$\Omega_4 > \Omega_2 > \Omega_6$	Present work
BZLP: 2.5Pr	2.87	3.72	1.48	$\Omega_4 > \Omega_2 > \Omega_6$	Present work
$(Ge_{30}Ga_5Se_{65})_{100-x}$ $(Pr_2Se_3)x$	6.00	16.8	5.00	$\Omega_4 > \Omega_2 > \Omega_6$	[220]

$59.99TeO_2$ -$25WO_3$ – $15PbF_2$ – $0.01Pr_6O_{11}$	4.782	6.148	2.208	$\Omega_4 > \Omega_2 > \Omega_6$	[221]
TeWLiK	8.56	9.64	2.80	$\Omega_4 > \Omega_2 > \Omega_6$	[222]
TeWNaK	9.39	9.55	2.81	$\Omega_4 > \Omega_2 > \Omega_6$	[222]
Phosphate	4.19	4.29	6.40	$\Omega_6 > \Omega_2 > \Omega_4$	[224]
Mixed halide	2.70	4.40	5.40	$\Omega_6 > \Omega_2 > \Omega_4$	[225]
ZnAlBiB 1.0Pr	7.36	4.46	4.17	$\Omega_2 > \Omega_4 > \Omega_6$	[228]
ZBP5	3.94	1.34	1.23	$\Omega_2 > \Omega_4 > \Omega_6$	[277]
$40GaS_{3/2}$.$40GeS_2$.20Cs :Br Pr^{3+}: GeAsGaSe	9.05	7.26	7.28	$\Omega_2 > \Omega_6 > \Omega_4$	[223]

The Ω_2 parameter of the BZLP 0.1Pr glass is greater than those of the earlier reported glasses [221,222,225–227] and is comparable to those of Pr^{3+}doped ZnAlBiB glasses reported by Mahamuda et al. [228]. The higher value of Ω_2 parameter observed for BZLP 0.1Pr glass implies a greater degree of covalency of the Pr^{3+} ions bonding with the oxygen ligand, which is verified by the bonding parameters listed in Table 5.2 and may also be an indication of a greater degree of asymmetry in the ion sites around the Pr^{3+} ions. In contrast, higher value of Ω_4 implies more rigidity of host medium around the Pr^{3+} ions [147,229]. For the present glass system, J-O intensity parameter Ω_4 increases as the concentration of Pr^{3+} ions rise from BZLP:0.01Pr to BZLP:0.1Pr and then decreases up to BZLP:2.5Pr. Greater the value of Ω_4 intensity parameter for prepared glasses indicates the rigidity of host material in which Pr^{3+} ions are located [230].

The optical band gap is a vital parameter and was calculated for Pr^{3+} ions doped BZLP glass samples based on recorded absorption spectra. The optical band gap for glass samples are estimated through using the relation 3.1 given in chapter 3.

The value of $\alpha(v)$ was estimated using the relation 4.1 given in chapter 4. The E_{opt} values were acquired for direct and indirect allowed transitions by extrapolating the linear section of the Tauc's plot [$(ahv)^{1/n}$ versus (hv)] as presented in Fig. 5.3 with n = ½. The estimated direct bandgap E_{opt} values for Pr^{3+} ions doped BZLP glass samples have been listed in Table 5.1 and lie in the range 3.48-4.07 eV.

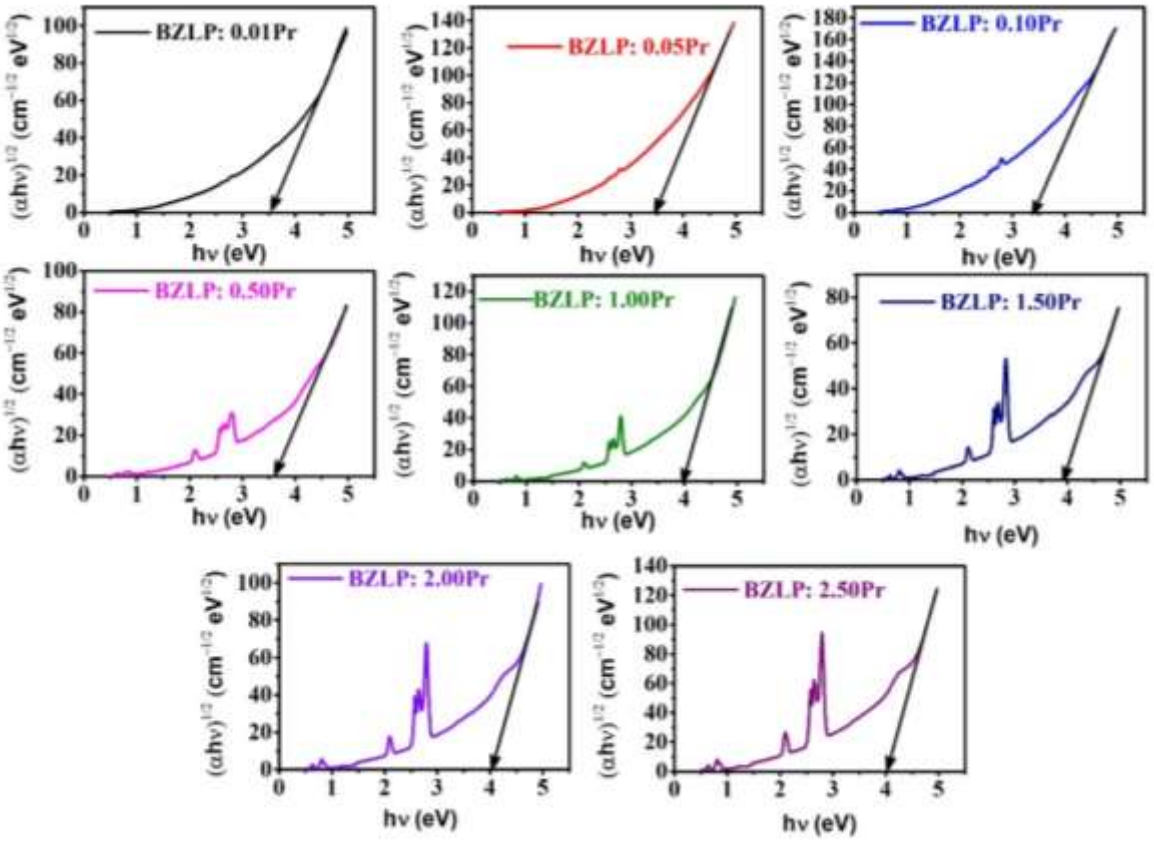

Fig. 5.3*. Indirect bandgap plot of Pr^{3+} doped BZLP glasses with varying concentration from 0.01 to 2.50 mol%.*

5.3.4. PL characteristics of glass:

PL excitation spectrum of BZLP1.0Pr glass sample was recorded in 400 to 500 nm range with monitoring emission wavelength λ_{em} = 604 nm and has been presented in Fig. 5.4. Three excitation peaks ascribed to $^3H_4 \rightarrow {}^3P_2$, $^3P_1$,$^3P_0$ transitions of Pr^{3+} ions, respectively can be seen. The most intense excitation was perceived at 445 nm corresponding to $^3H_4 \rightarrow {}^3P_2$ transition and this selected for recording the photoluminescence emission spectra of all prepared glass samples at room temperature [217].

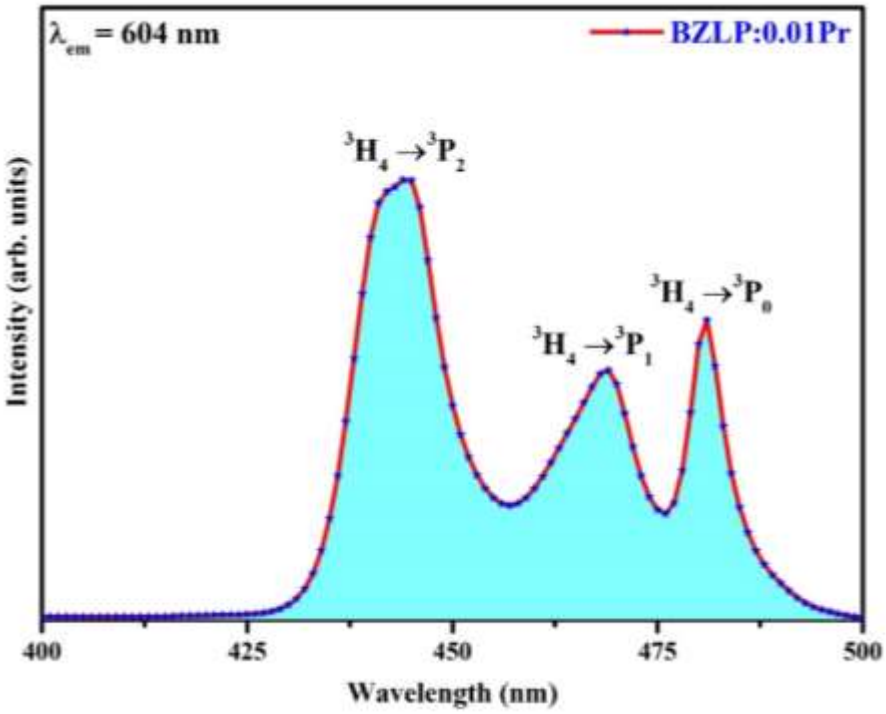

Fig. 5.4. *The excitation spectrum recorded for BZLP:0.01Pr glass under 604 emission wavelength.*

The PL spectra of Pr^{3+}doped BZLP glasses at λ_{ex} = 445 nm have been presented in Fig. 5.5. Emission peaks were noticed at 604, 616 and 647 nm corresponding to $^1D_2 \rightarrow {}^3H_4$, $^3P_0 \rightarrow {}^3H_6$ and $^3P_0 \rightarrow {}^3F_2$ transitions of Pr^{3+} ions respectively. Among the emission peaks, the dominant

one is due to $^1D_2 \rightarrow {}^3H_4$ transition at 604 nm. In the emission spectra ranging between 600 to 620 nm, emission bands ($^1D_2 \rightarrow {}^3H_4$ and $^3P_0 \rightarrow {}^3H_6$) are observed, which are overlapped in proximity. The peak observed in the red region: $^3P_0 \rightarrow {}^3H_6$ has better sharpness as the concentration of Pr^{3+} ions is increased beyond 0.5 mol% while $^1D_2 \rightarrow {}^3H_4$ transition loses its sharpness at this concentration. The band maxima shift from 604 nm to 616 nm as the concentration of dopant ion is increased [231–233]. The intensity of the peaks increased with increase in Pr^{3+} ions content up 0.1 mol% and decreased afterwards.

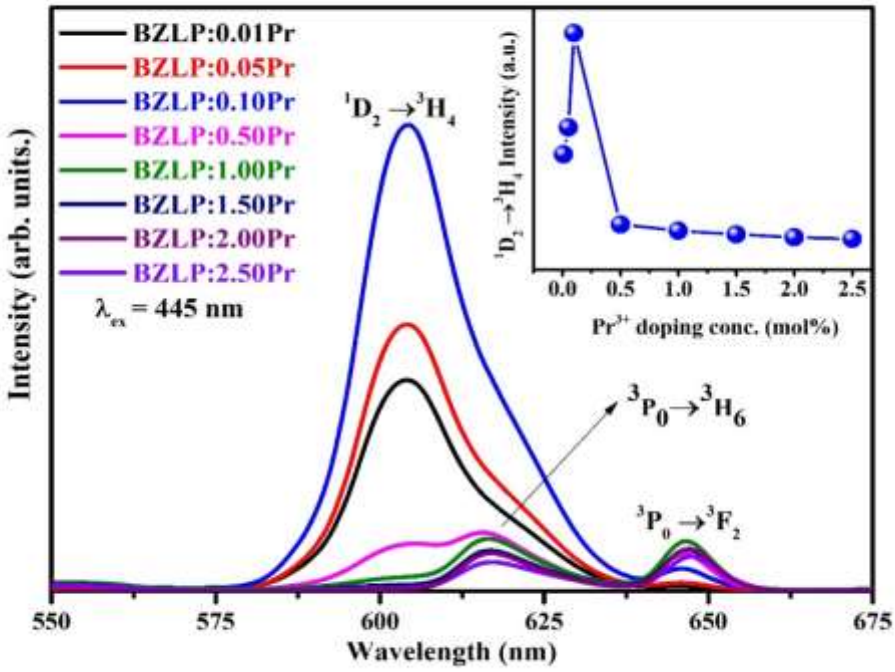

Fig. 5.5. *Emission spectra of Pr^{3+} doped BZLP glasses with varying the doping concentration from 0.01 to 2.50 mol%. Inset plot shows the variation of the emission intensity related to $^1D_2 \rightarrow {}^3H_4$ transition with Pr^{3+} ions concentration.*

This is due to concentration quenching. This occurs as soon as the interionic distance among the Pr^{3+} ions become lesser than the critical distance the minimum distance between two doping ions. In this condition, the energy migration amongst dopant Pr^{3+} ions happens via radiation less transfer either by multiphonon or cross-relaxation process [234].The inset plot of Fig. 5.5 demonstrates the change in PL intensity with concentration of Pr^{3+} ions in BZLP glasses.

The excitations, non-radiative and radiative emissions of Pr^{3+} ions in BZLP glass and cross-relaxation channels (CRC) were well clarified by the energy level diagram as demonstrated in Fig. 5.6. The energy level diagram shows the absorption of specific energy and subsequently movement of ions from the ground state to a specific excited state. After a certain time, the excited ions return to the ground level via radiation less and radiative emissions. As per the energy of presented levels of Pr^{3+}, the possible CRC responsible for the concentration quenching are as below [230]:

$$CRC\ 1: {}^3P_0 + {}^3H_4 \rightarrow {}^1D_2 + {}^3H_6$$

$$CRC\ 2: {}^3P_0 + {}^3H_4 \rightarrow {}^3H_6 + {}^1D_2$$

$$CRC\ 3: {}^3P_0 + {}^3H_4 \rightarrow {}^1G_4 + {}^1G_4$$

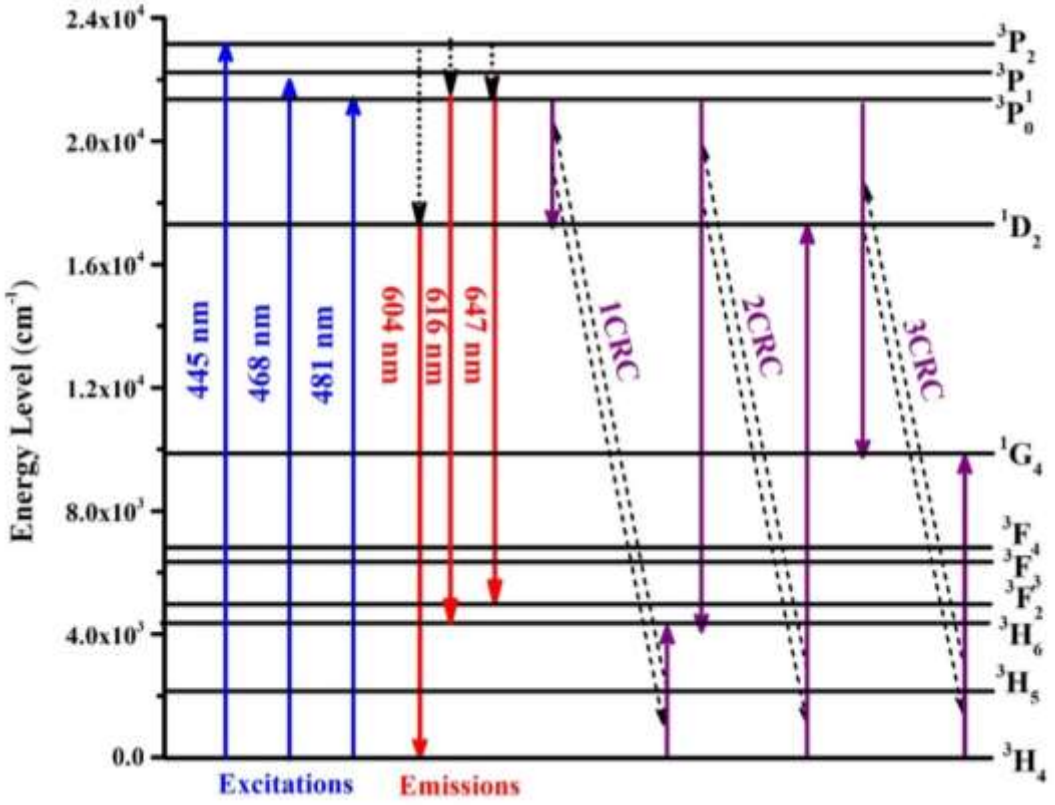

Fig. 5.6. *Energy level diagram of Pr^{3+} doped BZLP glasses.*

The non-radiative energy transfer takes place in rare-earth-doped luminescent materials due to the multipolar interaction among dopant ions. Dexter theory predicts three kinds of mechanisms for interionic multipolar interactions between the dopant ions. As per the theory the PL intensity is related to the amount of doping ion content in the host system as [235]:

$$log\left(\frac{I}{c}\right) = logf - \frac{s\,log(c)}{d} \qquad (5.1)$$

here I denotes the PL intensity, c is the the Pr^{3+} ion concentration in BZLP glass samples, d denotes the dimension of the compound having the value of $d = 3$. f signifies a constant, which is unaffected by doping ion concentration. The parameter s describes the type of multipolar interaction within the adjacent Pr^{3+} ions in BZLP glass samples. The value of parameter s is 6

for dipole-dipole interaction, 8 for dipole-quadrupole inetraction and 10 for quadrupole-quadrupole multipolar interaction [236]. For this research work, the value of parameter s was estimated using the slope of the linear fitted plot of $log\ (I/c)$ versus $log(c)$ as shown in Fig.5.7 and was found to be 1.485. Therefore, the estimated value of parameter s was 4.455 which is close to 6. This proves that the non-radiative multipolar interaction between the Pr^{3+} ions is dipole-dipole in nature. In accordance with Dexter Theory, the emission and absorption spectrum of doped glasses will overlap. The visible range emission and absorption spectrum of the $^1D_2$ transition, as well as the cross relaxation channel overlap as shown in Fig. 5.8 [234]. This spectral overlap enables us to comprehend the resonant energy transfer between excited and unexcited Pr^{3+} ions.

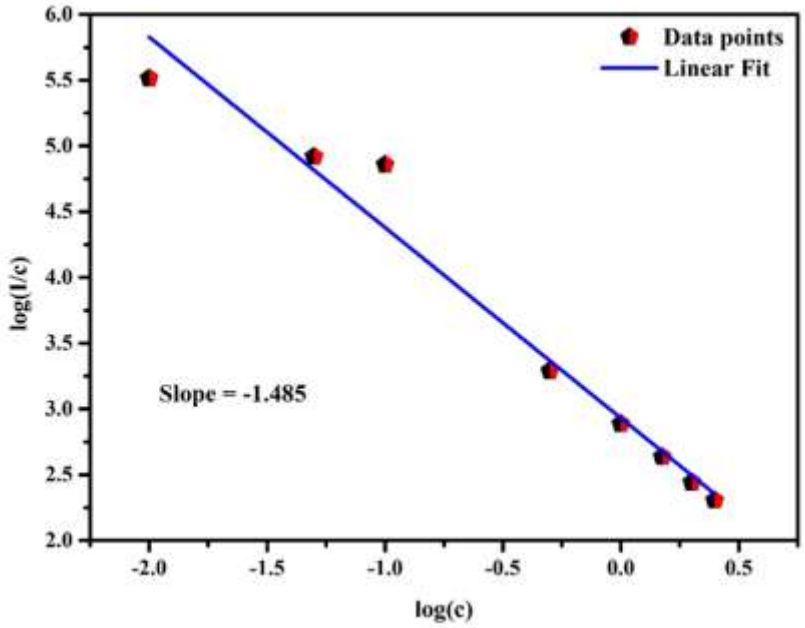

Fig. 5.7*. Relation between log (I/c) and log (c) for different concentrations of* Pr^{3+}.

The photoluminescence performance for Pr^{3+} doped BZLP glasses is estimated by calculating the parameters like radiative transition probability (A_R), total transition probability (A_T), radiative lifetime (τ_R) and luminescence branching ratio (β_R) with the aid of J-O intensity

parameters measured from the absorption spectra. These parameters have been listed in Table 5.3. To explore the luminescent process, the radiative transition probability (A_R), total transition probability (A_T), radiative lifetime $\tau_R(a_j, b_{j'})$ and the luminescence branching ratio β_R $(a_j, b_{j'})$ for fluorescent levels can be computed by using the following equations 1.9, 1.10, 1.11 & 1.12 given in chapter 1 An essential parameter is stimulated emission cross-section (σ_{se}) and its value dictates high gain and low threshold for lasing applications and calculated by using relation 1.13 given in chapter 1. A_R, A_T, β_R and τ_R radiatitve parameters computed for Pr^{3+} doped BZLP glasses for all fluoroscent transitions are listed in Table 5.4.

Table 5.4. Transition probability (A_R) (s^{-1}), luminescence branching ratio (β_R), total transition probability (A_T) (s^{-1}) and radiative lifetime ($\boldsymbol{\tau_R}$) (μs) for the observed emission transitions of Pr^{3+} ions in BZLP glass.

Sample name	Transition	A_R	A_T	β_R	τ_R
BZLP: 0.01Pr	$^3P_1 \rightarrow {}^3F_3$	10071.61	48833.47	0.2062	20
	$^1D_2 \rightarrow {}^3H_4$	978.62	3947.08	0.2479	253
BZLP: 0.05Pr	$^3P_1 \rightarrow {}^3F_3$	17721.88	66333.76	0.2672	15
	$^1D_2 \rightarrow {}^3H_4$	1372.52	6371.21	0.2154	156
BZLP: 0.1Pr	$^3P_1 \rightarrow {}^3F_3$	32900.21	110698.7	0.2972	9
	$^1D_2 \rightarrow {}^3H_4$	2001.65	11082.17	0.1806	90
BZLP: 0.5Pr	$^3P_1 \rightarrow {}^3F_3$	19264.42	68643.08	0.2806	14
	$^1D_2 \rightarrow {}^3H_4$	1293.03	6665.77	0.194	150
BZLP: 1.0Pr	$^3P_1 \rightarrow {}^3F_3$	13848.99	54324.4	0.2549	18

	$^1D_2 \rightarrow {}^3H_4$	1073.6	5003.91	0.2146	199
BZLP: 1.5Pr	$^3P_1 \rightarrow {}^3F_3$	13504.31	51079.94	0.2644	19
	$^1D_2 \rightarrow {}^3H_4$	1000.98	4811.39	0.208	207
BZLP: 2.0Pr	$^3P_1 \rightarrow {}^3F_3$	13605.71	53053.52	0.2565	18
	$^1D_2 \rightarrow {}^3H_4$	816.25	4636.94	0.176	215
BZLP:2.5Pr	$^3P_1 \rightarrow {}^3F_3$	13488.58	52998.95	0.2075	18
	$^1D_2 \rightarrow {}^3H_4$	799.31	4589.27	0.1742	217

Other radiative parameters like λ_p (peak wavelength), $\Delta\lambda_p$ (effective band width), β_R, β_{exp}diative and experimental brnching ratio) σse, (stimulated emission cross section) σ_{se} x Δλp (gain bandwidth) and σ_{se} x τ_R (optical gain parameters) are represented in Table 5.5 for all reported glasses. Fluorescent Branching ratio (β_R) is another significant parameter for lasing action and its value should be around 0.5. From Table 5.5, it is noticed that β_R values for high intense transition $^1D_2 \rightarrow {}^3H_4$ decreases as the concentration of Pr^{3+} ions increase up to 0.1 mol% and after that increases as the concentration increases upto 2.5 mol%. This might be due to fluorescent quenching of $^1D_2 \rightarrow {}^3H_4$ transition [230,237–239] . Moreover, higher value of stimulated emission cross-section (σse) is essential for luminescent transition thereby showing that the glass can be used as an active medium for laser. From Table 5.5, it is noticed that σse has maximum value for BZPL:0.1Pr glass for transition $^1D_2 \rightarrow {}^3H_4$.

Table 5.5. Emission peak wavelength (λ_P)(nm), effective band widths ($\Delta\lambda_P$)(nm), measured and experimental branching ratios (β_R & β_{exp}), stimulated emission cross-sections (σ_{se}) (cm^2), gain band width ($\sigma_{se} \times \Delta\lambda_P$) ($cm^3$) and optical gain parameter ($\sigma_{se} \times \tau_R$) ($cm^2$ s) parameters for the emission transitions for Pr^{3+} ions in BZLP glasses.

Spectral parameters	**BZLP: 0.01Pr**	**BZLP: 0.05Pr**	**BZLP: 0.1Pr**	**BZLP: 0.5Pr**	**BZLP: 1.0Pr**	**BZLP: 1.5Pr**	**BZLP: 2.0 Pr**	**BZLP: 2.5Pr**
$^1D_2 \rightarrow {}^3H_4$								
λ_P	604	604	604	604	604	604	604	604
$\Delta\lambda p$	18.67	18.90	19.54	16.01	14.97	14.50	14.19	15.63
β_R	0.247	0.215	0.180	0.194	0.214	0.2080	0.176	0.174
β_{exp}	0.88	0.94	0.95	0.37	0.48	0.45	0.56	0.39
σ_{se}	29.20	39.13	53.42	41.21	35.45	32.71	26.97	23.50
$\sigma_{se} \times \Delta\lambda_P$	54.54	73.98	104.41	66.00	53.07	47.45	38.30	36.74
$\sigma_{se} \times \tau_R$	7.39	6.10	4.80	6.18	7.05	6.77	5.79	5.10

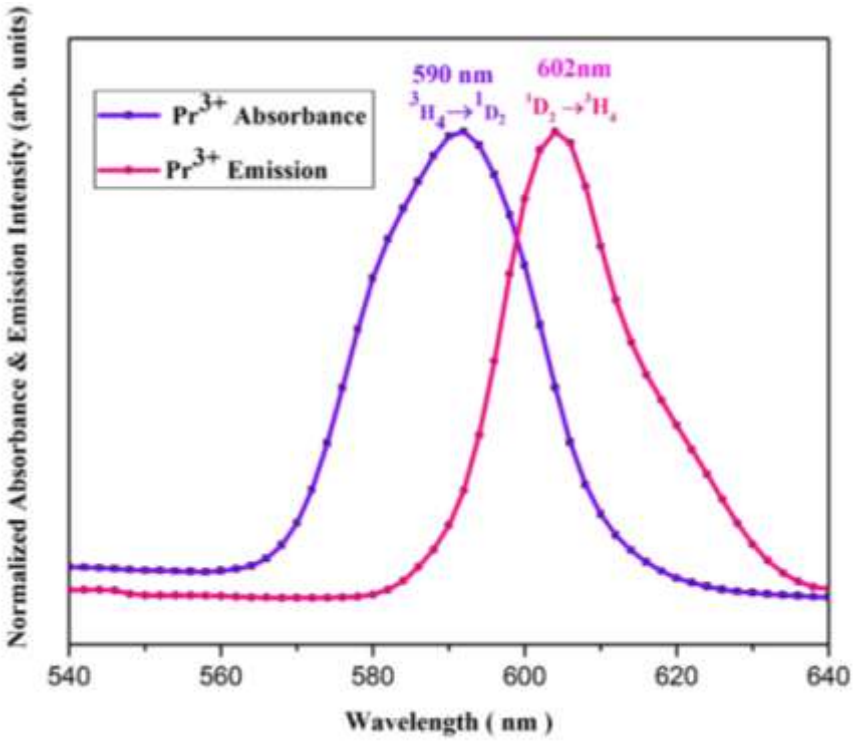

Fig. 5.8*. Spectral overlap of absorbance & emission spectrum of BZLP:0.1 glass for transition* $^1D_2 \rightarrow {}^3H_4$

Furthermore, a glassy material doped with RE ions having high values of gain bandwidth (σ_{se} x $\Delta\lambda p$) and optical gain parameters (σ_{se} x τ_R) can be used in construction of optical fibre. As it is evident from Table 5.5, BZLP:0.1Pr glass has high values for all radiative parameters as compared to other reported glasses. Therefore, BZLP:0.1Pr i.e. 0.1 mol% of Pr^{3+} doped BZLP glass is best fitted for reddish –orange laser transition at 604 nm.

5.3.5. Colorimetric study:

Chromaticity color coordinates of Pr^{3+} doped BZLP glass samples were evaluated based on PL results at λ_{ex} = 445 nm. And have been shown in Table 5.6. The estimated color coordinates lie in the red region of the CIE chromaticity diagram as shown in Fig. 5.9.

Table 5.6 CIE co-ordinates of Pr^{3+} ions in BZLP glasses.

Name of the sample	CIE co-ordinates	
	***X* co-ordinate**	***Y* co-ordinate**
BZLP: 0.01Pr	0.606	0.386
BZLP: 0.05Pr	0.628	0.363
BZLP: 0.1Pr	0.629	0.367
BZLP: 0.5Pr	0.571	0.416
BZLP: 1.0Pr	0.554	0.4231
BZLP: 1.5Pr	0.544	0.440
BZLP: 2.0 Pr	0.532	0.307
BZLP: 2.5 Pr	0.506	0.469

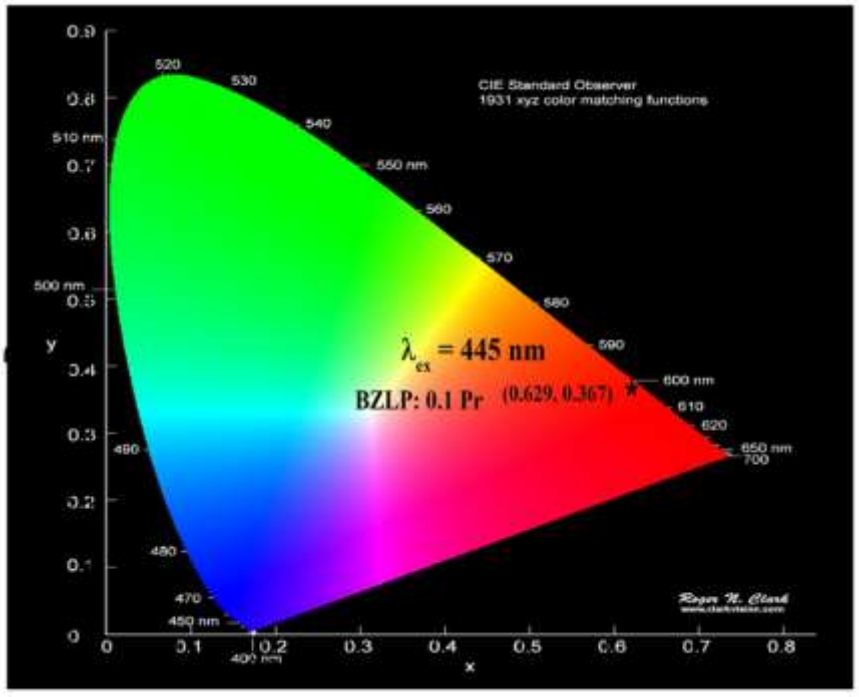

Fig.5.9: *CIE chromaticity coordinates of BZLP:0.10Pr glass.*

Further, the color purity is one of the vital parameters stating how pure or monochromatic a light for utilization in photonic applications. The color purity (CP) for all the glass samples were calculated via using equation 4.2 given in chapter 4

. The calculated color purity for the optimized glass was found to be 98.61%. The highly pure color of the Pr^{3+} doped BZLP glass samples make them an ideal candidate as a red light-emitting constituent in W-LEDs.

5.3.6. PL decay analysis:

PL decay profiles for Pr^{3+} doped BZLP glass samples have been documented at λ_{ex} = 445 nm and λ_{em} = 604 nm and shown in Fig. 5.10. The curves follow an exponential behaviour. The most proper fitting was attained for the bi-exponential function given by relation 1.17 in chapter 1 Click or tap here to enter text.

g.5.10: *PL decay curves of Pr^{3+} doped BZLP glasses with varying the doping concentration from 0.01 to 2.50 mol% under 445 nm excitation and emission at 604 nm.*

. The average (τ_{avg}) decay time for Pr^{3+} doped BZLP glass samples was assessed with the help formula 1.18 given in chapter 1 Click or tap here to enter text.

The τ_{avg} recorded decay profile of all glass samples was depicted in Table 5.7.

Table 5.7. Experimental lifetime (τ_{exp}) (μs), radiative lifetime (τ_R) (μs), quantum efficiency (η), and non-radiative decay rates (W_{NR}) (s^{-1}) for Pr^{3+} ions in BZLP glasses.

Sample	τ_{exp} (μs)	τ_R (μs)	η (%)	W_{NR}
BZLP: 0.01Pr	91	253	35.96	7036
BZLP: 0.05Pr	89	156	57.05	4825
BZLP: 0.1Pr	87	90	96.66	383
BZLP: 0.5Pr	86	150	57.33	4961
BZLP: 1.0Pr	85	199	42.71	6739
BZLP: 1.5Pr	83	207	40.09	7217
BZLP: 2.0 Pr	80	215	37.20	7848
BZLP: 2.5 Pr	75	217	34.56	8725

The average decay time decreased with an increase of Pr^{3+} ions in the glass lattice. This is due to reduced distance between the Pr^{3+} ions there by enhancing the non-radiative energy transfer. The estimated average decay time for BZLP:0.1Pr was τ_{avg} = 2.57 ms which reduced to τ_{avg} = 1.23 ms for BZLP:2.50 Pr glass. From Table 5.7, it is seen that τ_{exp} values are less than τ_R. This small variation between τ_{exp} and τ_R values arise due to multi phonon relaxation process. In this case τ_{exp} , τ_R and non-radiative decay rate (W_{NR}) are related by equation 3.4 given in chapter 3

Table 5.7. contains the W_{NR} values t determined using the aforementioned equation. Another crucial factor utilized to assess the luminescence intensity of reported glasses is the quantum efficiency (η %). By calculating the ratio between τ_{exp} and τ_R, quantum efficieny for prepared glasses has been estimated and presented in Table 5.7. It is evident from Table 5.7 that up to 0.1 mol% (BZLP:0.1Pr) glass, the value of η % rises and after that declines with increasing Pr^{3+} ions concentration. Furthermore , Table 5.8 represents the comparison between several radiative parameters with the other reported glasses in literature [237,240,241].

Table 5.8 Comparison of emission characteristics parameters like effective band widths ($\Delta\lambda_P$)(nm), measured branching ratio (β_R) and stimulated emission cross-sections (σ_{se} x 10^{-22}) (cm^2) of transition $^1D_2 \rightarrow {}^3H_4$ in different Pr^{3+} doped glasses.

Name of the sample	$\Delta\lambda_P$	β_R	σ_{se}	η (%)	References
BZLP: 0.01Pr	18.67	0.2479	29.20	35.96	Present work
BZLP: 0.05Pr	18.90	0.2154	39.13	57.05	Present work
BZLP: 0.1Pr	19.54	0.1806	53.42	96.66	Present work
BZLP: 0.5Pr	16.01	0.1940	41.21	57.33	Present work
BZLP: 1.0Pr	14.97	0.2146	35.45	42.71	Present work
BZLP: 1.5Pr	14.50	0.2080	32.71	40.09	Present work
BZLP: 2.0 Pr	14.19	0.1760	26.97	37.20	Present work
BZLP: 2.5 Pr	15.63	0.1742	23.50	34.56	Present work
0.1 Pr:NaAlGdP	16.50	0.82	27.64	78	[248]
ZNBBP-1	26.48	0.34	16.49	-	[249]
LiPbAlBPr 1.0	18.09	0.41	46.1	86	[237]

It has been observed that stimulated emission cross section of the Pr^{3+} BZLP doped glasses have larger value than other reported glasses [241,242] and are comparable with that of Pr^{3+} doped LiPbAlB glass reported by Nisha et. al [234] . From the data in Table 5.8, BZLP:0.1Pr

glass had the best quantum efficiency and stimulated emission cross section as compared to other reported glasses. Therefore, under 445 nm excitation, BZLP:0.1Pr glass is most suited for lasing emission in the reddish orange region.

5.3.7. Temperature-dependent PL (TD-PL) characteristics:

Thermal stability is one of the vital requirements of the luminescent materials for utility in W-LEDs applications. So, using the temperature dependent-photoluminescence (TD-PL) spectra, the thermal stability of the prepared glass samples was examined. The TD-PL spectra were reported at excitation wavelength of λ_{ex} = 445 nm as presented in Fig. 5.11.

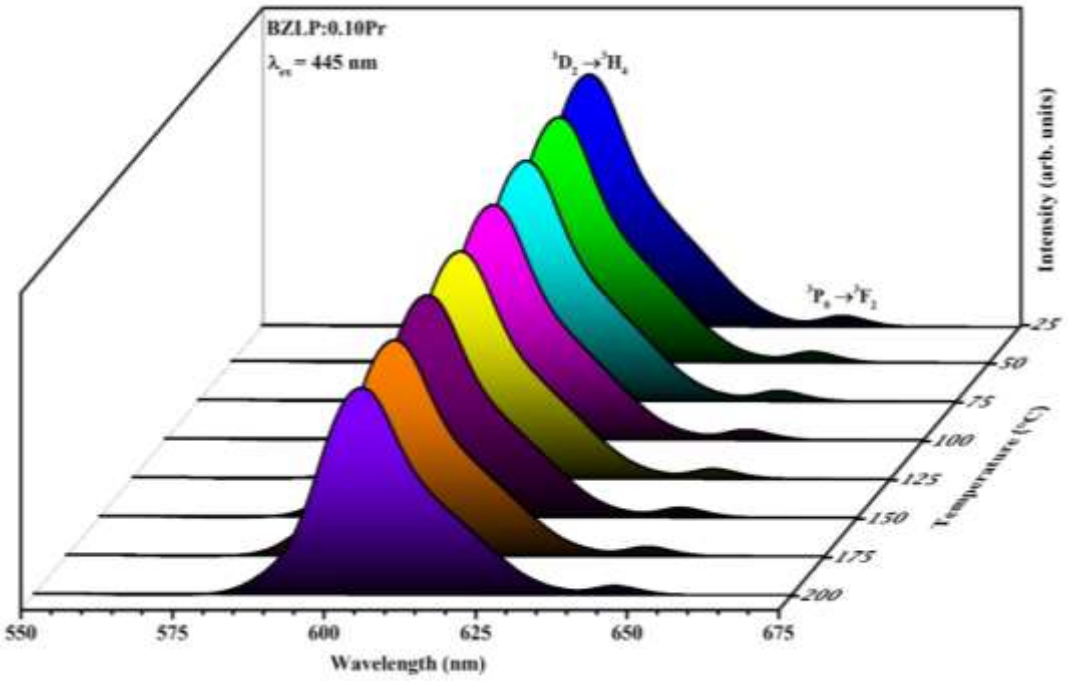

Fig.5.11*. TDPL spectra of optimized BZLP:0.10Pr glass with temperature varying from 27 ˚C to 200 ˚C under 445 nm excitation wavelength.*

It is evident that with an increase in temperature from 300 K to 473 K, PL intensity diminishes gradually but the spectral shape/peak position is unaffected. Further, the activation energy (ΔE) was evaluated using the equation 3.5 given in chapter 3

The value of ΔE was assessed via the slope of the linear fitted plot between $ln((I_0/I_T)-1)$ and $1/K_BT$ as shown in Fig.5. 12 [243]. The activation energy was found to ΔE = 0.175 eV for BZLP:0.1Pr glass. Inset plot of Fig.5.12 reveals the PL intensity reduced from 88.12 % at 423 K to 82.61 % at 473 K, which shows that glass samples have brilliant thermal stability.

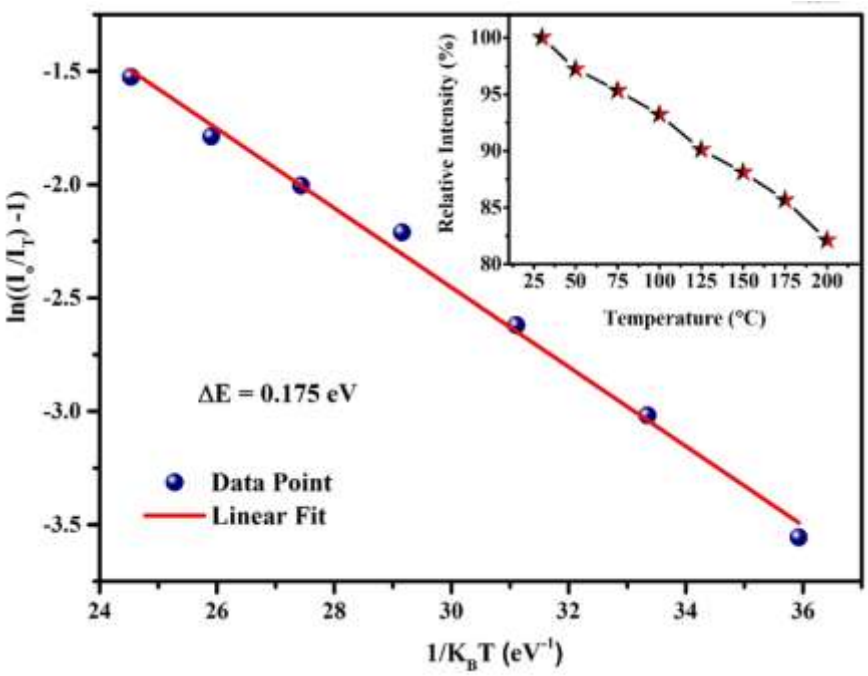

Fig. 5.12. *Graph between $ln[(I_o/I_T)-1]$ and $(1/K_BT)$ for BZLP:0.10Pr glass. The inset plot shows the decrease in relative emission intensity with rise in temperature from 27 ˚C to 200 ˚C.*

5.4. Conclusions:

Trivalent praseodymium doped BZLP glass samples were synthesized through melt quenching route and their structural, physical and optical properties were studied for utility in luminescent

device applications. The diffraction pattern confirmed the unstructured and nonexistent crystalline character of host glass. Absorption spectra showed several bands in ultraviolet, visible and infrared regions. The indirect optical bandgap was estimated using Tauc's plot for each glass and was found to be in the range 3.48-4.07 eV. Using J-O parameters derived from the absorption spectrum, several radiative parameters were assessed for the reported fluorescence peaks of Pr^{3+} ions in BZLP glass samples. The PL spectra at 445 nm excitation shows prominent emission peak at 604 nm due to $^1D_2 \rightarrow {}^3H_4$ transition of Pr^{3+} ions. Beyond 0.10 mol% of Pr^{3+} ion concentration, quenching effect is observed due to dipole-dipole type of interaction between the dopant ions as confirmed by the Dexter plot. For the transitions $^1D_2 \rightarrow {}^3H_4$, stimulated emission cross-section, branching ratios and quantum efficiency were assessed. The CIE coordinates for the as prepared glasses fall in deep-red region. The average lifetime values at λ_{ex} = 445 nm for 604 nm emission were observed to decrease with an increase in Pr^{3+} ion content in BZLP glasses. The TD-PL study shows that the glass has an excellent thermal stability with activation energy ΔE = 0.175 eV. After analyzing the several evaluated radiative parameters, it was revealed that amongst all the Pr^{3+} doped BZLP glass samples, BZLP:0.1Pr glass can be used as a deep red-emitting component in blue pumped white LED and other luminescent device applications.

CHAPTER 6

SUMMARY AND FUTURE SCOPE OF THE WORK

The current chapter provides a summary of the general research effort given in this dissertation as well as the specific conclusions reached from the findings. This chapter also explores how the current work might be expanded upon and utilized going forward to guide new lines of investigation.

6.1. Summary:

The present researchers working in the field of glass science & technology the scholar has prepared variety of glasses using the numerous glass formers along with network formers and studied their spectroscopic properties. Among various glass formers, phosphate is one of the suitable glass formers owing to distinctive properties like clear visibility in the wide-ranging spectrum, softening, less melting temperature, high thermal stability, high RE ion solubility and low dispersion. Phosphate glasses possess various applications in photonic devices but it has some limitations because of its hygroscopic nature and poor chemical stability. To overcome these limitations, network modifiers (BaO, Li_2O) and intermediate (ZnO) have been added to the host glass, which can increase chemical stability and reduce thermal expansions. Moreover, ZnO helps to overcome hygroscopic nature and increases the solubility of RE ions. All the above-discussed characteristic features possessed by the chemical species P_2O_5, Li_2O, BaO and ZnO prompted the scholar to prepare a glassy system namely barium zinc lithium phosphate (BZLP) glass. Phosphate based glasses doped with RE ions are effective in improving the

luminescent characteristics of a materials to have potential applications in the field of optoelectronics.

Dy^{3+} activated BZLP glasses are effectively absorbing UV, visible and NIR radiation having the optical bandgap in the 3.64 - 3.76 eV range. Radiative properties of distinguished glowing levels of Dy^{3+} ions in BZLP glasses were measured through J–O parameters. The PL spectra of BZLP glasses reveal three sharp peaks, out of which yellow emission (575 nm) was the more intense as compared with blue, and red emission under 350 nm excitation wavelength. The decay curves show the exponential in nature. The calculated CIE coordinates are in good approximation with standard white light points (0.33, 0.33) of equal energy and lie in the visible region. The values of CCT of BZLP glasses fall in the bright white light and make them suitable for w-LEDs. Relatively high activation energy BZLP glass doped with 1.5 mol% of Dy^{3+} ion concentration measured from the recorded TD-PL spectrum reveals excellent thermal stability for it. From the various calculated radiative parameters especially quantum efficiency and stimulated emission cross-section, it was summarized that among various Dy^{3+} activated BZLP glasses, (the one with 1.5 mol% of Dy^{3+} ion concentration) is quite suitable for the fabrication of visible photonic devices such as yellow lasers and w-LEDs.

The XRD pattern recorded for Tb^{3+} doped glasses confirmed their glassy nature. UV- vis spectra were employed to estimate the energy band gap for Tb^{3+} doped BZLP glasses via Tauc's plot, which is found in the range of 4.57-4.19 eV. The dominant emission attributed to the $^5D_4 \rightarrow {}^7F_5$ transition gave the intense green emission at 542 nm under 373 nm excitation wavelength. All the evaluated coordinates were situated in the green region of the CIE diagram. The chromaticity coordinates for BZLP glass with 0.5 mol% of Tb^{3+} ions show CIE coordinates (0.309, 0.597) which matches well with green emitting standard data. The PL decay profiles

of Tb^{3+} doped BZLP glasses are found bi-exponential in nature. A significantly slighter decrease in emission intensity with rising temperature and the high activation energy value (0.161 eV) suggests that the prepared glasses have good thermal stability. The above-mentioned characteristics indicate the suitability of Tb^{3+} doped BZLP glasses for green color emitting components useful in various photonic device applications such as display devices and w-LEDs.

Trivalent praseodymium doped BZLP glass samples were synthesized through melt quenching route and their structural, physical and optical properties were studied for utility in luminescent device applications. The diffraction pattern confirmed the unstructured and nonexistent crystalline character of host glass. Absorption spectra showed several bands in ultraviolet, visible and infrared regions. The indirect optical bandgap was estimated using Tauc's plot for each glass and was found to be in the range 3.48-4.07 eV. Using J-O parameters derived from the absorption spectrum, several radiative parameters were assessed for the reported fluorescence peaks of Pr^{3+} ions in BZLP glass samples. The PL spectra at 445 nm excitation shows prominent emission peak at 604 nm due to $^1D_2 \rightarrow {}^3H_4$ transition of Pr^{3+} ions. Beyond 0.10 mol% of Pr^{3+} ion concentration, quenching effect is observed due to dipole-dipole type of interaction between the dopant ions as confirmed by the Dexter plot. For the transition $^1D_2 \rightarrow {}^3H_4$, stimulated emission cross-section, branching ratios and quantum efficiency were assessed. The CIE coordinates for the as prepared glasses fall in deep-red region. The average lifetime values at λ_{ex} = 445 nm for 604 nm emission were observed to decrease with an increase in Pr^{3+} ion content in BZLP glasses. The TD-PL study shows that the glass has an excellent thermal stability with activation energy ΔE = 0.175 eV. After analyzing the several evaluated radiative parameters, it was revealed that amongst all the Pr^{3+} doped BZLP glass samples,

BZLP:0.1Pr glass can be used as a deep red-emitting component in blue pumped white LED and other luminescent device applications.

6.2. Future scope of the work:

1. The host glasses are improved for better photonic device application by altering the alkaline and alkaline-earth metals.
2. To investigate the energy transfer processes between the sensitizer and activator incorporated into phosphate glass hosts and thereby to measure quantum efficiency
3. By applying heat to various phosphate glasses over varying lengths of time at a temperature slightly below the glass transition point, glasses may be converted into glassy ceramics and studied their radiative properties.
4. Fabrication of proto type LED devices utilizing appropriate technology to assess the usability of the produced glasses in real-world situations.

REFERENCES:

[1] G.C. Righini, F. Enrichi, L. Zur, M. Ferrari, J Phys Conf Ser 1221 (2019).

[2] C. Zhu, Y. Yang, X. Liang, S. Yuan, G. Chen, J Lumin 126 (2007) 707–710.

[3] A.S. Rao, Y.N. Ahammed, R.R. Reddy, T.V.R. Rao, Spectroscopic Studies of Nd 3q-Doped Alkali Fluoroborophosphate Glasses, 1998.

[4] E.F. Schubert, Cambridge University Press, New York, . 2nd ed (2005).

[5] C.K.J. K.U. Kumar, P.Babu, Ch.Basavapoornima, R.Praveena, D. S. Rani, Physica B: Condens. Matter. 646 (2022) 413427.

[6] V. Venkatramu, P. Babu, I.R. Martín, V. Lavín, J.E. Muöoz-Santiuste, T. Tröster, W. Sievers, G. Wortmann, C.K. Jayasankar, Journal of Chemical Physics 132 (2010).

[7] B. Minnaert, P. Veelaert, Energies (Basel) 7 (2014) 1500–1516.

[8] J. Pisarska, L. Zur, W.A. Pisarski, Physica Status Solidi (A) Applications and Materials Science 209 (2012) 1134–1140.

[9] D. Chen, Z. Wan, Y. Zhou, X. Zhou, Y. Yu, J. Zhong, M. Ding, Z. Ji, ACS Appl Mater Interfaces 7 (2015) 19484–19493.

[10] J. Zhou, Q. Liu, W. Feng, Y. Sun, F. Li, Chem Rev 115 (2014) 395–465.

[11] H. Rawson, Inorganic Glass- Forming System academic press, N.Y. (1967).

[12] C. Feldmann, T. Justel, C.R. Ronda, P.J. Schmidt, Adv Funct Mater 13 (2003) 511–516.

[13] Guokui. Liu, B. Jacquier, (2010) 550.

[14] A.A. Setlur, Electrochemical Society Interface 18 (2009) 32–36.

[15] V.R. Bandi, M. Jayasimhadri, J. Jeong, K. Jang, H.S. Lee, S.S. Yi, J.H. Jeong, J Phys D Appl Phys 43 (2010).

[16] K. Li, H. Lian, R. Van Deun, Dalton Transactions 47 (2018) 2501–2505.

[17] C.C. Lin, A. Meijerink, R.S. Liu, Journal of Physical Chemistry Letters 7 (2016) 495–503.

[18] Z.C. Wu, J.X. Shi, J. Wang, M.L. Gong, Q. Su, J Solid State Chem 179 (2006) 2356–2360.

[19] N. Lohia, V. V. Jaiswal, S. Bishnoi, G. Swati, S.N. Sharma, M. Mohapatra, D. Haranath, Ceram Int 46 (2020) 4079–4085.

[20] M. Jayasimhadri, K. Jha, B. V. Ratnam, H.J. Woo, K. Jang, A.S. Rao, D. Haranath, J Alloys Compd 711 (2017) 395–399.

[21] A. Kudo, Chemistry of Materials 9 (1997) 664–669.

[22] B.R. Judd, J Chem Phys 44 (1966) 839–840.

[23] X. Wang, Q. Liu, Y. Bu, C.S. Liu, T. Liu, X. Yan, RSC Adv 5 (2015) 86219–86236.

[24] A. Jha, B. Richards, G. Jose, T. Teddy-Fernandez, P. Joshi, X. Jiang, J. Lousteau, Prog. Mater Sci. 57 (2012) 1426–1491.

[25] B. Hou, M. Jia, P. Li, G. Liu, Z. Sun, Z. Fu, Inorg Chem 58 (2019) 7939–7946.

[26] S. Al-Waisawy, W.M. Jadwisienczak, J.T. Wright, D. Pendrill, F. Rahman, J Lumin 169 (2016) 196–203.

[27] Y. Gao, J. Qiu, D. Zhou, Journal of the American Ceramic Society 100 (2017) 2901–2913.

[28] D. Chen, W. Xiang, X. Liang, J. Zhong, H. Yu, M. Ding, H. Lu, Z. Ji, J Eur Ceram Soc 35 (2015) 859–869.

[29] Y. Gao, S. Murai, K. Shinozaki, J. Qiu, K. Tanaka, ACS Appl Electron Mater 1 (2019) 961–971.

[30] M. Wilding, Y. Badyal, A. Navrotsky, J Non Cryst Solids 353 (2007) 4792–4800.

[31] M. Mohapatra, V. Natarajan, S. V. Godbole, J Non Cryst Solids 386 (2014) 115–120.

[32] A. Okasha, A.M. Abdelghany, S.Y. Marzouk, Journal of Materials Research and Technology 9 (2020) 59–66.

[33] S.N.S. Yaacob, M.R. Sahar, E.S. Sazali, Z.A. Mahraz, K. Sulhadi, Solid State Sci 81 (2018) 51–57.

[34] J.A. Duffy, M.D. Ingram, J Non Cryst Solids 21 (1976) 373–410.

[35] C.R. Ronda, (2008) 260.

[36] M. Anand Pandarinath, G. Upender, K. Narasimha Rao, D. Suresh Babu, J. Non-Cryst. Solids 433 (2016) 60–67.

[37] S. Davison, R.G. Newton, Routledge (2008).

[38] J. Lin, Y. Lu, X. Li, F. Huang, C. Yang, M. Liu, N. Jiang, D. Chen, ACS Energy Lett 6 (2021) 519–528.

[39] P. Yasaka, J. Kaewkhao, in: Proceedings - 2015 4th International Conference on Instrumentation, Communications, Information Technology and Biomedical Engineering, ICICI-BME 2015, Institute of Electrical and Electronics Engineers Inc., 2016, pp. 4–15.

[40] G.C. Righini, F. Enrichi, L. Zur, M. Ferrari, J Phys Conf Ser 1221 (2019) 012028.

[41] L. Mishra, A. Sharma, A.K. Vishwakarma, K. Jha, M. Jayasimhadri, B. V Ratnam, K. Jang, A.S. Rao, R.K. Sinha, J Lumin 169 (2016) 121–127.

[42] S. Kumar Ray, Y.K. Kshetri, S. Wohn Lee -, P. Linna Guo, Y. Wang, J. Zhang, al -, nanotubes Zepeng Li, J. Wang, L. Wang, E. Erol, N. Vahedigharehchopogh, O. Kıbrıslı, elikbilek Ersundu, A. Erç in Ersundu, Journal of Physics: Condensed Matter 33 (2021) 483001.

[43] Y. Wang, W. Zheng, Y. Lu, P. Li, S. Xu, J. Zhang, J Lumin 237 (2021) 118152.

[44] L.D. Pye, R. Locker, M.J. Plodinec, Materials Science Research 15 (1983) 627–637.

[45] F. N, A. G, YMER Digital 21 (2022) 111–126.

[46] Y. Zheng, B. Chen, H. Zhong, J. Sun, L. Cheng, X. Li, J. Zhang, Y. Tian, W. Lu, J. Wan, T. Yu, L. Huang, H. Yu, H. Lin, Journal of the American Ceramic Society 94 (2011) 1766–1772.

[47] Optical Nonlinearities in Chalcogenide Glasses and Their Applications (2007) 1–28.

[48] A.G. Clare, P.F. Wachtel, J.D. Musgraves, Springer Handbooks (2019) 595–616.

[49] J.D. Musgraves, J. Hu, L. Calvez, (2019) 1851.

[50] M. Giordano, D. Leporini, M.P. Tosi, (1996) 1–392.

[51] Luminescence: Phenomena, Materials and Applications & Special Attention to Borate Host Materials, n.d.

[52] L.U. Khan, Z.U. Khan, Handbook of Materials Characterization (2018) 345–404.

[53] J.R. Lakowicz, Principles of Fluorescence Spectroscopy Principles of Fluorescence Spectroscopy, 2006.

[54] G.S. Opelt, J Chem Phys 37 (1962) 511–520.

[55] V. Bhatia, D. Kumar, A. Kumar, V. Mehta, S. Chopra, A. Vij, S.M.D. Rao, S.P. Singh, Journal of Materials Science: Materials in Electronics 30 (2019) 677–686.

[56] L.G. Van Uitert, J Electrochem Soc 114 (1967) 1048–1053.

[57] Q. Wang, M. Liao, Q. Lin, M. Xiong, Z. Mu, F. Wu, J Alloys Compd 850 (2021).

[58] A. Kitai, Luminescent Materials and Applications, John Wiley & Sons Ltd, England, 2008.

[59] . R.D. Peacock, Struct. Bond. Berlin 22 (1975) 83-122

[60] Q. Chen, B. Miao, P.S. Kumar, S. Xu, Opt Mater (Amst) 116 (2021) 111093.

[61] M. Dalal, V.B. Taxak, S. Chahar, J. Dalal, A. Khatkar, S.P. Khatkar, J Alloys Compd 686 (2016) 366–374.

[62] B.M. Walsh, Advances in Spectroscopy for Lasers and Sensing (2006) 403–433.

[63] N. Deopa, A.S. Rao, Opt Mater (Amst) 72 (2017) 31–39.

[64] N. Deopa, M.K. Sahu, P.R. Rani, R. Punia, A.S. Rao, J Lumin 222 (2020) 117166.

[65] N. Deopa, A.S. Rao, S. Mahamuda, M. Gupta, M. Jayasimhadri, D. Haranath, G.V. Prakash, J Alloys Compd 708 (2017) 911–921.

[66] N. Deopa, A.S. Rao, A. Choudhary, S. Saini, A. Navhal, M. Jayasimhadri, D. Haranath, G. Vijaya Prakash, Mater Res Bull 100 (2018) 206–212.

[67] A. Ćirić, Ł. Marciniak, M.D. Dramićanin, Scientific Reports 2022 12:1 12 (2022) 1–10.

[68] B. Zhou, Z. Li, C. Chen, Minerals 7 (2017) 203.

[69] K. Maheshwari, A.S. Rao, Opt Mater (Amst) 137 (2023) 113533.

[70] A. Zakery, S.R. Elliott, Springer Series in Optical Sciences 135 (2007) 1–193.

[71] D.H. Ravishanker Yadav, Atif F. Khan, Ashish Yadav, Harish Chander, V.S. and S.C. Bipin Kr. Gupta, Opt Express 17 (2009) 116258.

[72] M.K. Sahu, M. Jayasimhadri, Journal of Materials Science: Materials in Electronics 33 (2022) 5201–5213.

[73] N. Deopa, B. Kumar, M.K. Sahu, P.R. Rani, A.S. Rao, J Non Cryst Solids 513 (2019) 152–158.

[74] R. Shi, L. Ning, Y. Huang, Y. Tao, L. Zheng, Z. Li, H. Liang, ACS Appl Mater Interfaces 11 (2019) 9691–9695.

[75] K. Maheshwari, Ravita, A. Prasad, Y. Tayal, A.S. Rao, Opt Mater (Amst) 140 (2023).

[76] B.P. Choudhary, N.B. Singh, (2023) 79–112.

[77] G. Galleani, S.H. Santagneli, Y. Ledemi, Y. Messaddeq, O. Janka, R. Pöttgen, H. Eckert, Journal of Physical Chemistry C 122 (2018) 2275–2284.

[78] J.-L. Cia, R.-Y. Yi, C.-J. Zhao, S.-T. Tie, Ju.-Y. Shen, Mater Res Bull 57 (2014) 85–90.

[79] K.R. Vighnesh, B. Ramya, S. Nimitha, A. Wagh, M.I. Sayyed, E. Sakar, H.A. Yakout, A. Dahshan, S.D. Kamath, Opt Mater (Amst) 99 (2020) 109512.

[80] M. Kuwik, J. Pisarska, W.A. Pisarski, Materials 13 (2020) 1–20.

[81] G. Sole, L.E. Bausa, D. Jaque, An Introduction to the Optical Spectroscopy of Inorganic Solids, John Wiley & Sons Ltd, England, 2005.

[82] W.T. Carnall, P.R. Fields, K. Rajnak, J. Chem. Phys. 49 (2003) 4424.

[83] K.N. Shinde, S.J. Dhoble, H.C. Swart, K. Park, Phosphate Phosphors for Solid-State Lighting, Springer Series in Materials Science, vol 174. Springer, Berlin, Heidelberg. (2012).

[84] V. Dubey, R. Tiwari, M. Pradhan, G. Rathore, C. Sharma, R. Tamrakar, Journal of Luminescence and Applications 1 (2014) 30–39.

[85] L. Alexander, H.P. Klug, J Appl Phys 21 (1950) 137–142.

[86] K. Rajnak, B.G. Wybourne, J Chem Phys 41 (1964) 565–569.

[87] B.D. Cullity, Addision-Wesley Publishing COMPANY 2 edition (1978) 0–555.

[88] L. Berzina-Cimdina, N. Borodajenko, Infrared Spectroscopy - Materials Science, Engineering and Technology (2012).

[89] C.S. Pappas, P.A. Tarantilis, P.C. Harizanis, M.G. Polissiou, Appl Spectrosc 57 (2003) 23–27.

[90] K. Jha, M. Jayasimhadri, J Lumin 194 (2018) 102–107.

[91] R.E. Hummel, Encyclopedia of Analytical Chemistry (2000).

[92] N. Fuhrmann, E. Baum, J. Brübach, A. Dreizler, Review of Scientific Instruments 82 (2011).

[93] A Kumar, S. Tripathi, a D. Deshmukh, D. Haranath, P. Singh, a M. Biradar, J Phys D Appl Phys 46 (2013) 195302.

[94] J.S. Kim, Y.H. Park, S.M. Kim, J.C. Choi, H.L. Park, Solid State Commun 133 (2005) 445–448.

[95] V.K. Rai, Applied Physics B 2007 88:2 88 (2007) 297–303.

[96] J. Brübach, C. Pflitsch, A. Dreizler, B. Atakan, Prog Energy Combust Sci 39 (2013) 37–60.

[97] A.A. Reddy, M.C. Sekhar, K. Pradeesh, S.S. Babu, G.V. Prakash, J Mater Sci 46 (2011) 2018–2023.

[98] S. Selvi, G. Venkataiah, S. Arunkumar, G. Muralidharan, K. Marimuthu, Physica B Condens Matter 454 (2014) 72–81.

[99] Y.N.C. Ravi Babu, P. Sree Ram Naik, K. Vijaya Kumar, N. Rajesh Kumar, A. Suresh Kumar, J Quant Spectrosc Radiat Transf 113 (2012) 1669–1675.

[100] A. Srinivasa Rao, B. Rupa Venkateswara Rao, M.V.V.K.S. Prasad, J. V. Shanmukha Kumar, M. Jayasimhadri, J.L. Rao, R.P.S. Chakradhar, Physica B Condens Matter 404 (2009) 3717–3721.

[101] A.S. Rao, Y.N. Ahammed, R.R. Reddy, T.V.R. Rao, Spectroscopic Studies of Nd 3q-Doped Alkali Fluoroborophosphate Glasses, 1998.

[102] Y. Tayal, A.S. Rao, Opt Mater (Amst) 107 (2020).

[103] A.A. Reddy, M.C. Sekhar, K. Pradeesh, S.S. Babu, G.V. Prakash, J Mater Sci 46 (2011) 2018–2023.

[104] Y.G. Choi, J. Heo, ..3 Txm Emission and Multiphonon Relaxation Phenomena in PbO-BizO3-Ga203 Glasses Doped with Rare-Earths, 1997.

[105] J.S. Kim, K.T. Lim, Y.S. Jeong, P.E. Jeon, J.C. Choi, H.L. Park, Solid State Commun 135 (2005) 21–24.

[106] C. Zhu, Y. Yang, X. Liang, S. Yuan, G. Chen, J Lumin 126 (2007) 707–710.

[107] H. Masai, Y. Yamada, Y. Suzuki, K. Teramura, Y. Kanemitsu, T. Yoko, Sci Rep 3 (2013).

[108] K. Jha, M. Jayasimhadri, J Alloys Compd 688 (2016) 833–840.

[109] R.J. Amjad, M.R. Dousti, M.R. Sahar, Current Applied Physics 15 (2015) 1–7.

[110] M. Higuchi, R. Sasaki, J. Takahashi, J Cryst Growth 311 (2009) 4549–4552.

[111] Z. Yan, X. Zhongzi, L. Chunhua (t%&-Q), N. Yam, Z. Qitu, Optical Properties of Dy3 + Doped in Boroaluminasilicate Glass, 2007.

[112] P. Manasa, C.K. Jayasankar, Spectrochim Acta A Mol Biomol Spectrosc 212 (2019) 315–321.

[113] Y.H. Zhang, D.S. Li, X. Zhao, E.Y.B. Pun, H. Lin, J Alloys Compd 728 (2017) 1279–1288.

[114] C. Madhukar Reddy, G.R. Dillip, B. Deva Prasad Raju, Journal of Physics and Chemistry of Solids 72 (2011) 1436–1441.

[115] A.M. Babu, B.C. Jamalaiah, J.S. Kumar, T. Sasikala, L.R. Moorthy, J Alloys Compd 509 (2011) 457–462.

[116] I. Khan, G. Rooh, R. Rajaramakrishna, N. Srisittipokakun, C. Wongdeeying, N. Kiwsakunkran, N. Wantana, H.J. Kim, J. Kaewkhao, S. Tuscharoen, J Alloys Compd 774 (2019) 244–254.

[117] P. Rekha Rani, M. Venkateswarlu, S. Mahamuda, K. Swapna, N. Deopa, A.S. Rao, J Alloys Compd 787 (2019) 503–518.

[118] S. Tian, Y. Lun, Y. Sun, D. Chen, G. Tang, Q. Qian, Z. Yang, J Non Cryst Solids (2021) 121313.

[119] P. Babu, V. Chandrappa, N. Vijaya, C.K. Jayasankar, H.J. Seo, Physica B Condens Matter 614 (2021) 413037.

[120] R.J. Amjad, T.O. Sales, A. Sattar, C. Jacinto, M.R. Dousti, J Lumin 231 (2021) 117839.

[121] R.S. Gedam, D.D. Ramteke, in: AIP Conf Proc, 2012, pp. 561–562.

[122] W.T. Carnall, P.R. Fields, K. Rajnak, J Chem Phys 49 (1968) 4424–4442.

[123] A.H. Khafagy, M.A. Ewaida, A.A. Higazy, M.M. S Ghoneim, I.Z. Hager, R. El-bahnasawy, Infrared Spectra and Composition Dependence Investigations of the Vitreous V205/P205 System, 1992.

[124] R. Lakshmikantha, R. Rajaramakrishna, R. V. Anavekar, N.H. Ayachit, Mater Chem Phys 133 (2012) 249–252.

[125] Y.B. Saddeek, Physica B Condens Matter 406 (2011) 562–566.

[126] A.M. E®mov, V.G. Pogareva, Water-Related IR Absorption Spectra for Some Phosphate and Silicate Glasses, n.d.

[127] M. Kumar, A.S. Rao, Opt Mater (Amst) 109 (2020) 110356.

[128] E. Mansour, G. El-Damrawi, Physica B Condens Matter 405 (2010) 2137–2143.

[129] R.S. Gedam, D.D. Ramteke, in: AIP Conf Proc, 2012, pp. 561–562.

[130] M. Altaf, M.A. Chaudhry, M. Zahid, 14 (2003) 253–259.

[131] C. Klixbull, J.$ Rgensen, The Nephelauxetic Series, Vol 4, Prog.Inorg.chem, 1962.

[132] A. Srinivasa Rao, B. Rupa Venkateswara Rao, M.V.V.K.S. Prasad, J. V. Shanmukha Kumar, M. Jayasimhadri, J.L. Rao, R.P.S. Chakradhar, Physica B Condens Matter 404 (2009) 3717–3721.

[133] B.R. Judd, Physical Review 127 (1962) 750–761.

[134] N. Deopa, A.S. Rao, J Lumin 192 (2017) 832–841.

[135] M. Reddi Babu, N. Madhusudhana Rao, A. Mohan Babu, N. Jaidass, C. Krishna Moorthy, L. Rama Moorthy, Optik (Stuttg) 127 (2016) 3121–3126.

[136] A. Lira, A. Speghini, E. Camarillo, M. Bettinelli, U. Caldiño, Opt Mater (Amst) 38 (2014) 188–192.

[137] S.N. Rasool, L. Rama Moorthy, C.K. Jayasankar, Solid State Sci 22 (2013) 82–90.

[138] C.B. Annapurna Devi, S. Mahamuda, M. Venkateswarlu, K. Swapna, A. Srinivasa Rao, G. Vijaya Prakash, Opt Mater (Amst) 62 (2016) 569–577.

[139] K. Swapna, S. Mahamuda, A. Srinivasa Rao, M. Jayasimhadri, T. Sasikala, L. Rama Moorthy, Ceram Int 39 (2013) 8459–8465.

[140] Y.C. Ratnakaram, D. Thirupathi Naidu, A. Vijayakumar, J.L. Rao, Opt Mater (Amst) 27 (2004) 409–417.

[141] Y.B. Shin, J. Heo, Mid-Infrared Emissions and Multiphonon Relaxation in Dy 3‡-Doped Chalcohalide Glasses, n.d.

[142] R.R. Jacobs, M.J. Weber, IEEE J Quantum Electron 11 (1975) 846–847.

[143] B.C. Jamalaiah, L.R. Moorthy, H.J. Seo, J Non Cryst Solids 358 (2012) 204–209.

[144] M. Reddi Babu, N. Madhusudhana Rao, A. Mohan Babu, N. Jaidass, C. Krishna Moorthy, L. Rama Moorthy, Optik (Stuttg) 127 (2016) 3121–3126.

[145] P. Manasa, C.K. Jayasankar, Spectrochim Acta A Mol Biomol Spectrosc 212 (2019) 315–321.

[146] N. Luewarasirikul, H.J. Kim, P. Meejitpaisan, J. Kaewkhao, Opt Mater (Amst) 66 (2017) 559–566.

[147] M. Vijayakumar, K. Marimuthu, J Alloys Compd 629 (2015) 230–241.

[148] T.G.V.M. Rao, A. Rupesh Kumar, K. Neeraja, N. Veeraiah, M. Rami Reddy, Spectrochim Acta A Mol Biomol Spectrosc 118 (2014) 744–751.

[149] T. Sasikala, L. Rama Moorthy, A. Mohan Babu, T. Srinivasa Rao, J Solid State Chem 203 (2013) 55–59.

[150] V. Uma, K. Marimuthu, G. Muralidharan, J Fluoresc 26 (2016) 2281–2294.

[151] K. Siva Rama Krishna Reddy, K. Swapna, S. Mahamuda, M. Venkateswarlu, A.S. Rao, G. Vijaya Prakash, Opt Mater (Amst) 85 (2018) 200–210.

[152] S. Zulfiqar Ali Ahamed, C. Madhukar Reddy, B. Deva Prasad Raju, Opt Mater (Amst) 35 (2013) 1385–1394.

[153] D.L. Dexter, J.H. Schulman, J Chem Phys 22 (1954) 1063–1070.

[154] J. Suresh Kumar, K. Pavani, A. Mohan Babu, N. Kumar Giri, S.B. Rai, L.R. Moorthy, J Lumin 130 (2010) 1916–1923.

[155] T. Srihari, C.K. Jayasankar, Opt Mater (Amst) 69 (2017) 87–95.

[156] P. Karthikeyan, R. Vijayakumar, K. Marimuthu, Physica B Condens Matter 521 (2017) 347–354.

[157] F. Zaman, J. Kaewkhao, N. Srisittipokakun, N. Wantana, H.J. Kim, G. Rooh, Opt Mater (Amst) 55 (2016) 136–144.

[158] R. Casesa, M.A. Chamarroa, R. Alcalaa, V.D. Rodriguezb, Optical Properties of Nd 3~and Dy3~ions in ZnF 2-CdF2 Based Glasses, 1991.

[159] C. Venkateswarlu, M. Seshadri, Y.C. Ratnakaram, Opt Mater (Amst) 33 (2011) 799–806.

[160] P. Babu, K.H. Jang, E.S. Kim, L. Shi, R. Vijaya, V. Lavín, C.K. Jayasankar, H.J. Seo, J Non Cryst Solids 356 (2010) 236–243.

[161] R.D. Peacock, The Intensities of Lanthanide f +-~ FTransitions, 22nd ed., struct.Bond, 1975.

[162] C.S. McCamy, Color Res Appl 17 (1992) 142–144.

[163] S. Kaur, A.K. Vishwakarma, N. Deopa, A. Prasad, M. Jayasimhadri, A.S. Rao, Mater Res Bull 104 (2018) 77–82.

[164] K. Jha, A.K. Vishwakarma, M. Jayasimhadri, D. Haranath, J Alloys Compd 719 (2017) 116–124.

[165] M.K. Sahu, J. Mula, Journal of the American Ceramic Society 102 (2019) 6087–6099.

[166] Ravita, A.S. Rao, J Lumin 239 (2021) 118325.

[167] P. Vani, G. Vinitha, M.I. Sayyed, M.M. AlShammari, N. Manikandan, Nuclear Engineering and Technology 53 (2021) 4106–4113.

[168] A. Kaur, A. Khanna, M. González-Barriuso, F. González, Journal of Materials Science: Materials in Electronics 32 (2021) 17266–17281.

[169] N. Deopa, A.S. Rao, S. Mahamuda, M. Gupta, M. Jayasimhadri, D. Haranath, G.V. Prakash, J Alloys Compd 708 (2017) 911–921.

[170] A. Tamang, A. Hongsingthong, V. Jovanov, P. Sichanugrist, B.A. Khan, R. Dewan, M. Konagai, D. Knipp, Sci. Reports 6 (2016) 29639.

[171] Ravita, A.S. Rao, J Lumin 239 (2021) 118325.

[172] A.S.R. A. Kumar, Anu, M.K. Sahu, Ravita, S. Dahiya, N. Deopa, A. Malik, R. Punia, J Lumin 244 (2022) 118676.

[173] Ravita, A. S.Rao, J Lumin (2021) 118689.

[174] J. Gou, J. Fan, S. Zuo, M. Luo, Y. Chen, X. Zhou, Y. Yang, B. Yu, S.F. Liu, Journal of the American Ceramic Society 100 (2017) 4011–4020.

[175] F. Enrichi, C. Armellini, S. Belmokhtar, A. Bouajaj, A. Chiappini, M. Ferrari, A. Quandt, G.C. Righini, A. Vomiero, L. Zur, J Lumin 193 (2018) 44–50.

[176] Y. Zheng, B. Chen, H. Zhong, J. Sun, L. Cheng, X. Li, J. Zhang, Y. Tian, W. Lu, J. Wan, T. Yu, L. Huang, H. Yu, H. Lin, Journal of the American Ceramic Society 94 (2011) 1766–1772.

[177] C. Zuo, Z. Zhou, L. Zhu, A. Xiao, Y. Chen, Mater Res Bull 83 (2016) 155–159.

[178] Y. Tayal, A.S. Rao, Opt Mater (Amst) 107 (2020) 110070.

[179] M. Kumar, A.S. Rao, Opt Mater (Amst) 109 (2020) 110356.

[180] M. Jayasimhadri, K. Jang, H.S. Lee, B. Chen, S.S. Yi, J.H. Jeong, J Appl Phys 106 (2009) 013105.

[181] J.F.M. dos Santos, V.S. Zanuto, A.C.C. Soares, E. Savi, L.A.O. Nunes, M.L. Baesso, T. Catunda, J Lumin 240 (2021) 118430.

[182] R.T. Karunakaran, K. Marimuthu, S. Surendra Babu, S. Arumugam, Physica B Condens Matter 404 (2009) 3995–4000.

[183] A. Kumar, Anu, M.K. Sahu, Ravita, S. Dahiya, N. Deopa, A. Malik, R. Punia, A.S. Rao, J Lumin 244 (2022) 118676.

[184] A.S. Rao, Y.N. Ahammed, R.R. Reddy, T.V.R. Rao, Opt Mater (Amst) 10 (1998) 245–252.

[185] J.A. Duffy, J Non Cryst Solids 109 (1989) 35–39.

[186] W.T. Carnall, P.R. Fields, K. Rajnak, J Chem Phys 49 (2003) 4447.

[187] Ravita, A. S.Rao, J Lumin (2021) 118689.

[188] K. Jha, M. Jayasimhadri, J Alloys Compd 688 (2016) 833–840.

[189] H. Tiantian, X.Y. Sun, J. Yu, Y. Gu, L. Xia, Z.X. Wen, H. Guo, X. Ye, J Lumin 244 (2022) 118737.

[190] B. Szpikowska-Sroka, N. Pawlik, T. Goryczka, M. Bańczyk, W.A. Pisarski, J Lumin 188 (2017) 400–408.

[191] F. Enrichi, C. Armellini, S. Belmokhtar, A. Bouajaj, A. Chiappini, M. Ferrari, A. Quandt, G.C. Righini, A. Vomiero, L. Zur, J. Lumin. 193 (2018) 44–50.

[192] M. Kumar, A.S. Rao, Opt Mater (Amst) 120 (2021) 111439.

[193] Y.C. Fang, X.R. Huang, Y. Der Juang, S.Y. Chu, Journal of the American Ceramic Society 95 (2012) 1613–1618.

[194] M.K. Sahu, S. Bishnoi, G. Swati, M. Jayasimhadri, D. Haranath, Int J Appl Ceram Technol 19 (2022) 488–497.

[195] G. Swati, D. Bidwai, D. Haranath, Nanotechnology 31 (2020) 364007.

[196] Y.C. Fang, X.R. Huang, Y. der Juang, S.Y. Chu, Journal of the American Ceramic Society 95 (2012) 1613–1618.

[197] F.G. Montoya, A. Peña-García, A. Juaidi, F. Manzano-Agugliaro, Energy Build 140 (2017) 50–60.

[198] B. Minnaert, P. Veelaert, Energies (Basel) 7 (2014) 1500–1516.

[199] T.H. Kim, W. Wang, Q. Li, Front Chem Sci Eng 6 (2012) 13–26.

[200] X. Chen, P. Dai, X. Zhang, C. Li, S. Lu, X. Wang, Y. Jia, Y. Liu, Inorg Chem 53 (2014) 3441–3448.

[201] R.J. Xie, N. Hirosaki, N. Kimura, K. Sakuma, M. Mitomo, Appl Phys Lett 90 (2007) 191101.

[202] J. Chen, Y. Liu, L. Mei, H. Liu, M. Fang, Z. Huang, Sci Rep 5 (2015) 9673.

[203] S. Kaur, M. Jayasimhadri, A.S. Rao, J Alloys Compd 697 (2017) 367–373.

[204] N. Deopa, A.S. Rao, J Lumin 192 (2017) 832–841.

[205] R.A. Talewar, S. Mahamuda, K. Swapna, A.S. Rao, J Alloys Compd 771 (2019) 980–986.

[206] K. Jha, M. Jayasimhadri, D. Haranath, K. Jang, J Alloys Compd 789 (2019) 622–629.

[207] J. Gou, J. Fan, S. Zuo, M. Luo, Y. Chen, X. Zhou, Y. Yang, B. Yu, S.F. Liu, Journal of the American Ceramic Society 100 (2017) 4011–4020.

[208] K. Jha, M. Jayasimhadri, Journal of American Ceramic Society (2017) 1402–1411.

[209] C. Madhukar Reddy, B. Deva Prasad Raju, N. John Sushma, N.S. Dhoble, S.J. Dhoble, Renewable and Sustainable Energy Reviews 51 (2015) 566–584.

[210] C.B. Annapurna Devi, S. Mahamuda, M. Venkateswarlu, K. Swapna, A. Srinivasa Rao, G. Vijaya Prakash, Opt Mater (Amst) 62 (2016) 569–577.

[211] W. Hordijk, G. Blasse, J Lumin 6 (1973) 137–139.

[212] C.Y. Morassuti, L.H.C. Andrade, J.R. Silva, M.L. Baesso, F.B. Guimarães, J.H. Rohling, L.A.O. Nunes, G. Boulon, Y. Guyot, S.M. Lima, J Lumin 210 (2019) 376–382.

[213] D. Manzani, D. Pabœuf, S.J.L. Ribeiro, P. Goldner, F. Bretenaker, Opt Mater (Amst) 35 (2013) 383–386.

[214] P.P. Pawar, S.R. Munishwar, R.S. Gedam, J Alloys Compd 660 (2016) 347–355.

[215] . S. Mahamuda, K. Swapna, A. Srinivasa Rao, T. Sasikala, L. Rama Moorthy, Physica B Condens Matter 428 (2013) 36–42.

[216] W.T. Carnall, P.R. Fields, K. Rajnak, J Chem Phys 49 (1968) 4424–4442.

[217] T.H. S. Tanabe, T. Ohyagi, N. Soga, Phys. Rev. B 46 (2018) 3305.

[218] M.B. Saisudha, J. Ramakrishna, Optical Absorption of Nd 3‡ , Sm 3‡ and Dy 3‡ in Bismuth Borate Glasses with Large Radiative Transition Probabilities, n.d.

[219] S. Mahamuda, K. Swapna, M. Venkateswarlu, A.S. Rao, S.L. Shakya, G.V. Prakash, J Lumin (2014).

[220] M.B. Saisudha, J. Ramakrishna, Optical Absorption of Nd 3‡ , Sm 3‡ and Dy 3‡ in Bismuth Borate Glasses with Large Radiative Transition Probabilities, n.d.

[221] M.F. P. N eemec, J Non Cryst Solids 302 (2002) 1018–1022.

[222] M. Venkateswarlu, M.V.V.K.S. Prasad, K. Swapna, S. Mahamuda, Ceram Int 40 (2014) 6261–6269.

[223] C.B. Annapurna, S. Mahamuda, K. Swapna, M. Venkateswarlu, A.S. Rao, G.V. Prakash, J Non Cryst Solids 498 (2018) 345–351.

[224] H. Dantanarayana, E. Faber, A.B. Seddon, T.M. Benson, S. Sujecki, 36 (2014) 1076–1082.

[225] M. Czaja, 32 (2010) 547–553.

[226] N.F.B. M.A. Newhouse, R.F. Bartholomew, B.G. Aitken, L.J. Button, IEEE Photonics Technology Letters 6 (1994) 189–191.

[227] I. Pal, A. Agarwal, S. Sanghi, M.P. Aggarwal, 509 (2011) 7625–7631.

[228] S. Mahamuda, K. Swapna, A. Srinivasa Rao, T. Sasikala, L. Rama Moorthy, Physica B Condens Matter 428 (2013) 36–42.

[229] V.H. Rao, P.S. Prasad, K.S. Babu, 101 (2020).

[230] S. Mahamuda, K. Swapna, A. Srinivasa Rao, T. Sasikala, L. Rama Moorthy, Physica B Condens Matter 428 (2013) 36–42.

[231] . M. So, A. Górny, L. Zur, M. Ferrari, G.C. Righini, W.A. Pisarski, J. Pisarska, (2018).

[232].. H.H. Caspers, H.E. Rast, R.A. Buchanan, 2124 (1965) 1–6.

[233] . P. Ramakrishna, R.K. Padhi, S. Kumar, D.K. Mohapatra, H. Jena, B.S. Panigrahi, Opt Mater (Amst) 134 (2022) 113121

[234] N. Deopa, A.S. Rao, S. Mahamuda, M. Gupta, M. Jayasimhadri, D. Haranath, G.V. Prakash, J Alloys Compd 708 (2017) 911–921.

[235] Y. Tayal, A.S. Rao, Opt Mater (Amst) 117 (2021) 111112.

[236]. N. Deopa, B. Kumar, M.K. Sahu, P.R. Rani, A.S. Rao, J Non Cryst Solids 513 (2019) 152–158.

[237] D.V.R. Murthy, B.C. Jamalaiah, T. Sasikala, L. Rama Moorthy, M. Jayasimhadri, K. Jang, H.S. Lee, S.S. Yi, J.H. Jeong, Physica B Condens Matter 405 (2010) 1095–1100.

[238] G. Lakshminarayana, K.M. Kaky, S.O. Baki, S. Ye, A. Lira, I. V. Kityk, M.A. Mahdi, J Alloys Compd 686 (2016) 769–784.

[239] M. Venkateswarlu, M.V.V.K.S. Prasad, K. Swapna, S. Mahamuda, Ceram Int 40 (2014) 6261–6269.

[240] N. Wantana, E. Kaewnuam, N. Chanthima, H.J. Kim, J. Kaewkhao, 267 (2022).

[241] V. Hegde, C.S.D. Viswanath, N. Chauhan, K.K. Mahato, S.D. Kamath, Opt Mater (Amst) 84 (2018) 268–277.

[242] N. Wantana, E. Kaewnuam, N. Chanthima, H.J. Kim, J. Kaewkhao, 267 (2022).

[243] G. Zhu, Z. Li, C. Wang, X. Wang, F. Zhou, M. Gao, S. Xin, Y. Wang, Dalton Transactions 48 (2019) 1624–1632.